ABSTRACT

Title of Dissertation:	THE IMPACT OF TRANSLATIONAL FIDELITY ON HUMAN HEALTH
	Carolina Marques dos Santos Vieira, Doctor of Philosophy, 2018
Dissertation directed by:	Professor and Chair, Jonathan D. Dinman, Department of Cell Biology and Molecular Genetics

Ribosomopathies are a class of diseases resulting from mutations in genes encoding ribosomal proteins and ribosome biogenesis factors. Pleiotropic clinical presentations of different ribosomopathies has been taken as evidence of specialized ribosomes. Alternatively, gene dosage effects have been proposed to account for the observed differences. A yeast genetics approach was used to address this issue. Due to a historical gene duplication event, *S. cerevisiae* cells harbor two ohnologs for most ribosomal proteins. Deletion of one yeast ribosomal protein ohnolog was used to mimic haploinsufficiency in diploid cells (i.e. pseudo-haploinsufficient yeast). Further, insertion of a second copy of the undeleted ohnolog into the locus of the deleted ohnolog enabled separation of effects due to gene dosage from those due to ribosomal protein ohnolog identity. We found that significant changes in translational fidelity in the ribosomal protein ohnolog deletion strains were corrected by ohnolog

duplication. Changes in gene dosage, particularly as they may affect the abundance of an enzyme as central as the ribosome, can impart stress through far reaching effects on cellular metabolism. Thus, as an orthogonal approach, we also examined the stress profiles of cells harboring the *cbf5-D95A* allele (model of X-linked Dyskeratosis Congenita) and the *rps23a-R69K* allele (model of MacInnes Syndrome). RNA-seq analysis revealed increased expression of proteins involved in response to oxidative stress in *cbf5-D95A* cells. Growth curve analysis revealed a longer plateau of the *cbf5-D95A* cells upon reaching stationary phase, suggestive of a pre-adaptive stress response. Decreased ROS abundance, tunicamycin resistance and increased basal levels of HAC1 mRNA in the mutant cells support this hypothesis. Similar results were observed with regard to the ohnolog deletion strains. Taken as a whole, these data support the gene dosage model as opposed to the specialized ribosome hypothesis with the caveat that this conclusion is limited to yeast cells growing in rich medium.

THE IMPACT OF TRANSLATIONAL FIDELITY ON HUMAN HEALTH

by

Carolina Marques dos Santos Vieira

Dissertation submitted to the Faculty of the Graduate School of the
University of Maryland, College Park, in partial fulfillment
of the requirements for the degree of
Doctor of Philosophy
2018

Advisory Committee:
Professor Jonathan D. Dinman, Chair
Professor Najib El-Sayed
Associate Professor Antony M. Jose
Associate Professor Kan Cao
Associate Professor Lisa Taneyhill, Dean's Representative

Dedication

This dissertation is dedicated to my parents for all their love. They have been an immense source of inspiration and support in my life. Without them, I would not have made it this far.

Acknowledgements

I would like to thank my advisor, Dr. Jon Dinman, for the years of mentorship, support, patience, and encouragement. To my committee: thank you for your time and guidance.

I would also like to thank past and present lab members of the Dinman lab, especially Dr. Joe Briggs, Dr. Denis Wafula, Dr. Ashton Trey Belew, Joe Kendra, Alex Olson, Swaksha Rachuri, Cassie Moomau, Dr. Alicia Cheek, Dr. Suna French, Dr. Sharmishtha Musalgaonkar, Dr. Vivek Advani, Dr. John Jones, Dr. Bin Chen. You have been great colleagues and friends. Thank you for the valuable discussions, experimental troubleshoot, and for the fun moments inside and outside of the lab.

To all graduate students and post-docs I have interacted with during my time at the University: thank you both for your assistance with experiments and for your friendship.

To all my friends who have helped me stay sane during my time in graduate school, thank you. A special thank you goes to Maria Osso and Lisa Starr for being some of my biggest cheerleaders.

To the staff of the Department of Cell Biology and Molecular Genetics, especially to Moly Burke, Sharon Fabricante, Teresa Thompson, Dorothea O'Toole, Megan Leung, Priyanka Vengat, and Errica Philpott: thank you for all you have done for me, both from an administrative standpoint, but also as friends.

I would like to thank my family for all the years of support, and for their patience as they watched me from an ocean away for the last nine years. Thank you for your understanding and unwavering love. I will forever be in your debt.

Finally, a big thank you to my husband, Angel Galvez, for his love and support. Without him, none of this would have been possible. Thank you for helping me make it through to the end. Thank you, also, for always being there for me, for listening, and for making me laugh even when graduate school life got rough.

This work was supported in part by NIH grant R01HL119439 to Dr. Jonathan D. Dinman, and three fellowships to Carolina Marques dos Santos Vieira (Graduate School Summer Research Fellowship, CMNS Dean's Fellowship, MOCB-CA Summer Fellowship).

Thank you to Dr. Susan Baserga and Dr. Sherif Abou Elela for kindly providing us with yeast strains, and to Dr. Alyson MacInnes for providing us with patient-derived cell lines. These were instrumental to completing the work discussed in this dissertation.

Table of Contents

List of Tables

List of Figures

List of Abbreviations

ANOVA	Analysis of variance
ATP	Adenosine triphosphate
BTDD	Brachycephaly, trichomegaly, and developmental delay
cDNA	Complementary DNA
CMV	Cytomegalovirus
CO_2	Carbon dioxide
cpm	Counts per million
DBA	Diamond Blackfan Anemia
DE	Differential expression or differentially expressed
DMEM	Dubelco's modified eagle medium
DNA	Deoxyribonucleic acid
dT	Deoxythymine
EDTA	Ethylenediaminetetraacetic acid
ETS	External transcribed spaces
FBS	Fetal bovine serum
GTP	Guanosine triphosphate
H	Hour
H_2O_2	Hydrogen peroxide
ICA	Isolated Congenital Asplenia
IGV	Integrative Genomics Viewer
ITS	Internal transcribed spaces
LB	Luria-Bertani broth
LCL	Lymphoblast cell line
LiOAc	Lithium acetate
M	Molar
MCINS	MacInnes Syndrome
min	Minutes
ml	Milliliter
mm	millimeter
mM	Millimolar
mRNA	Messenger ribonucleic acid
µg	Microlgram
µl	Microliter
µM	Micromolar
ng	Nanogram
nm	Nanometer
NMD	Nonsense mediated mRNA decay
OD	Optical density
OMIM	Online Mendelian Inheritance in Man
PBS	Phosphate buffered saline
PCA	Principal component analysis
PCR	Polymerase chain reaction
PEG	Polyethylene glycol
PMSF	Phenylmethylsulfonylfluoride

Poly (A)	Poly adenosine
Pre-rRNA	Pre-ribosomal ribonucleic acid
PRF	Programmed ribosomal frameshifting
RNA	Ribonucleic acid
RNA-Seq	RNA sequencing
RPMI	Roswell Park Memorial Institute medium
rRNA	Ribosomal ribonucleic acid
sec	Seconds
siRNA	Small interfering ribonucleic acid
snoRNA	Small nucleolar ribonucleic acid
SOC	Super optimized broth with catabolite repression
TE	Tris and EDTA buffer
tRNA	Transfer ribonucleic acid
Ts/+	*Tail short*/+ phenotype in mouse
UTR	Untranslated region
WT	Wild-type
X-DC	X-linked Dyskeratosis Congenita
YPAD	Yeast extract, peptone, adenine sulfate, and dextrose medium

Chapter 1: Introduction

The ribosome

The ribosome is the molecular machine responsible for the synthesis of proteins. This macromolecule is older than cellular life itself, dating back ~4 billion years[1,2]. It is hypothesized that cellular life has evolved around the ribosome. Ribosomal RNAs (rRNAs) and ribosomal proteins are assembled into ribosomes in a complex maturation process (**Figure 1**). The large ribosomal subunit (60S) in the yeast ribosome is composed of 5S, 5.8S, and 25S rRNAs, and 33 ribosomal proteins[3]. The small ribosomal subunit (40S) is composed of 18S rRNA and 46 ribosomal proteins[3].

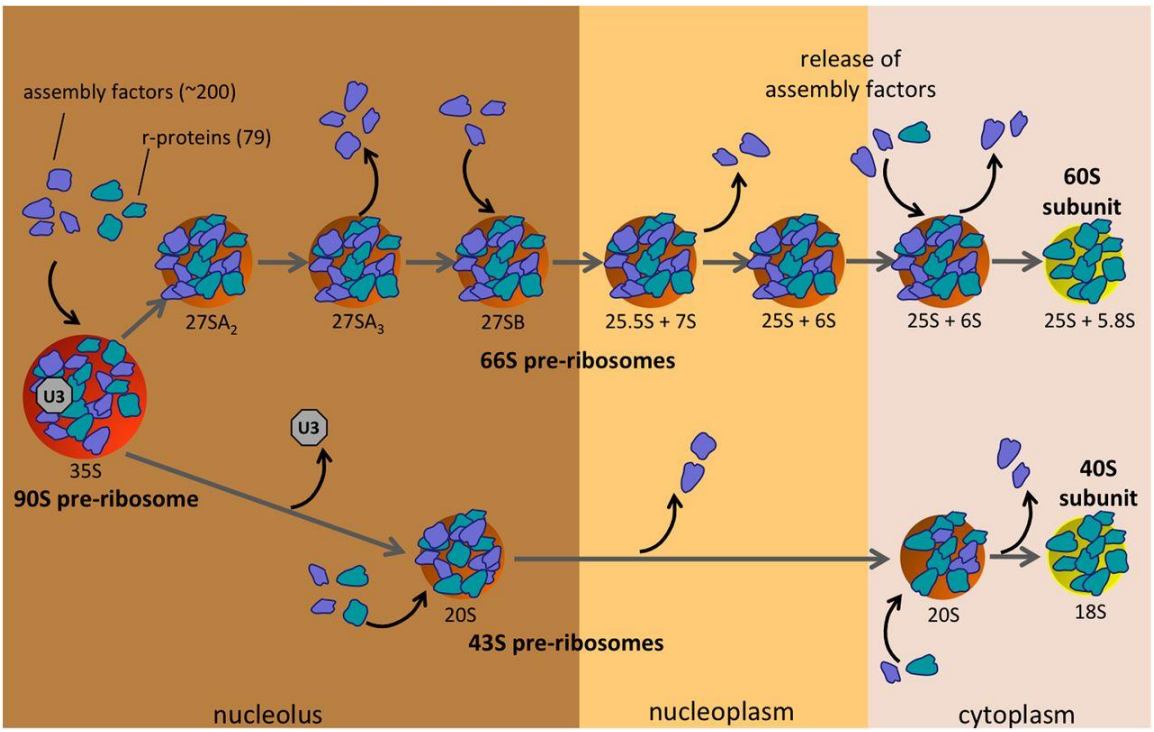

Figure 1. Maturation of ribosomes into large (60S) and small (40S) subunits

Sequential assembly of the pre-ribosome intermediates happens with the assistance of ~200 assembly factors (shown in purple). rRNAs are represented in red (early), orange (middle), or yellow (late), and their sedimentation coefficient is displayed. Ribosomal proteins are shown in teal and assemble into the pre-ribosomes at all stages of maturation. Figure from Woolford and Baserga, 2013[3].

The two ribosomal subunits function together to decode messenger RNA (mRNA) into proteins[4–6]. The small subunit contains the decoding center where base pairing between the mRNA codon and the transfer RNA (tRNA) anticodon allow for discernment of correct aminoacyl tRNAs (**Figure 2**). The large subunit contains the peptidyl transferase center where as the name indicates peptidyl transfer occurs via a transesterification reaction wherein the nascent peptide is transferred from a peptidyl tRNA in the ribosomal P-site onto an incoming aminoacyl tRNA located in the ribosomal A-site (**Figure 2**).

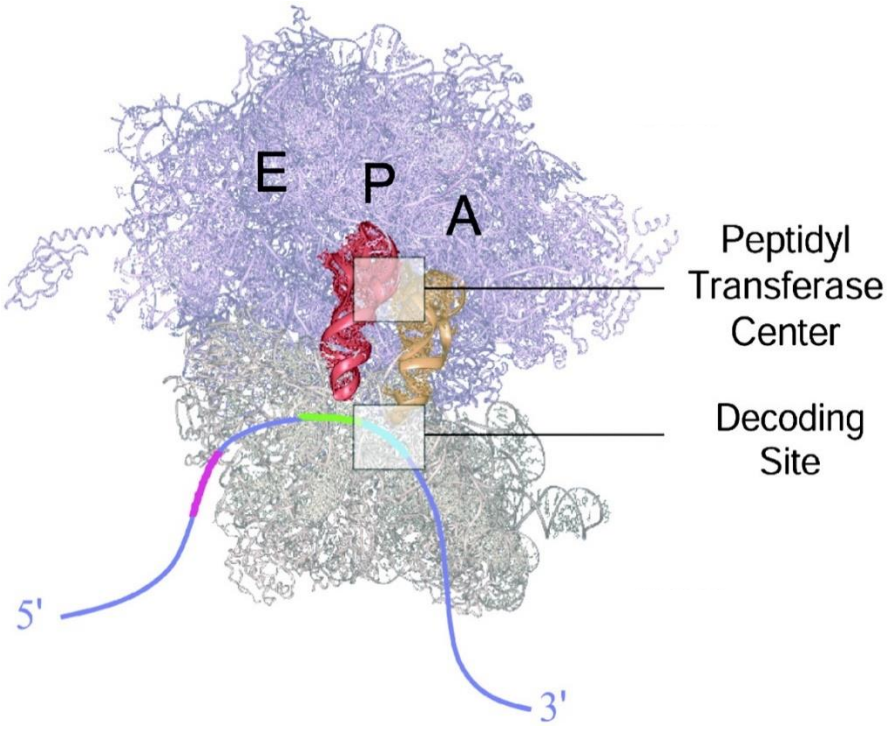

Figure 2. Peptidyl transferase center and decoding center of the ribosome
Ribosome with A-, P-, and E- sites labeled. Large subunit is shown in purple, and small subunit in grey. Aminoacyl tRNA is shown in orange at the A-site, and the peptidyl tRNA is shown in red on the P-site. The location of the peptidyl transferase center and decoding center are highlighted. Image adapted from Blanchard et al., 2004[5].

Ribosomopathies

Given the centrality of the ribosome for life, the discovery that organisms could survive despite the presence of mutations in genes encoding ribosomal proteins was somewhat surprising. In *Drosophila melanogaster*, the appearance of the *Minute* phenotype (characterized by slow development, small size, and thin bristles) has been independently attributed to mutations in 64 ribosomal protein genes. These haploinsufficient mutations leading to

reduced overall protein synthesis were the first indication that the ribosomal deficiencies may underlie certain human disease states[7,8,17,9–16].

This class of disorders, called ribosomopathies, is often characterized by anemia and in some cases bone marrow failure early in life, and by cancer if patients survive in early adulthood [18–20]. This transition from a hypoproliferative phenotype (anemia) to a hyperproliferative phenotype (cancers, such as leukemia) is known as Dameshek's riddle[18,21]. In a classic paper published in 1967, Dr. William Dameshek proposed that some sort of repair mechanism was able to react to an initial damage, thus providing at least some cells the ability to grow, albeit abnormally[21]. The subsequent identification of mutations affecting the ribosome as underlying this class of diseases, termed 'ribosomopathies', marked a critical breakthrough toward understanding this paradox[18].

In ribosomopathies, the first insult to a cell is the mutation in a ribosomal protein or ribosome biogenesis factor. This leads to ribosome biogenesis defects and changes in protein expression. The population of cells carrying these mutations are under selective pressure to synthesize enough ribosomes. Revertants or cells carrying second site suppressor mutations that inactivate ribosome biogenesis quality control mechanism thus have a selective advantage. Although these cells are able to synthesize enough ribosomes, they remain defective in their ability to carry out accurate protein synthesis (**Figure 3**)[18,22]. A well-studied example involves cells carrying the R98S mutation in *RPL10* (encoding uL16), which initially causes ribosome biogenesis defects

and a slow growing phenotype. Hematopoietic stem cells require high rates of cellular proliferation in order to supply enough erythrocytes to supply the body with a constant supply of new blood cells. Those carrying the *RPL10-R98S* mutation are under selective pressure to proliferate, selecting for suppressor mutations that eventually cause the cancerous phenotype, T-cell acute lymphoblastic leukemia[23].

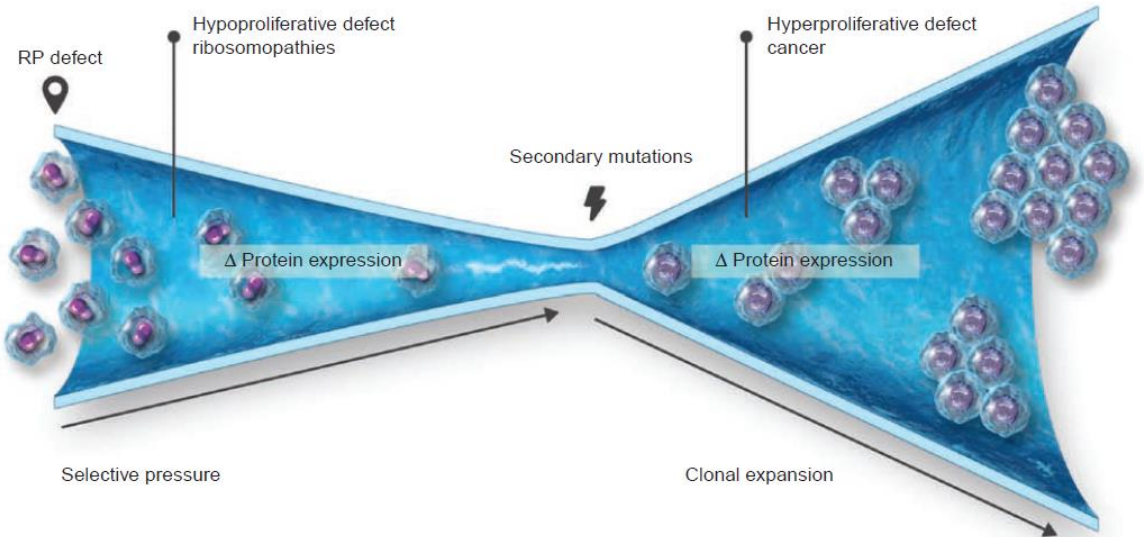

Figure 3. Ribosomopathies: Transition from a hypoproliferative to a hyperproliferative phenotype

Model of ribosomal protein defect leading to a hypoproliferative phenotype. This places selective pressure on the cells to acquire secondary mutations. These mutations could then cause a hyperproliferative phenotype, leading to clonal expansion of cells with an altered translational phenotype. Figure from Sulima et al., 2017[22].

An extensive list of ribosomopathies have been characterized. This work will focus on the five summarized below (**Table 1**).

Table 1. A selective list of ribosomopathies, including their clinical features and mutated genes, and the ribosomal proteins they encode

Ribosomopathy	Human Gene	Clinical Features	Yeast Gene	Protein
X-linked Dyskeratosis Congenita (X-DC)	*DKC1*	Cytopenia, skin hyperpigmentation, and nail dystrophy	*CBF5*	Dyskerin
Diamond-Blackfan Anemia (DBA)	19 RP genes (*RPS19* in ~ 25% of cases)	Anemia, growth defects, and congenital abnormalities	*RPS19*	Most commonly eS19
Isolated Congenital Asplenia (ICA)	*RPSA*	Absence of the spleen	*RPS0*	uS2
5q- Syndrome	*RPS14*	Anemia	*RPS14*	uS11
MacInnes Syndrome	*RPS23*	Short stature, microcephaly, fetal finger pads, simian palmar creases, hearing loss	*RPS23*	uS12

Table adapted from Narla and Ebert, 2010 and Nakhoul et al., 2014[19,20].

Diamond Blackfan Anemia

Diamond-Blackfan Anemia (DBA, OMIM #105650) was first identified in 1938 as a hypoplastic anemia[24]. DBA is an autosomal dominant disease that occurs at a rate of between 5 and 7 people per million live births[25–30]. Most patients present with macrocytic anemia (defined as red blood cells larger than normal, and with lower levels of hemoglobin)[26–28,30–33], bone marrow failure[27,29,33], short stature[25,28,30], craniofacial abnormalities[25,28–30,32,34], heart congenital malformations[28,30,32,34], and thumb abnormalities[25,32,34].

To date, DBA has been associated with mutations in 19 ribosomal protein genes: *RPS19* (accounting for ~25% of cases[27,35]), *RPS7*, *RPS10*,

RPS17, *RPS24*, *RPS26*, *RPS27*, *RPS28*, *RPS29*, *RPL3*, *RPL5*, *RPL9*, *RPL11*, *RPL15*, *RPL18*, *RPL26*, *RPL27*, *RPL31*, and *RPL35A*[27,28,40,41,30,31,34–39]. DBA tends to be caused by inactivating mutations, resulting in haploinsufficiency for the ribosomal proteins they encode (eS19, eS7, eS10, eS17, eS24, eS26, eS27, eS28, uS14, uL3, uL18, uL6, uL5, eL15, eL18, uL24, eL27, eL31, and eL33, respectively). Patients with mutations in *GATA1*, which encodes a transcription factor involved in erythroid differentiation, and *TSR2*, which encodes a protein involved in pre-rRNA processing and which binds directly to eS26, have also been identified[36,42,43]. DBA patients have a higher risk of cancer, most commonly in the form of acute myeloid leukemia and osteogenic sarcoma[30,32,39,44].

Isolated Congenital Asplenia

Isolated Congenital Asplenia patients (ICA, OMIM #271400) are born without a spleen and have no other developmental defects[29,45–47]. This autosomal dominant ribosomopathy afflicts 0.51 people per million live births[29,46,48]. Patients with ICA are more susceptible to bacterial infections, and a large portion die of sepsis in childhood[29,48]. *De novo* heterozygous mutations in gene *RPSA*, encoding ribosomal protein uS2, leading to haploinsufficiency for uS2, were identified in ICA patients[46,49].

5q- Syndrome

5q- Syndrome (OMIM #153550) is due to deletion of a portion of the long arm of chromosome 5. This results in haploinsufficiency for the *RPS14* gene, encoding ribosomal protein uS11, a component of the 40S ribosomal subunit[49–53]. This disorder affects 1 in 20,000 people in the USA[54]. This syndrome is a subtype of myelodysplastic syndrome, which in a quarter of the patients progresses to acute myeloid leukemia[19,29,51,53,55]. Patients present with macrocytic anemia, and high platelet counts[52,53,55–57].

X-linked Dyskeratosis Congenita

X-linked Dyskeratosis Congenita (X-DC, OMIM #30500) is a ribosomopathy caused by mutations in the *DKC1* gene. *DKC1* encodes dyskerin, a conserved pseudouridine synthase that catalyzes the conversion of certain uridines in rRNA to pseudouridines[58–60]. Small nucleolar RNAs (snoRNAs) called H/ACA RNAs guide pseudouridylation[61–63] by transiently base pairing with the rRNA and specifically targeting the uridines to be modified[64]. The H/ACA RNAs contain two hairpin structures, the H domain and the ACA box, separated by a single stranded region. Dyskerin is conserved from humans through yeast, where the gene is called *CBF5*[58,65–67]. One in every million males is affected by X-DC[29].

MacInnes Syndrome

MacInnes Syndrome (OMIM #617412) is a ribosomopathy caused by mutations in the *RPS23* gene, encoding protein uS12[68]. This novel ribosomopathy was identified by our collaborator Dr. Alyson MacInnes. The two known patients presented with short stature and craniofacial malformations[68], similar to what is observed in DBA patients. One of the patients was additionally diagnosed with intellectual disability and autism spectrum disorder[68]. Contrary to DBA, MacInnes Syndrome patients did not present with anemia or any other hematologic symptoms[68].

Ribosome biogenesis defects in ribosomopathies

Ribosomopathies are due to genetic abnormalities in ribosomal proteins or ribosome biogenesis factors. As such, it was deemed important to study the effects of the mutations associated with ribosomopathies on ribosome biogenesis. The central part of ribosome biogenesis is pre-rRNA processing (**Figures 4 and 5**), around which ribosomal proteins and ribosome biogenesis factors assemble as described above. Pre-rRNA processing has been studied in patient-derived cells and model organisms.

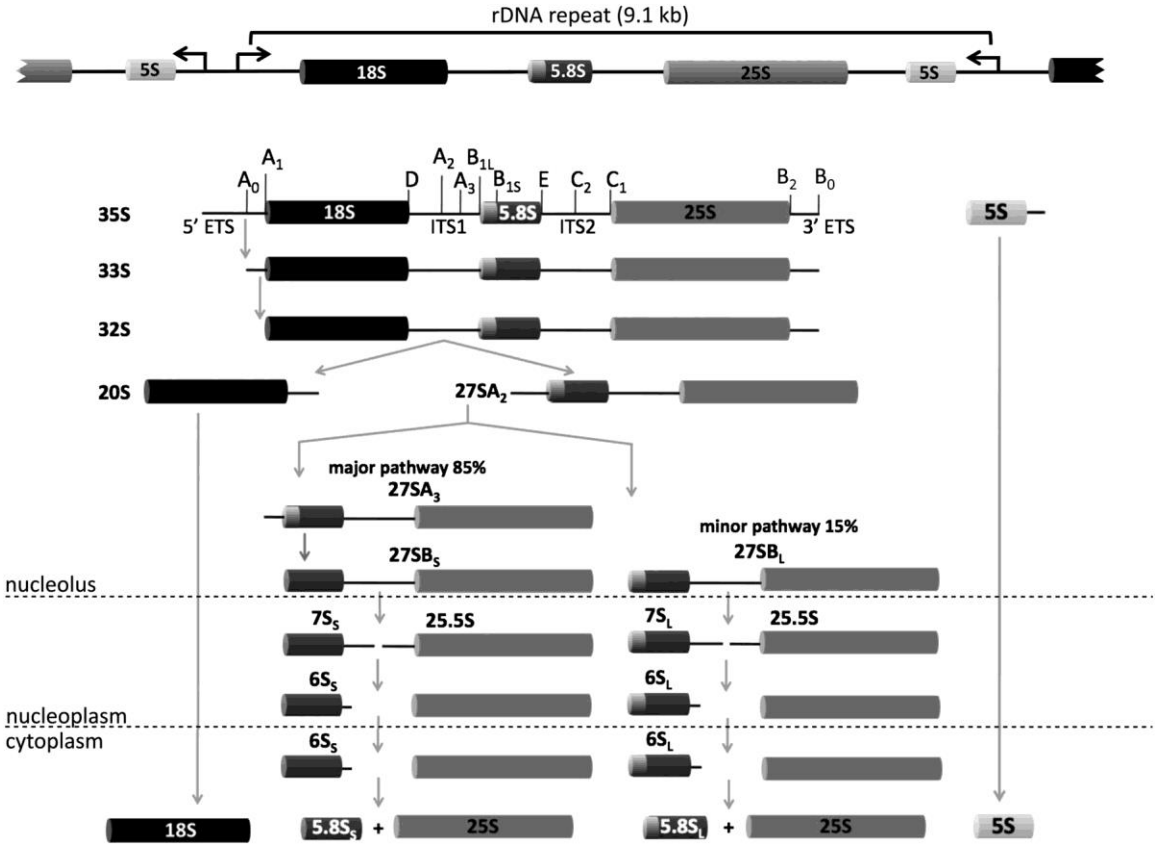

Figure 4. Yeast pre-rRNA processing

The 35S pre-rRNA is transcribed by RNA polymerase I, while pre-5S rRNA is transcribed by RNA polymerase III. External and internal transcribed spacers (ETS and ITS) are removed by a series of endonucleolytic and exonucleolytic steps during ribosome assembly. This series of processes starts in the nucleolus and continues through the nucleoplasm and cytoplasm, as the forming ribosome subunits are exported out of the nucleolus. Figure from Woolford and Baserga, 2013[3].

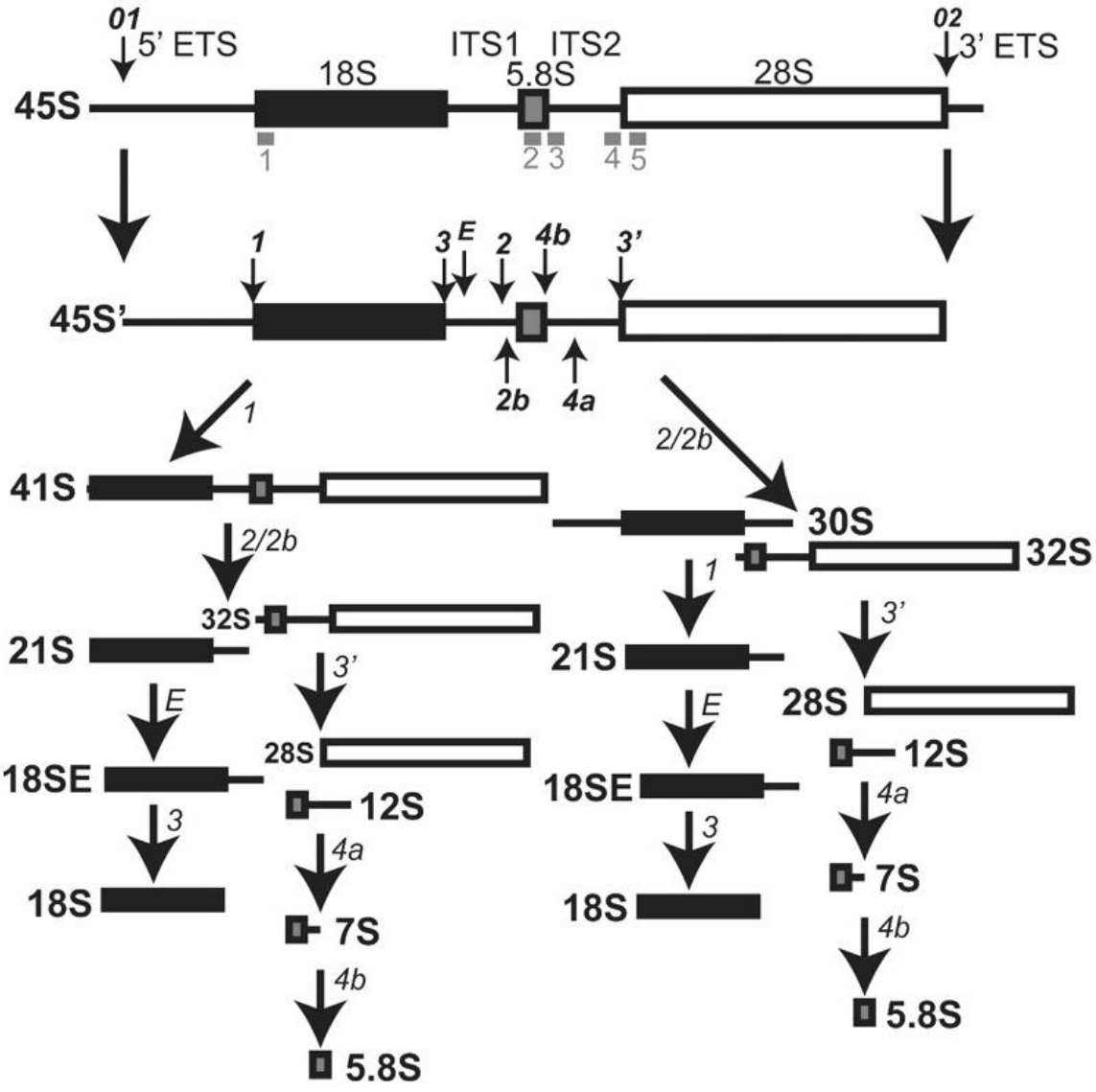

Figure 5. Human pre-rRNA processing

Depiction of pre-rRNA processing in human cells. External and internal transcribed spacers (ETS and ITS) are removed by a series of endonucleolytic and exonucleolytic steps during ribosome assembly. This series of processes starts in the nucleolus and continues through the nucleoplasm and cytoplasm, as the forming ribosome subunits are exported out of the nucleolus. Figure from Farrar et al., 2008[39].

Ribosomopathies are associated with ribosome biogenesis defects

Ribosome biogenesis defects associated with ribosomopathies has been most well documented in patient-derived DBA cells and in models of this disease. The yeast eS19 protein shares 50% identity with the human eS19. It is encoded by ribosomal protein genes *RPS19A* and *RPS19B* ohnologs, closely related genes resulting from a genome duplication event that occurred in *Saccharomyces cerevisiae* approximately 100 million years ago[69]. Analysis of ribosome biogenesis in yeast *rps19bΔ* cells revealed that 18S rRNA production is compromised as documented by an increase in accumulation of 35S pre-rRNAs[70]. Polysome profiling in *rps19bΔ* cells revealed a smaller 40S peak and fewer polysomes[70]. Independently of which yeast *rps19* ohnolog was deleted, 40S subunits were retained in the nucleus[70], presumably because of a defect in small subunit assembly that affects nuclear export.

Ribosome biogenesis defects have been documented in cells derived from DBA patients, as well as in cells in which a ribosomal protein associated with a DBA diagnosis had been knocked down by either siRNA or shRNA. Fibroblasts derived from DBA patients with mutations in *RPS19* showed accumulation of 21S pre-rRNA[71]. Hematopoietic progenitor TF-1 cells in which *RPS19* was knocked down had reduced 18S rRNA levels, accumulation of 21S pre-rRNA, and a reduction in 40S subunits on polysome profiles[72]. Similarly, HeLa cells in which *RPS19* had been knocked down displayed a smaller 40S subunit peak on polysome profiles, as well as a decrease in 18S pre-rRNA[71].

HeLa cells in which *RPS10* or *RPS26* mRNAs were knocked down by siRNA displayed a reduction in 18S rRNA[27]. Lymphoblast cell lines (LCLs) derived from DBA patients with mutations in either *RPS10* or *RPS26* showed higher levels of 18S-E pre-rRNA, suggesting a defect in processing 18S rRNA[27]. *RPS27* knockdown on K562 cells (erythroid lineage) led to increased accumulation of 30S pre-rRNA, and a decrease in abundance of 21S and 18S-E pre-rRNA[73], indicating an earlier defect in rRNA processing. Observations regarding accumulation of pre-rRNAs and changes to polysome profiles in cells that either carry mutations to *RPS19*, *RPS10*, *RPS26*, or *RPS27*, or cells which have had expression of the mRNAs encoding their respective proteins knocked down indicated defects in rRNA processing required for small ribosomal subunit assembly.

Studies examining the effects of large subunit ribosomal proteins implicated in DBA diagnosis have also revealed ribosome biogenesis defects. Lymphoblastoid cells from DBA patients carrying mutations in *RPL5* and *RPL11* showed increase in accumulation of 32S, 30S, 18S-E, and 12S pre-rRNAs[30]. Knockdown of *RPL5* and *RPL11* in HeLa cells led to a decrease in the 60S peak in polysome profiles[30]. Knock down of *RPL15* in HeLa cells led to a decrease in the 60S peak and half-mers appearing in the polysome profile of these cells[28]. In HeLa cells in which *RPL15* has been knocked down, there was an increase in accumulation of 32S and 12S pre-rRNAs (precursors to 28S and 5.8S rRNAs), and a higher ratio of 41S, 30S, and 18S-E pre-rRNAs to 21S

pre-rRNA[28]. The same observations were made in HeLa cells in which *RPL26* had been knocked down[37].

Additional studies of DBA-associated mutations in large subunit ribosomal proteins generated similar observations. Sucrose gradient fractionation of *RPL3*, *RPL19*, and *RPL26* siRNA knock downs in HeLa cells revealed decreased levels of free 60S subunits, as well as decreased in 80S monosomes and polysomes peaks[37]. Knock down of *RPL19* in HeLa cells led to accumulation of 32S pre-rRNA, which was also seen in lymphoblasts from a DBA patient carrying a heterozygous *RPL19* mutation[37]. Knock down of *RPL26* in HeLa cells resulted in decreased abundances of 30S, 21S, and 12S pre-rRNAs, and an increase in 41S pre-rRNA[37], suggesting an earlier defect in rRNA processing. The effects seen in levels of 41S, and 21S pre-rRNAs were recapitulated in patient cells with a mutation in *RPL26*[37]. Knock down of *RPL27* in K562 cells (erythroid lineage) led to accumulation of 32S pre-rRNA[73]. UT-7/Epo cells (human leukemic cell lines requiring erythropoietin for growth) where *RPL35A* had been knocked down displayed a smaller 60S subunit peak in a polysome profile, consistent with the accumulation of 45S and 41S pre-rRNA observed in these cells[39,74]. These observations were consistent with defects in processing of rRNAs required for assembly of the large subunit of the ribosome.

In sum, it is clear that ribosome biogenesis is a common denominator in DBA, both in patient-derived cells and in DBA models. Depending on the ribosomal protein that was affected, effects in rRNA processing of either the

small or large subunit were observed. It is also clear that mutations in small subunit proteins reduced the size of 40S peaks, and that large subunit protein mutants conferred reductions in size of 60S peaks in polysome profiles. Taken together, this information supports the hypothesis that DBA pathology is likely due to defective ribosome synthesis, and not due to a specialized function of any one ribosomal protein[39].

Ribosome biogenesis defects have been documented in other ribosomopathies as well. With regard to ICA, uS2 is a component of the small ribosomal subunit and when deleted leads to lower amounts of 18S-E pre-rRNA, indicating that there is a defect in processing 21S pre-rRNA (precursor to 18S rRNA, in the small subunit of the ribosome)[75]. Regarding 5q- syndrome, uS11 haploinsufficiency leads to accumulation of 30S pre-rRNA, and lower levels of 18S-E pre-rRNA[53], suggesting defects in 18S rRNA processing.

Translational Fidelity

Although the effects of mutations involved in ribosomopathies on ribosome biogenesis have been well documented, there remains a large gap in knowledge with respect to the effects of these mutations on translational fidelity. Faithful translation of a message depends on three factors: 1) aminoacyl-tRNA synthetases must pair the correct amino acid and tRNA, 2) ribosomes must select cognate aminoacyl-tRNAs, and 3) ribosomes must be able to proofread and correct wrongful selection events[76–81].

In order to understand the effects of ribosomopathies on translational fidelity, it is imperative to establish baselines regarding what are considered

'normal' error rates. The frequency of errors by the aminoacyl-tRNA synthetase is 10^{-6} or lower due to its editing capabilities[79,82,83]. The ribosome incorporates a missense amino acid at a rate of 10^{-4} to 10^{-5} in wild-type (WT) cells [79,84–86]. Nonsense suppression occurs at a rate of 3 to 4 x 10^{-4} at UAA and UAG codons in WT cells[87]. The rate of non-programmed ribosomal frameshifting is ~ 0.01% for WT ribosomes[88,89]. The frequency of proofreading error by the ribosome is 0.055% in WT cells[90]. In general, these parameters ensure that error rates are on the order of 10^{-3} to 10^{-4} errors per codon in WT cells[76,79,91–95].

Translational fidelity defects

While a high level of translational accuracy is required for proper protein synthesis, there are exceptions to the rules. These are called translational recoding events. This section will give overview of four examples of recoding.

Programmed -1 Ribosomal Frameshifting (-1 PRF)

Programmed -1 ribosomal frameshifting (-1 PRF) was first identified in the region of overlap between the *gag* and *pol* genes of retroviruses[96–98] (**Figure 6**). In retroviruses and many other RNA viruses, -1 PRF events encode C-terminally extended peptides, allowing viral genomes to maximize their information/coding capacity[99].

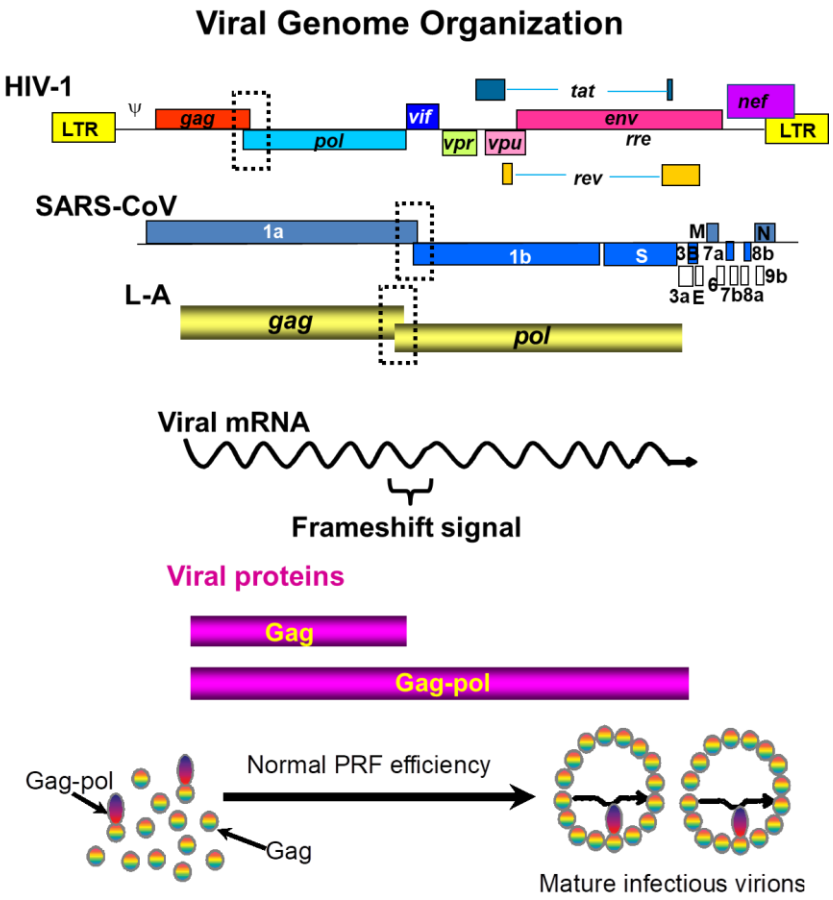

Figure 6. -1 PRF events in viruses

-1 PRF events in viruses encode C-terminally extended proteins for translation of gag and pol proteins. Controlled rates of -1 PRF allow for correct stoichiometric ratios to form a mature infectious virion. Figure from Advani, 2015[100].

Numerous studies of viral -1 PRF signals led to the determination of the basic elements of 1- PRF signals. They are divided into three parts, consisting of a heptameric slip site with the consensus sequence of N NNW WWH (where N denotes any 3 identical nucleotides, W denotes 3 consecutive As or Us, H denotes any nucleotide but G, and spaces indicate incoming frame), a short spacer, and a downstream RNA structural element (**Figure 7A**)[89,101].

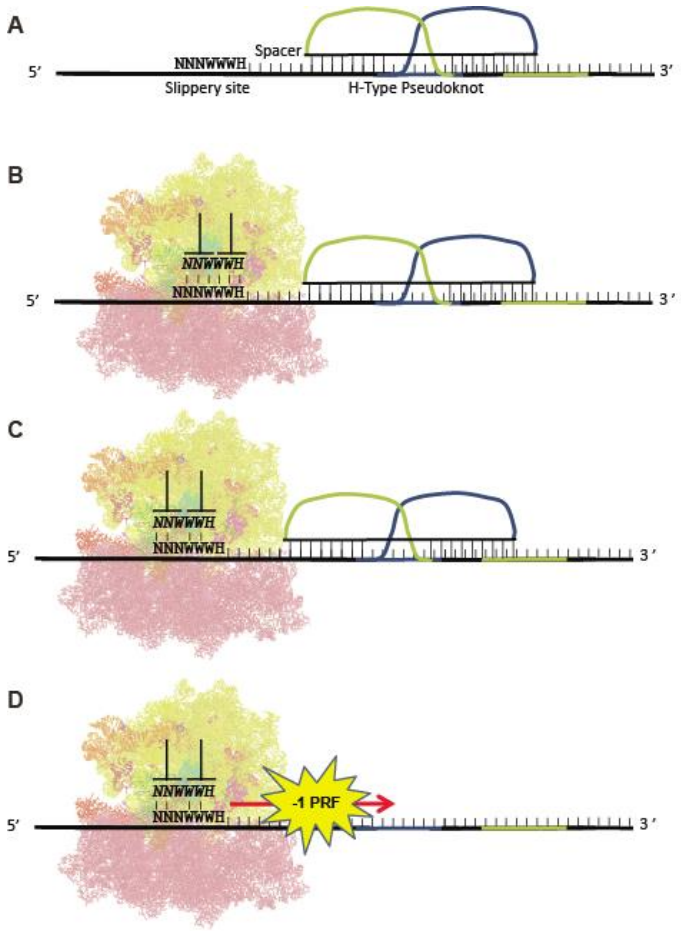

Figure 7. Structure and mechanism of -1 PRF signals

(A) -1 PRF signal consist of a heptameric slippery site, a short spacer, and a downstream secondary structure. **(B)** The downstream structure, in this case a pseudoknot, forces the elongating ribosome to pause with its A- and P-site tRNAs positioned over the slippery site. **(C)** The ribosome slips one base in the 5' direction, and non-wobble base pairing occurs between the tRNAs and the slippery site. **(D)** Once the downstream structure is resolved, the ribosome resumes translation in the -1 frame. Figure from Belew and Dinman, 2015[102].

When a translating ribosome encounters the secondary structure, it is forced to pause with its A- and P-site tRNAs over the slippery site (**Figure 7B**). During this pause, the tRNAs that are paired to the slippery site can slip in the 5' direction by one base, and re-pair their non-wobble bases to the -1 frame codons of the slippery site (**Figure 7C**). By this kinetic partitioning model, once

the downstream secondary structure has been resolved, the elongating ribosome will continue to decode the message reading in the -1 frame (**Figure 7D**)[102].

Analysis of the known viral frameshift signals allowed for the creation of PRFdb, a database available at prfdb.umd.edu, containing the predicted -1 PRF signals in 17 eukaryotic genomes[101]. PRFdb shows that ~10% of genes contain predicted -1 PRF signals[101]. In eukaryotes, cellular -1 PRF events are predicted to redirect translating ribosomes to premature termination codons (**Figure 8A**), targeting messages for degradation through the Nonsense-Mediated mRNA Decay (NMD) pathway (**Figure 8B**)[88,102–104]. An inverse exponential relationship between the efficiency of -1 PRF and mRNA steady state abundance has been demonstrated (**Figure 9**)[104–106].

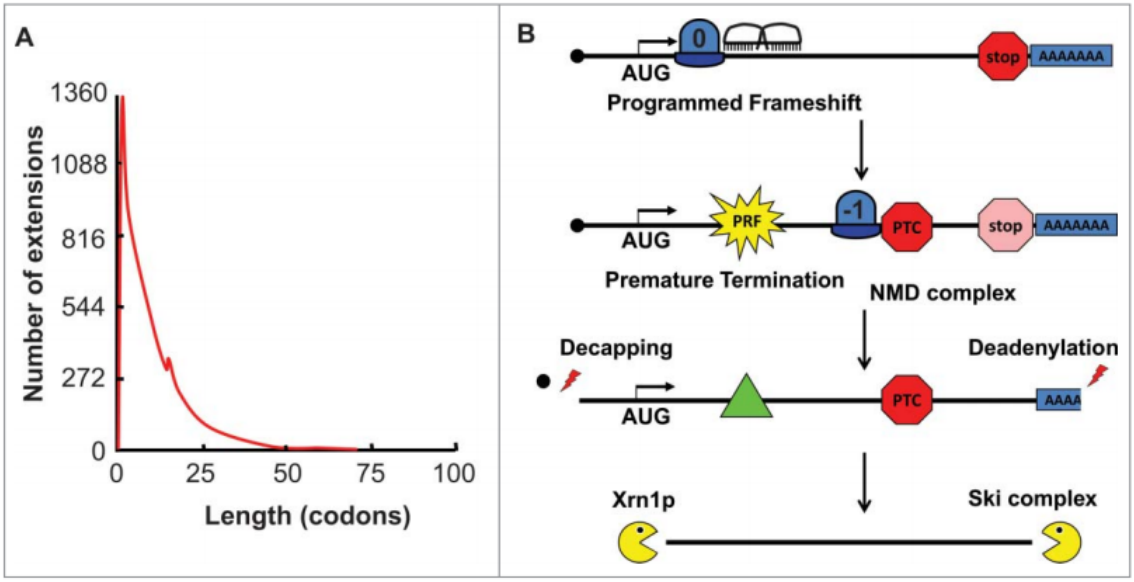

Figure 8. -1 PRF signals in eukaryotes functions as mRNA destabilizing elements

(A) Data from PRFdb (-1 PRF database available at prfdb.umd.edu) plotting the number of C-terminal extensions (y-axis) and their length in codons (x-axis) shows that 99% of -1 PRF events direct the ribosome to a stop codon within 30 codons. **(B)** -1 PRF events direct the ribosome to premature termination codons, triggering the recruitment of the nonsense mediated mRNA decay (NMD) complex to the mRNA. This results in deadenylation and decapping of the mRNA, making it a substrate for exonucleolytic degradation. Figure from Belew and Dinman, 2015[102].

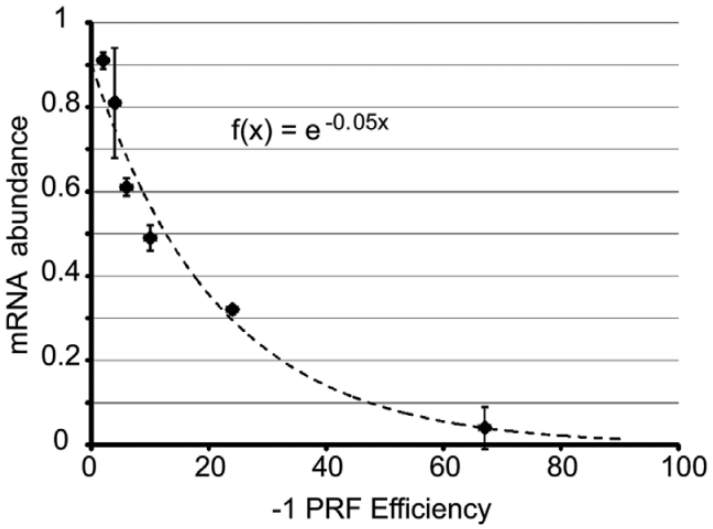

Figure 9. -1 PRF leads to degradation of message through the NMD pathway

Demonstration of the inverse exponential relationship between frameshifting efficiency (x-axis) and mRNA abundance (y-axis). Figure from Advani and Dinman, 2015[106].

Genetic evidence and mathematical modeling indicate that kinetic partitioning leading to -1 PRF can occur at three different steps in the elongation cycle[99,107]. A frameshifting event can occur as the ribosome translocates into (**Figure 10, box 1**) or out of (**Figure 10, box 3**) the slippery site, or during accommodation of the aminoacyl-tRNA into the A-site of the slippery site (**Figure 10, box 2**)[99,107]. The underlying biophysical mechanism thorough which -1 PRF is hypothesized to occur is the torsional restraint model[108]. In all three cases, GTP hydrolysis provides energy for unpairing of tRNAs from the zero frame codons[107].

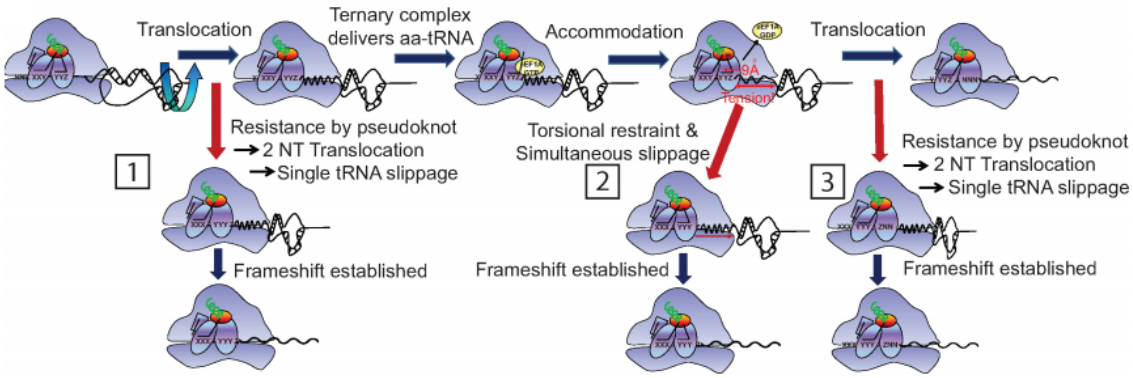

Figure 10. Possible paths to -1 PRF

-1 PRF can occur at three different times during translation of the slippery site. The first is directed by secondary structure as the ribosomes translocates into the slippery site. The second is as a result of torsional strain created by accommodation of aminoacyl-tRNA into the slippery site. The third path is directed by secondary structure as the ribosome translocates out of the slippery site. Tension is relieved by base pairing breaking, ribosome slipping in the 5' direction by one base, and base pairing reforming. Figure from Dinman, 2012[99].

Programmed +1 Ribosomal Frameshifting (+1 PRF)

Another translational recoding exception is programmed +1 ribosomal frameshifting (+1 PRF). As opposed to -1 PRF, the ribosome slips one nucleotide in the 3' direction at the time of a +1 PRF event. A heptameric slippery site is also required for +1 PRF events, while the downstream structure is optional. In +1 PRF events, ribosomal pause can be caused by either rare codons requiring rare, low abundance cognate tRNAs, or downstream secondary structures[109,110]. Messages requiring a +1 PRF event have been described in viruses, bacteria, yeast, and mammalian cells[109–113]. The *OAZ1* +1 PRF signal, conserved from yeast to humans, is the most well-studied. *OAZ1* encodes ornithine decarboxylase antizyme[109,112,113]. There is a negative

feedback mechanism between the amount of polyamines in the cell and the level of frameshifting in the OAZ1 mRNA[109,112].

Missense and termination codon (nonsense) suppression

Other forms of translational recoding are due to ribosome decoding errors. Missense suppression occurs when the ribosome incorporates either a near- or non-cognate amino acid in place of the amino acid that was encoded in the mRNA. This is sometimes due to scarcity of the amino acid, just like +1 PRF. Nonsense suppression takes place when the ribosome incorporates a suppressor tRNA, as opposed to a release factor, at a termination codon. This causes the ribosome to continue decoding the mRNA past the stop codon. This mechanism is used by some viruses to translate gag-pol fusion proteins[114,115] and by in all organisms to encode selenocysteine, the 21st amino acid[116–118].

Translational fidelity reporters

Translational fidelity profiles are often assayed in living cells through the use of dual reporter plasmids[119–121]. In this project, dual luciferase reporters were used. The control zero frame readthrough reporter contains *Renilla* and firefly luciferases in the zero frame (**Figure 11A**). Dual luciferase reporters used to monitor rates of -1 PRF, +1 PRF, and nonsense suppression contain *Renilla* in the zero frame, followed by a test sequence in such a way that firefly luciferase is in the -1, +1, and zero frames, respectively (**Figure 11B**). Normally, only *Renilla* luciferase would be translated, but when a translational

recoding event takes place firefly luciferase will also be translated. To monitor rates of missense suppression, the firefly luciferase of the zero frame readthrough control was mutated (either near- or non-cognate as indicated, **Figure 11C**) in the catalytic site. While a fusion protein will always be translated, firefly luciferase will only be catalytically active if the ribosome misincorporates arginine at residue 218 (**Figure 11C**). Translational recoding is calculated as a ratio of ratios (**Figure 11D**)[119,122].

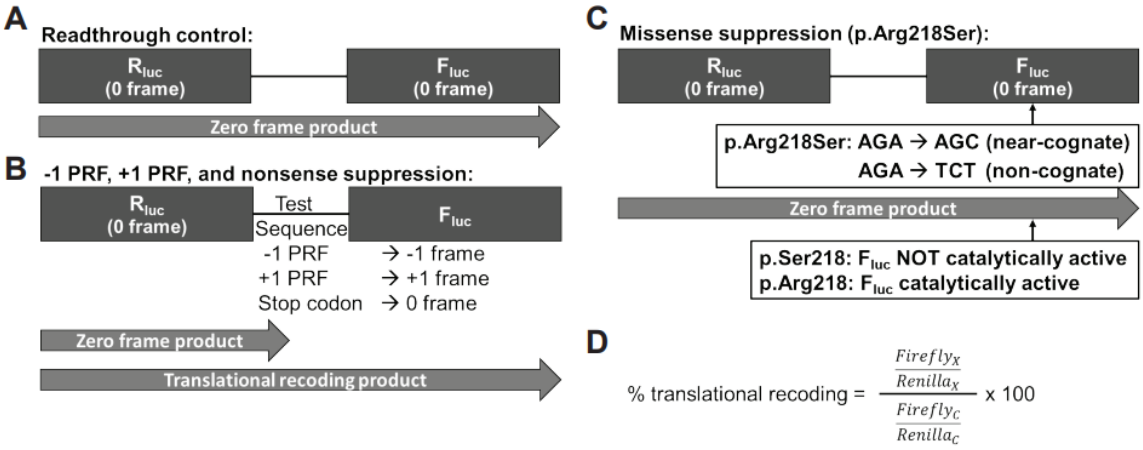

Figure 11. Dual luciferase reporters used to measure translational recoding

(A) Zero frame readthrough control contains *Renilla* and firefly luciferases in the zero frame. **(B)** Dual luciferase reporters used to monitor rates of -1 PRF, +1 PRF, and nonsense suppression contain *Renilla* in the zero frame, and firefly luciferase in the indicated frame. **(C)** Dual luciferase reporter to measure missense suppression contains *Renilla* and firefly luciferases in the zero frame, and the firefly luciferase contains mutations at arginine 218 in the catalytic site. The near- and non-cognate mutations are listed. Only when the ribosome mistranslates and incorporates an arginine the firefly luciferase is catalytically active. **(A-C)** Zero frame and translationally recoding products are indicated. **(D)** Translational recoding is calculated as a ratio of ratios. Figure from Paolini et al., 2017[68].

Research overview

In this research program, we investigate the specialized ribosomes *vs.* gene dosage hypotheses. It is known that ribosome biogenesis defects are present in cells carrying mutations that lead to ribosomopathies. We endeavored to fill gaps in knowledge regarding ribosome translational fidelity in these cells. Our data suggests that gene dosage explains the defects observed in yeast pseudo-haploinsufficient models. Changes in termination codon suppression were observed in ribosomopathy patient-derived cells. We also showed that ribosomopathies pre-adapt the cells for handling stress. We acknowledge the limitation on the use of yeast as a model organism. While the yeast allowed us to genetically mimic the patients' ribosomal haploinsufficiency, the yeast are unicellular organisms with very little developmental biology. Whether specialized ribosomes may help explain pathology in ribosomopathy patients remains to be explored.

Chapter 2: Materials and Methods

Preparation of plasmid DNA

Small scale preparation of DNA was done using GeneJET Plasmid Miniprep Kit (Thermo Scientific, catalog # K0503), according to manufacturer's instructions. Large scale preparation of plasmid DNA was done using either Qiagen Plasmid *Plus* Midi Kit (Qiagen, catalog # 12943) or ZymoPURE™ II Plasmid Midiprep Kit (Zymo Research, catalog # D4201), according to manufacturer's instructions.

Bacterial transformations

NEB® 5-alpha competent E. coli

Between 30 and 50 µl of NEB® 5-alpha competent *E. coli* cells (NEB, catalog # C2988J) were thawed on ice and mixed with 500 ng of plasmid DNA (1-5 µl). Mixtures were pipetted up and down to mix, and incubated on ice for 30 minutes. Samples were then heat shocked at 42°C for 30 seconds, and placed on ice for 5 minutes. Room temperature SOC was added to the mixture to bring the volume up to 1 ml. Cells were allowed to grow for 60 minutes shaking at 37°C. One hundred µl of the mixture was plated on LB with 100 µg/ml carbenicillin plates, and incubated overnight at 37°C.

Stellar™ Competent Cells

Between 30 and 50 µl of Stellar™ competent cells (Clontech, catalog # 636766) were thawed on ice and mixed with 2 µl In-Fusion reaction mixture (from TaKaRa's In-Fusion® HD Cloning Kit, catalog # 639650). Mixtures were pipetted up and down to mix, and incubated on ice for 30 min. Samples were then heat shocked at 42°C for 45 seconds, and placed on ice for 2 minutes. SOC at 37°C was added to the mixture to bring the volume up to 500 µl. Cells were allowed to grow for 60 minutes shaking at 37°C. One hundred µl of the mixture were plated on LB with 100 µg/ml carbenicillin plates, and incubated overnight at 37°C.

Yeast transformations

Following the lithium acetate method[123,124], yeast cultures were grown overnight shaking at 30°C in liquid YPAD media to $OD_{600} \approx 1$, and 200-500 µl of culture were pelleted, washed with 200 µl of 0.1 M LiOAc/TE buffer, and resuspended in 100 µl of the same buffer. These cell suspensions were mixed with 15-18 µl of salmon sperm single stranded DNA (50 mg/ml), 500 ng of plasmid, and 500 µl of PEG/LiOAc/TE buffer, and incubated at 30°C for 1 hour. After a heat shock at 42°C for 7 minutes, the cells were pelleted, washed with 1 ml of water, resuspended in 60 µl of water, and plated on selective media.

Generation of *UPF1* gene deletion yeast strains

Generation of disruption cassette

UPF1 gene deletion strains were created following the protocol described by Hegemann et al.[125]. The disruption cassette was generated by PCR amplification from pJD1521 (i.e. pUG73[126]) using DreamTaq PCR Master Mix (Thermo Fisher Scientific, catalog # K1071) using the following primers: OL5' for KO yUPF1 and OL3' for KO yUPF1 v2 (sequences can be found in Appendix 4). These primers contain ~20 nucleotides that are complementary to pJD1521, and 45 nucleotides that are complementary to flanking regions of the *UPF1* gene. The thermocycling conditions were as follows: 1: 95°C for 5 minutes, 2: 95°C for 90 seconds, 3: 58°C for 50 seconds, 4: 72°C for 150 seconds, 5: steps 2-4 were repeated 29 times, 6: 72°C for 15 minutes. The PCR product is expected to be 2,518 base pairs consisting of 45 base pairs at either end complementary to flanking regions of *UPF1* gene, and internal 2,428 base pairs with the *LEU2* coding region. The PCR product was resolved on a 1.5% agarose gel stained with ethidium bromide, and product was excised and purified using GeneJET Gel Extraction Kit (Thermo Fisher Scientific, catalog # K0691), according to manufacturer's instructions.

Yeast transformation

Yeast strains yJD1524 (*ade2-1 can1-100 his3-11 leu2-3, 112 trp1-1 ura3-1 cbf5::TRP1 + CBF5 on pRS313*) and yJD1525 (*ade2-1 can1-100 his3-11 leu2-3, 112 trp1-1 ura3-1 cbf5::TRP1 + CBF5 D95A on pRS313*) were

transformed with *LEU2* cassette as described above, and plated on –leu media plates.

Verification of gene disruption by PCR

To verify if the *UPF1* gene had been successfully disrupted, colony PCR was carried out using DreamTaq PCR Master Mix (Thermo Fisher Scientific, catalog # K1071) using the following pairs of primers: A and B-M, C-M and D, A and B, C and D, and A and D (sequences can be found in Appendix 4). The thermocycling conditions were as follows: 1: 95°C for 7 minutes, 2: 95°C for 90 seconds, 3: 50°C for 120 seconds, 4: 72°C for 150 seconds, 5: steps 2-4 were repeated 34 times, 6: 72°C for 15 minutes. The resulting yeast strains were named yJD1745 (*ade2-1 can1-100 his3-11 leu2-3, 112 trp1-1 ura3-1 cbf5::TRP1* + *CBF5 on pRS313*) and yJD1746 (*ade2-1 can1-100 his3-11 leu2-3, 112 trp1-1 ura3-1 cbf5::TRP1* + *CBF5 D95A on pRS313*).

CBF5 **RNA-Seq experiments**

RNA extraction and cDNA sequencing

First experiment. Yeast cultures were grown overnight in YPAD media (yJD1524: 1 night, yJD1525: 2 nights) shaking at 30°C. Samples were backdiluted to $OD_{600} \approx 0.8$, and allowed to grow for 2 hours 30 minutes. Cells in 5 ml of media were pelleted at 4,000 x *g* for 2 minutes. Cell pellets were resuspended in 1 ml of TRIzol ® Reagent (Ambion, catalog # 15596018), and 250 µl of 0.5 mm zirconia beads (BioSpec Products, catalog # 11079105z)

were added to each sample. Samples were vortexed for 30 minutes at maximum speed at 4 ˚C. Samples were then centrifuged at 20,000 x *g* for 1 minute at 4˚C to clear lysate and settle zirconia beads. The 1 ml of supernatant from each sample was transferred into a clean microcentrifuge tube, and 200 µl of chloroform were added. Each tube was inverted 6 times, and incubated at room temperature for 3 minutes. Samples were centrifuged at 10,000 x *g* for 25 minutes in the cold room. The upper aqueous layer from each sample was transferred to a clean microcentrifuge tube, and 700 µl of cold 100% iso-propanol (Sigma-Aldrich, catalog # I9516-500ML) were added to each. Samples were incubated overnight at -20°C. RNA was then pelleted at 10,000 x *g* for 20 minutes. The supernatant was discarded and 1 ml of cold 75% ethanol (prepared from absolute ethanol, Pharmco-Aaper, catalog # 111000200, and nuclease-free water) was added to each sample. RNA was pelleted at 10,000 x *g* for 5 minutes, and supernatants discarded. The RNA pellets were washed a second time with 75% ethanol, air dried, and resuspended in 88 µl of nuclease-free water, 10 µl of 10X TURBO DNase buffer (Ambion, catalog # 4022G) and 2.5 µl of TURBO DNase (Ambion, catalog # 2238G2). Samples were incubated at 37°C for 30 minutes. To each sample, 15 µl of DNase inactivation reagent (Ambion, catalog # 8174G) were added. Tubes were flicked to mix every minute during a 5 minute incubation at room temperature. Samples were then centrifuged at 20,000 x *g* at room temperature for 1 minute. Each supernatant was transferred to a fresh tube, and 10 µl of 3 M sodium acetate (pH 5.5, Ambion, catalog # 9740) and 400 µl of 100% ethanol

(Pharmco-Aaper, catalog # 111000200) were added. Samples were incubated overnight at -80°C, and then pelleted at 20,000 x *g* for 20 minutes in the cold room. Supernatants were discarded, and pellets were resuspended in 1 ml of 75% ethanol (prepared from absolute ethanol, Pharmco-Aaper, catalog # 111000200, and nuclease-free water). Samples were pelleted at 20,000 *x g* for 15 minutes. Supernatants were discarded, RNA pellets were air dried, and resuspended in 50 µl of nuclease-free water.

Second experiment (2 batches). Yeast cultures were grown overnight in YPAD media (yJD1524 and yJD1745: 1 night, yJD1525 and yJD1746: 2 nights) shaking at 30°C. Samples were backdiluted to $OD_{600} \approx 0.8$, and allowed to grow for 2 hours 30 minutes. Cells in 3 ml of media were pelleted at 4,000 x *g* for 2 minutes. RNA was isolated using UltraClean® Microbial RNA Isolation Kit (Mo Bio, catalog # 15800-50) and On-Spin Column DNase I Kit (Mo Bio, catalog # 15100-50) according to manufacturer's instructions.

All experiments (3 batches). After DNase treatment, the RNA was further purified using the Qiagen RNeasy mini kit (Quiagen, catalog # 74104), poly(A)+ RNA was selected using oligo-dT following Illumina TruSeqv2 instructions and its integrity was assessed using an Agilent 2100 bioanalyzer. cDNA libraries were constructed using a TruSeq RNA Sample prep Kit Version II (Illumina, catalog # RS-122-2001) with an average size of ~300 nucleotides. Libraries

were sequenced on an Illumina HiSeq 1500 at the UMD Next Generation Sequencing Core / IBBR DNA Sequencing Facility.

Data quality assessment and visualization

Quality assessment of 50 nucleotide single-end reads was preformed via an initial evaluation with FastQC (https://www.bioinformatics.babraham.ac.uk/projects/fastqc/) and biopieces (https://biopieces.org). Illumina sequencing adapters and low quality sequences were removed with Trimmomatic[127]. The remaining sequences were mapped against the S288C strain of *Saccharomyces cerevisiae* using the Ensembl *S. cerevisiae* release 64 genome and annotation data (ftp://igenome:G3nom3s4u@ussd-ftp.illumina.com/Saccharomyces_cerevisiae/Ensembl/R64-1-1/Saccharomyces_cerevisiae_Ensembl_R64-1-1.tar.gz). Alignments were done using Bowtie 2[128] version 2.1.0. Alignments were compressed, sorted, and indexed using samtools[129] and counted against the set of annotated transcripts using HTSeq[130]. Example scripts and all tables resulting from analyses are available in an online repository at https://github.com/cmsvieira/scerevisiae_cbf5. The resulting count tables were passed to R for outlier testing, sample clustering, visualization, and differential expression analyses with the hpgltools package (http://github.com/elsayed-lab/hpgltools/). Tables with raw counts for all samples and conditions are

available as Datasets E1_written_20180606.xlsx and E1E2_written_20180212.xlsx in the online repository.

Differential expression and gene ontology analyses

Samples were tested for significant outliers using a mix of hierarchical clustering and principal component analysis. Non-expressed and weakly expressed genes, defined as having <2 reads per million in *n* of the samples, where *n* is the size of the smallest group of replicates, were removed prior to differential expression (DE) analysis. Multiple data normalization methods were tested, including a mix of: quantile, log transformation, and counts per million. Surrogate variables / batches were queried with a mix of methods from sva[131] to ruv[132]. The first batch of the second experiment was an outlier and was removed from further analysis (discussed in chapter 3). The removed batch contained samples hpgl0774 through hpgl0781, resulting in a total of 6 samples of *CBF5 UPF1* (hpgl0564 through hpgl0567, hpgl0782, and hpgl0786), 6 samples of *cbf5-D95A UPF1* (hpgl0568 through hpgl0571, hpgl0783, and hpgl0787), 2 samples of *CBF5 upf1Δ* (hpgl0784, and hpgl0788), and 2 samples of *cbf5-D95A upf1Δ* (hpgl0785, and hpgl0789) for analyses. Differential expression analyses were performed and compared using surrogate estimates from sva with limma[133], DEseq2[134], EdgeR[135], and a statistically uninformed basic method as a diagnostic control. Genes were considered 'significant' when the DEseq2 observed $|\log_2$ fold-change$|$ was equal or greater than 1.0 ($\log_2 FC \geq 1$) and the adjusted *P* value was less than 0.05. The set of significant

genes for each contrast of interest was passed to g:Profiler[136] through its R interface.

Translational fidelity: Dual luciferase assays

Yeast

Reporters. pJD376 (pYDL-LA)[119], pJD1018 (pYDL-EST2)[104], pJD1039 (pYDL-STN1)[104], and pJD1041 (pYDL-EST1)[104] were used to monitor rates of -1 PRF. Rates of +1 PRF were assayed using pJD377 (pYDL-EST3)[119]. pJD431 (pYDL-UAA), pJD432 (pYDL-UAG), and pJD433 (pYDL-UGA) were used to assay termination codon readthrough[119,137]. Suppression of an AGC near-cognate serine codon or a TCT non-cognate serine codon in the firefly luciferase catalytic site was assayed using pJD642 (pYDL-TCT_{218}), and pJD643 (pYDL-AGC_{218})[138,139]. pJD375 (pYDL-control)[119] was used as the zero frame dual luciferase reporter. All assays were performed in triplicate a minimum of three independent times.

Yeast transformations by lithium acetate method were carried out as described above. Transformants were plated on –ura plates, since dual luciferase reporters contain the URA3 gene.

Sample preparation of RPS23A strains. Transformed yeast cultures were grown overnight shaking at 30°C in H-tryptophan-uracil liquid media containing galactose and raffinose, and after 24 hours media was replaced with H-tryptophan-uracil liquid media containing dextrose. Samples were

backdiluted to OD_{600} = 0.5 and allowed to grow for 2 hours shaking at 30°C. Cells were pelleted by centrifugation, washed with phosphate buffered saline (PBS), and resuspended in PBS with 1mM phenylmethylsulfonylfluoride (PMSF). Glass beads (0.5 mm) were added to the cell suspensions, and samples were lysed on a bead-beater for 2 minutes or vortexed at max speed for 10 minutes. Twenty µl of supernatant were placed on a white 96-well plate for assay.

Sample preparation of ohnolog deletion and duplication strains. Transformed yeast cultures were grown overnight shaking at 30°C in –ura liquid media. Samples were backdiluted to OD_{600} = 0.4 and allowed to grow for 2 hours shaking at 30°C. Ninety µl of 1X Passive Lysis Buffer (PLB) (Pomega) and 10 µl of culture were combined on each well of a white 96-well plate, and assayed.

Mammalian cell lines

All DBA and MacInnes patient-derived cell lines listed below were kindly provided by Dr. Alyson MacInnes at euroDBA, and were deidentified by the providers.

Reporters for MacInnes Syndrome project. pJD2046 (pHDL-fullCMV-UAA)[68] was used to monitor termination codon readthrough. pJD2044 (pHDL-fullCMV-control)[68] was used as the zero frame dual luciferase reporter. To make these constructs, the CMV promoter/enhancer was PCR amplified from

the pCDNA3.1(+) plasmid template using the following oligonucleotide primers: CMVprom-forward and CMVprom-reverse (sequences can be found in Appendix 4). Primers were designed to have either *Kpn* I or *Pst* I restriction enzyme digest sites so that PCR amplicons could be digested and ligated into similarly digested pJD175f (pHDL-SV40-control)[105], and pJD1643 (pHDL-SV40-UAA)[100] dual luciferase reporter plasmids.

MacInnes Syndrome project. Deidentified fibroblasts (RPS23-F120I and RPS23-R67K were MacInnes Syndrome patient-derived cell lines, and C109 and 9E0872 were used as healthy controls) were transfected by electroporation using a Nucleofector II apparatus (Amaxa™) and the Amaxa™ Normal Human Dermal Fibroblasts Nucleofector kit (Lonza, catalog # VPD-1001), per the manufacturer's instructions. For each transfection, 4-5x10^5 cells were mixed with 3 µg of plasmid DNA. All assays were performed in triplicate a minimum of 3 times. 24 hours post-transfection, cell lysates were prepared using passive lysis buffer (Promega) and luciferase activities were determined using the Dual-Luciferase® Reporter Assay System (Promega, catalog # E1960), per the manufacturer's instructions.

Reporters for DBA project. A new generation of dual luciferase reporters was generated by Loughran, et al. to correct interference of test sequence with stability and activity of *Renilla* and firefly luciferases[121]. Plasmid pSGDluc, which contains tandem StopGo sequences (2A) on either side of the test

sequence[121], was kindly provided by Dr. John Atkins, at University College Cork. In order to disrupt the *Bam* HI/*Sal* I sites present downstream of the firefly luciferase coding sequence, complimentary oligonucleotides (BamSalKilT and BamSalKilB, sequences in Appendix 4) were ligated with linearized vector. The resulting plasmid was doubly digested with *Xho* I and *Apa* I, and the vector portion was used in Gibson assembly. A gBlock (sequence in Appendix 4) was used to insert the HIV -1 PRF signal[98,140] between new *Sal* I and *Bam* HI sites. After sequence verification, the resulting plasmid (pJD2256) was linearized with *BamHI* and *SalI*, and another set of complementary oligonucleotides (Alphahelixspacer-T2 and Alphahelixspacer-B2, sequences in Appendix 4) was used to insert an alpha helix spacer which creates an open reading frame encoding the peptide sequence: EAAAKEAAAKA. The resulting plasmid, pJD2257, was used as the zero frame dual luciferase reporter. pJD2337 (PEG10) was used to monitor -1 PRF, and pJD2349 (OAZ1) was used to monitor +1 PRF. pJD2443 (UAA), pJD2444 (UGA), and pJD2445 (UAG) were used to monitor stop codon readthrough. To make the constructs used to monitor PEG10[141,142] and OAZ1[109] mediated -1 and +1 PRF, a gBlock was inserted in linearized pJD2257 by Gibson Assembly (sequences in Appendix 4). To make the constructs used to monitor stop codon readthrough, sets of complimentary oligonucleotides (sequences in Appendix 4) were ligated with linearized pJD2257.

DBA project. Deidentified lymphoblast cell lines (RPL9 L20P (C.I.), and RPL9 c.-2+1 were DBA patient-derived cell lines, and F.T., NhnF, and NhnM were used as healthy controls) were transfected by electroporation using a Nucleofector II apparatus (Amaxa™) and the Amaxa™ Cell Line Nucleofector® Kit V (Lonza, catalog # VVCA-1003), per the manufacturer's instructions. For each transfection, 1.5 x 10^6 cells were mixed with 1.5 µg of plasmid DNA. All assays were performed in triplicate four times. Cell lysates were prepared using passive lysis buffer (Promega) and luciferase activities were determined using the Dual-Luciferase® Reporter Assay System (Promega, catalog # E1960), per the manufacturer's instructions 24 hours post-transfection.

Data analysis

Data were analyzed by taking the ratio of firefly luciferase to *Renilla* luciferase for each of the plasmids normalized to the same ratio obtained from the readthrough plasmid control in the same experiment. Data were plotted on GraphPad Prism as percent translational recoding, with each symbol representing one biological sample assayed in triplicate. Error bars represent standard deviation.

Cell culture

Deidentified patient-derived fibroblasts and lymphoblast cell lines (LCLs) mentioned above, as well as healthy control cell lines were generously provided to us by Dr. Alyson MacInnes, at the European Diamond Blackfan Anemia

foundation (euroDBA). Adherent cell lines (i.e. fibroblasts) were grown using Dulbecco's Modification of Eagle's Medium (DMEM, Corning, catalog # 10-013-CV) supplemented with 30% Fetal Bovine Serum (FBS, Gibco, catalog # 10437-028) and 1% penicillin/streptomycin (Gibco, catalog # 15140-122). Suspension cell lines (i.e. LCLs) were grown in Roswell Park Memorial Institute medium (RPMI, Lonza, catalog # 12-115F) supplemented with 30% FBS, 1% L-glutamine, and 1% penicillin/streptomycin. Cell lines were maintained in a humidified incubator at 37°C with 5% CO_2.

Growth curve experiments

Yeast cultures were grown overnight shaking at 30°C (1 day for yJD1524, 2 days for yJD1525). Cells were then backdiluted to OD_{600} = 0.05 with YPAD media to a final volume of 500 µl, in a 12-well clear plate. Growth was monitored for 47 hours in a BioTek Synergy HT microplate reader at 30°C, with readings taken every hour, after samples were shaken for one minute. Data were analyzed on Excel and growth curves made on GraphPad.

Reactive oxygen species: Amplex® Red assay

All experiments were carried out using Amplex® Red Hydrogen Peroxide/Peroxidase Assay Kit (Invitrogen cat# A22188), according to manufacturer's instructions with some modifications[143,144]. Wild-type yeast cells (yJD1524) were grown at 30°C in a Biotek Synergy HT plate reader for 22

hours. Readings for OD_{595} were collected every hour, after 1 minute of shaking. *cbf5-D95A* cells (yJD1525) were grown the same way for 42 hours. Knowing that 1 unit of OD_{600} corresponds to ~ 3 x 10^7 yeast cells, 2 x 10^7, 4 x 10^7, and 8 x 10^7 yeast cells were transferred into microcentrifuge tubes, and pelleted at 4,000 x *g* for 3 minutes. The cell pellets were resuspended in 500 µl of 1X Reaction buffer, incubated for 1 h shaking at 30°C. After that time, 100 µl of each sample were loaded in quadruplicate on a 96-well plate. To each well, 100 µl of 100 µM Amplex® Red reagent and 0.2U/ml HRP solution were added, and the sample incubated in the dark for 30 minutes. After that time, the fluorescence was measured in a Glomax Multi + Detection System (Promega) using the green filter (absorbance: 525 nm and emission: 580-640 nm). A standard curve was developed from samples of hydrogen peroxide (H_2O_2) dissolved at different concentrations in 1X Reaction Buffer. Final concentrations of H_2O_2 in the standard curve were 0, 0.015625, 0.03125, 0.0625, 0.125, 0.25, 0.5, 1, 2, 3, 4, and 5 µM.

Data analysis

Data for the wells without any cells or H_2O_2 was averaged and subtracted from every reading as background. Corrected duplicate readings of the H_2O_2 samples were averaged to plot a standard curve. Quadruplicate cell sample readings were averaged. Final H_2O_2 concentration in the well was calculated from the standard curve, and doubled to find the H_2O_2 concentration in the sample. Four independent experiments were carried out for each sample

and each plotted as a single point on the graph, along with mean and standard deviation, using GraphPad Prism.

Tunicamycin sensitivity assay

CBF5 strains

Yeast cultures (yJD1524 and yJD1525) were grown overnight in YPAD media shaking at 30°C. OD_{600} was taken, and samples backdiluted to OD_{600} = 0.6, and allowed to grow for 2 hours 30 minutes. Samples were diluted to OD_{600} = 0.1, and 10-fold serial dilutions were made, plated on YPAD plates containing either 0, 0.25, 0.5, or 1 µg/ml tunicamycin, and allowed to grow at 30°C. Photographs of the plates were taken daily.

Haploinsufficiency strains

Yeast cultures (yJD1732, 1739-1744, 1753-1754, and 1756-1760) were grown overnight in YPAD media shaking at 30°C. OD_{600} was taken, and samples backdiluted to OD_{600} = 0.6, and allowed to grow for 2 hours 30 minutes. Samples were diluted to OD_{600} = 0.1, and 10-fold serial dilutions were made, plated on YPAD plates containing either 0, 0.25, 0.5, or 1 µg/ml tunicamycin, and allowed to grow at 30°C. Photographs of the plates were taken daily.

RPS23A strains

Yeast cultures (yJD1729-1731) were grown overnight in –trp media containing galactose and raffinose shaking at 30°C. Media was replaced with –trp media containing dextrose 24 hours before the assay. OD_{600} was taken, and samples backdiluted to OD_{600} = 0.6, and allowed to grow for 2 hours 30 minutes. Samples were diluted to OD_{600} = 0.1, and 10-fold serial dilutions were made, plated on –trp plates containing dextrose, and either 0, 0.25, 0.5, or 1 µg/ml tunicamycin, and allowed to grow at 30°C. Photographs of the plates were taken daily.

HAC1 mRNA splicing

Treatment with tunicamycin

CBF5. Yeast cultures (yJD1524-1525) were grown overnight in YPAD media shaking at 30°C. OD_{600} was taken, and samples backdiluted to OD_{600} = 0.3, and allowed to grow for 1 hours 30 minutes shaking at 30°C. One µg/ml tunicamycin was added, and samples incubated for 1 hour shaking at 30°C.

RPS23. Yeast cultures (yJD1729-1731) were grown overnight in –trp media containing galactose and raffinose shaking at 30°C. Media was replaced with –trp media containing dextrose 24 hours before the assay. OD_{600} was taken, and samples backdiluted to OD_{600} = 0.3, and allowed to grow for 1 hours 30 minutes shaking at 30°C. One µg/ml tunicamycin was added, and samples incubated for 1 hour shaking at 30°C.

RNA isolation and cDNA synthesis

OD_{600} was determined, and $1x10^7$ yeast cells were collected after the 1 hour incubation with tunicamycin. RNA was isolated using Direct-zol™ RNA MiniPrep Plus kit (Zymo, catalog # R2072), according to manufacturer's instructions. cDNA was synthesized from 450 ng of RNA using iScript cDNA Synthesis Kit (Bio-Rad, catalog # 1708891), according to manufacturer's instructions.

PCR to determine HAC1 mRNA splicing status

Primers used were obtained from the literature[145], and the sequences are listed in Appendix 4. The PCR master mix contained 1X DreamTaq PCR MasterMix, 1 µM each of forward and reverse primer, and 2 µl of 1:10 cDNA dilution. The thermocycling conditions were as follows: 1: 95°C for 3 minutes, 2: 95°C for 30 seconds, 3: 58°C for 30 seconds, 4: 72°C for 60 seconds, 5: steps 2-4 were repeated 35 times, 6: 72°C for 15 minutes. The PCR products were resolved on a 1.5% agarose gel stained with ethidium bromide. Unspliced HAC1 mRNA is 363 bases, and the spliced HAC1 mRNA is 111 bases. rRNA was also resolved on a 1.5% agarose gel stained with GelStar (Lonza, catalog # 50535).

Chapter 3: Yeast models of X-DC, DBA, ICA, and 5q- Syndrome suggest that metabolic imbalances pre-adapt cells to stressors

Introduction

Ribosomopathies are a class of diseases caused by mutations in ribosomal proteins or ribosome biogenesis factors. As discussed in chapter 1, haploinsufficiency for these proteins has been shown to impart ribosome biogenesis defects in patient-derived cells and in ribosomopathy model systems. These defects were either in the small or large subunit depending on which ribosomal protein was mutated.

As discussed in detail in chapter 1, while most ribosomopathies present with anemia, they each have their own unique set of symptoms. A specialized ribosomes hypothesis has been formulated on the basis of these unique symptoms[20,29,146,147]. A study of *Rpl38* (eL38) mutant mouse embryos with homeotic transformations revealed that *Rpl38* transcripts were enriched in a tissue-specific manner in mice. Higher expression of *Rpl38* transcripts was detected in embryonic regions where the *Ts*/+ phenotype (characterized by a short and kinky tail and cleft palate) was observed. eL38 (as part of the ribosome) was shown to facilitate formation of 80S complex during translation initiation on some specific Hox mRNAs (the same ones that appeared as part of polysomes). eL38 gives the ribosome a regulatory role in tissue patterning[148].

Further studies are required to determine if heterogeneity of ribosomal proteins confers ribosomes “specialized” activity.

An alternative explanation posits that ribosomopathies are due to metabolic imbalance in the cells [149–151]. Supporters of this theory suggest that the mutations implicated in ribosomopathies lead to a lower concentration of ribosomes in the cells[149]. Lower ribosome concentrations can differentially affect translation of messages depending on rates of translation initiation[149,152]. *GATA1* has been used as an example to illustrate the effects of the rates of translation initiation. *GATA1* encodes a transcription factor involved in erythroid differentiation[36], and mutations in this gene have been implicated in DBA[36,43]. GATA1 mRNA has a highly structured region at the end of its 5’ UTR[153]. This renders GATA1 more sensitive to lower ribosome concentration and resulting changes in rates of translational initiation[149,153].

A yeast *cbf5-D95A* mutant originally developed by the laboratory of Dr. John Carbon[66] was subsequently re-engineered in the Dinman lab [100,154]. Cells harboring the *cbf5-D95A* mutation show decreased rRNA pseudouridylation content [66]. This results in production of ribosomes that have lower affinity for tRNAs both at the A- and the P-sites[154]. This in turn allows tRNAs to more readily slip along mRNAs, leading to increased rates of -1 PRF in yeast, in a *dkc1*^{m} hypomorphic mouse model, and in HeLa cells in which *DKC1* was knocked down by use of an siRNA[154]. Yeast cells carrying the *cbf5-D95A* mutation show hyperaccurate recognition of termination codons, consistent with the negative effects that this mutant confers on ribosomal affinities for

tRNAs (e.g. for suppressor tRNAs)[154]. It has also been determined by qRT-PCR that messages that contain -1 PRF signals are less abundant in *cbf5-D95A* cells than in WT cells[100]. This is likely due to the synergistic effects of increased levels of -1 PRF, which leads ribosomes to premature termination codons, and the increase in recognition of termination codons, which would lead to more efficient recruitment of the NMD complex and consequent degradation of the messages containing -1 PRF signals. In addition, *cbf5-D95A* cells have also been shown to have shorter telomeres than those present in WT cells[100], consistent with the progeria phenotype associated with X-DC[155,156]. In the current work, we have employed this system as a model of X-DC.

As diploid organisms, humans harbor two alleles of each of the ribosomal protein genes within their genome. In contrast, laboratory yeast strains are haploid. However, these yeast strains harbor two versions (A and B, called ohnologs) of most of the ribosomal protein genes as a result of a historical whole genome duplication event[69]. In the current study, we have capitalized on this to create pseudo-haploinsufficient yeast models of DBA (*RPS19* deletion since it is most commonly mutated in DBA patients), ICA (*RPS0*, which encodes uS2), and 5q- Syndrome (*RPS14*) by deleting one of the ribosomal protein gene ohnologs. Control yeast ohnolog duplication strains (kindly provided by Dr. Sherif Abou Elela at the University of Sherbrooke) harbor a second copy of the undeleted ribosomal protein ohnolog inserted into the locus of the one that had been deleted[157]. These cells allowed us to

determine, in yeast, whether translational fidelity differences were due to the ribosomal protein ohnolog that the cells were lacking or due to lower expression of the ribosomal protein.

The goals of the experiments in this chapter were to: 1) contribute to addressing the question of whether ribosomopathies are due to specialized ribosomes or gene dosage, 2) determine gene expression profile of yeast model of X-DC, and 3) investigate sensitivity to stress in yeast models of the ribosomopathies described here, i.e. X-DC, DBA, ICA, and 5q- Syndrome.

Results

Translational fidelity defects in yeast models of ribosomopathies resulting from haploinsufficiency of ribosomal proteins are due to gene dosage effects

In an effort to contribute to the specialized ribosomes or gene dosage dialogue[146,149], the translational fidelity profiles of the yeast models of DBA, ICA, and 5q-Syndrome, as well as of the control ohnolog duplication strains were determined. In order to monitor translational fidelity in these cells, dual luciferase reporters (described in chapter 1, **Figure 11**) were used to assay levels of -1 and +1 PRF, as well as nonsense and missense suppression. For this, each of the model yeast and control ohnolog duplication strains were transformed with a suite of dual luciferase reporter plasmids, and assayed using a dual luciferase assay kit (Promega).

Rates of -1 PRF were measured with a reporter containing the L-A frameshift signal[89]. Ohnolog-specific effects on -1 PRF were observed upon deletion of single ohnologs. In one case -1 PRF was enhanced (*rps0bΔ*), in others it was decreased (*rps0aΔ, rps14bΔ, rps19aΔ,* and *rps19bΔ*), and in one case it remained unchanged (*rps14aΔ*) (**Figure 12A-C)**. However, replacement of the deleted gene with a duplicated ohnolog corrected all -1 PRF defects (**Figure 12D-F**).

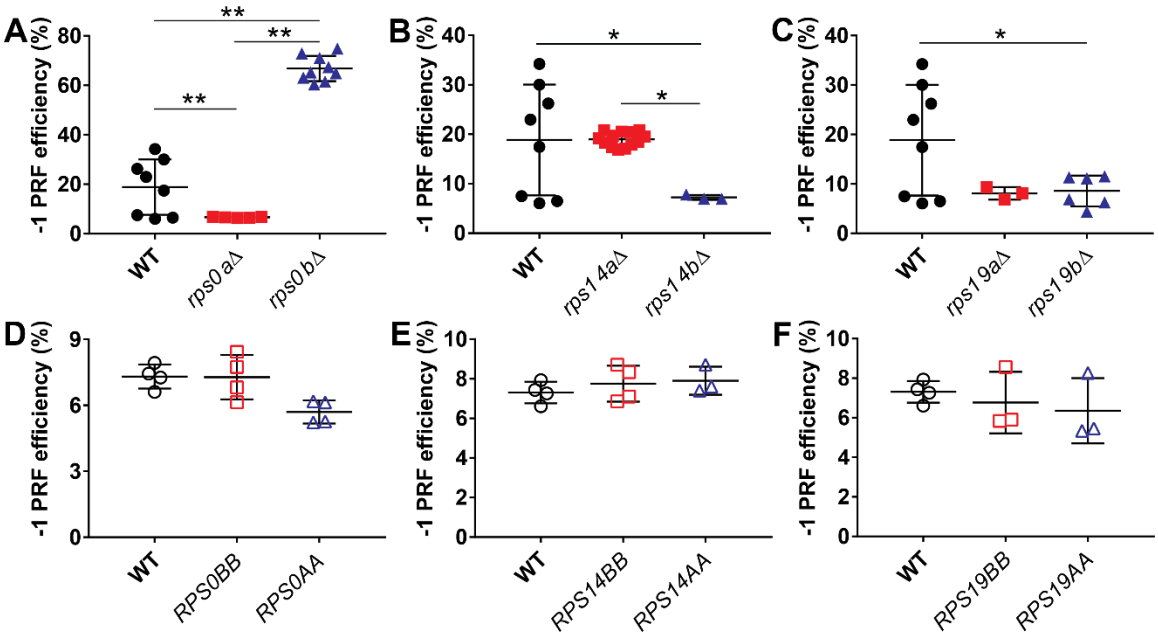

Figure 12. Programmed -1 Ribosomal Frameshifting promoted by the L-A signal in yeast models of haploinsufficiency

Rates of -1 PRF promoted by L-A in **(A)** *rps0Δ*, **(B)** *rps14Δ*, **(C)** *rps19Δ*, **(D)** *RPS0* duplication, **(E)** *RPS14* duplication, and **(F)** *RPS19* duplication strains. Each point represents an experimental replicate performed in triplicate. A minimum of 3 biological replicates were assayed in triplicate for each combination of yeast strain and plasmid. One-way ANOVA was used to determine significance: * $p<0.05$, and ** $p<0.01$.

Rates of +1 PRF were assayed with a dual luciferase reporter containing the frameshift signal for Ty*1*[110,158]. No statistically significant differences were

observed between any of the ohnolog deletion strains and the WT, or between the ohnolog duplication strains and the isogenic WT (**Figure 13**).

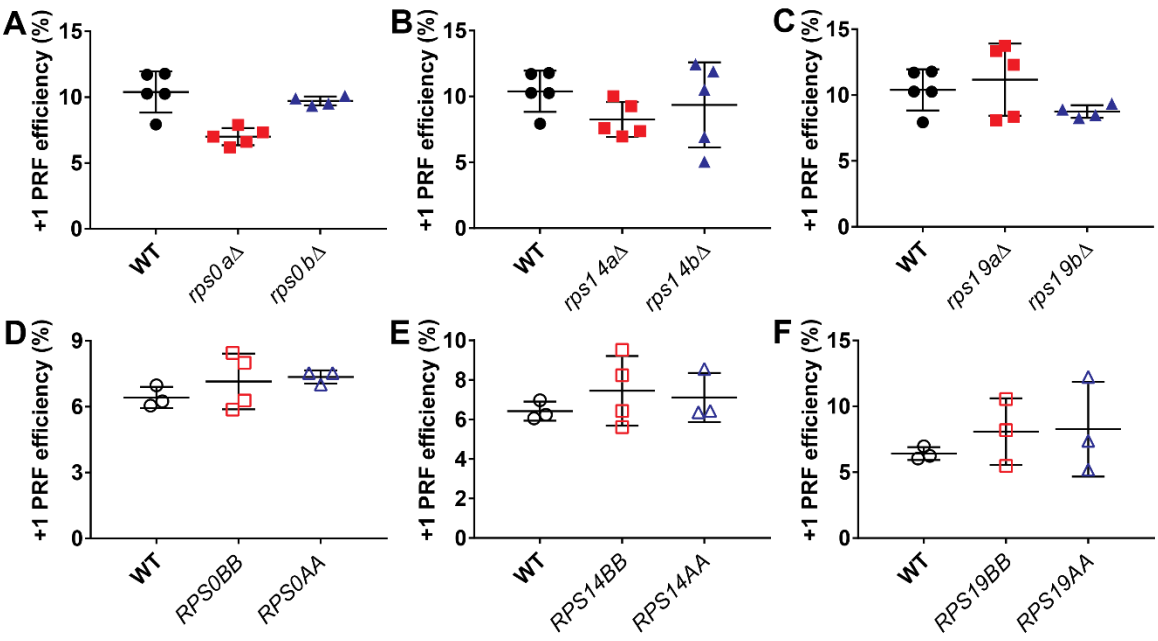

Figure 13. Programmed +1 Ribosomal Frameshifting promoted by the Ty1 signal in yeast models of haploinsufficiency

Rates of +1 PRF promoted by Ty*1* in **(A)** *rps0Δ*, **(B)** *rps14Δ*, **(C)** *rps19Δ*, **(D)** *RPS0* duplication, **(E)** *RPS14* duplication, and **(F)** *RPS19* duplication strains. Each point represents an experimental replicate performed in triplicate. A minimum of three biological replicates were assayed in triplicate for each combination of yeast strain and plasmid. One-way ANOVA did not find any statistically significant differences.

Stop codon readthrough was measured using reporters in which each of the stop codons was inserted in frame between *Renilla* and firefly luciferases in the zero frame[100]. No changes in UAA stop codon readthrough were observed in the ohnolog deletion strains (**Figure 14**), and thus UAA stop codon readthrough was not tested in ohnolog duplication strains.

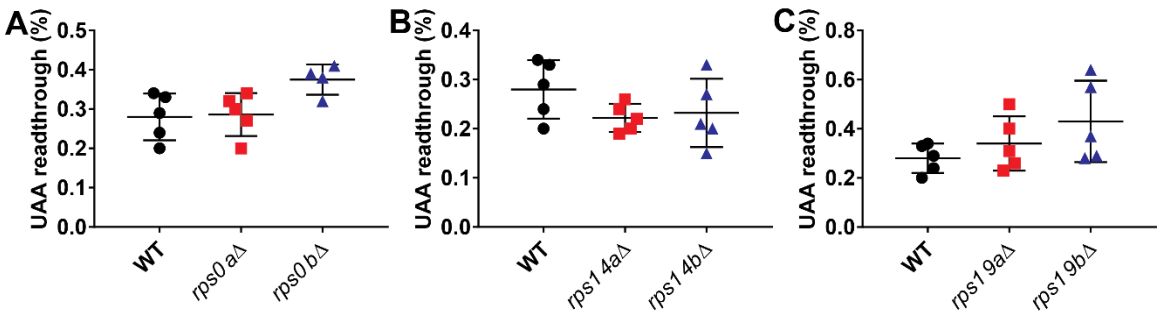

Figure 14. UAA stop codon readthrough in yeast models of haploinsufficiency

Rates of UAA stop codon readthrough in **(A)** *rps0Δ*, **(B)** *rps14Δ*, and **(C)** *rps19Δ* strains. Each point represents an experimental replicate performed in triplicate. A minimum of four biological replicates were assayed in triplicate for each combination of yeast strain and plasmid. One-way ANOVA did not find any statistically significant differences.

Ohnolog-specific effects on UAG stop codon readthrough were observed upon deletion of single ohnologs. In two cases UAG stop codon readthrough was enhanced (*rps0bΔ,* and *rps14aΔ*), and unchanged in all others (**Figure 15A-C)**. Again however, replacement of the deleted gene with a duplicated ohnolog corrected these translational fidelity defects (**Figure 15D-E**).

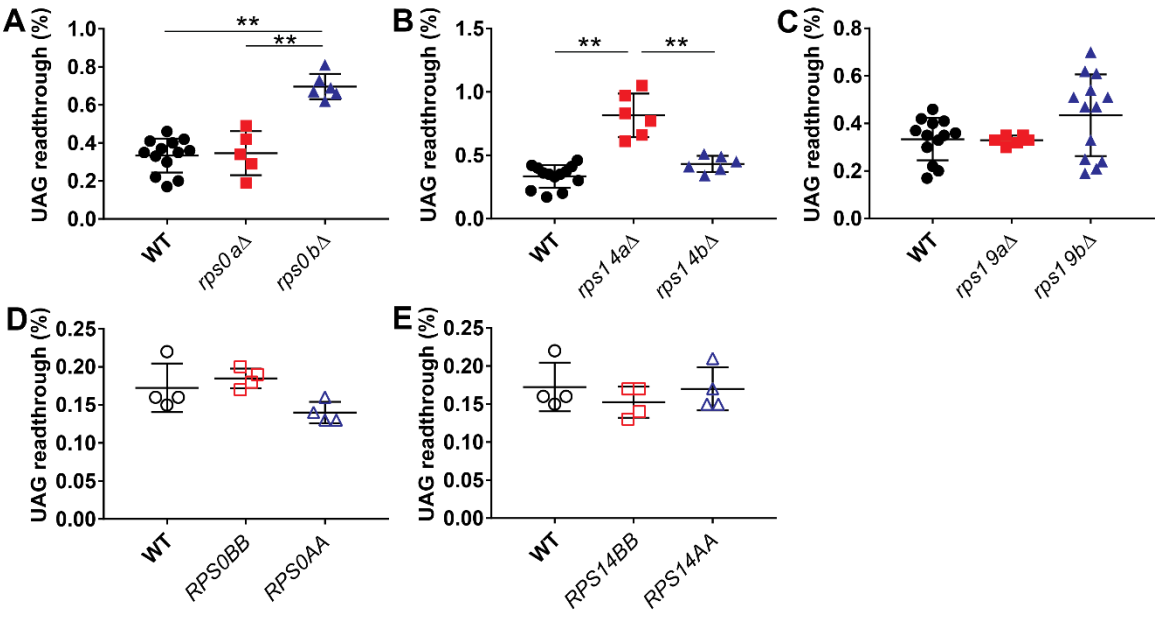

Figure 15. UAG stop codon readthrough in yeast models of haploinsufficiency

Rates of UAG stop codon readthrough in **(A)** *rps0Δ*, **(B)** *rps14Δ*, **(C)** *rps19Δ*, **(D)** *RPS0* duplication, and **(E)** *RPS14* duplication strains. Each point represents an experimental replicate performed in triplicate. A minimum of four biological replicates were assayed in triplicate for each combination of yeast strain and plasmid. One-way ANOVA was used to determine significance: ** $p<0.01$.

Ohnolog-specific effects on UGA stop codon readthrough were also observed upon deletion of single ohnologs. In two cases UGA stop codon readthrough was enhanced (*rps0bΔ,* and *rps14aΔ*), and unchanged in all others (**Figure 16A-C)**. However, replacement of the deleted gene with a duplicated ohnolog corrected these translational fidelity defects (**Figure 16D-E**).

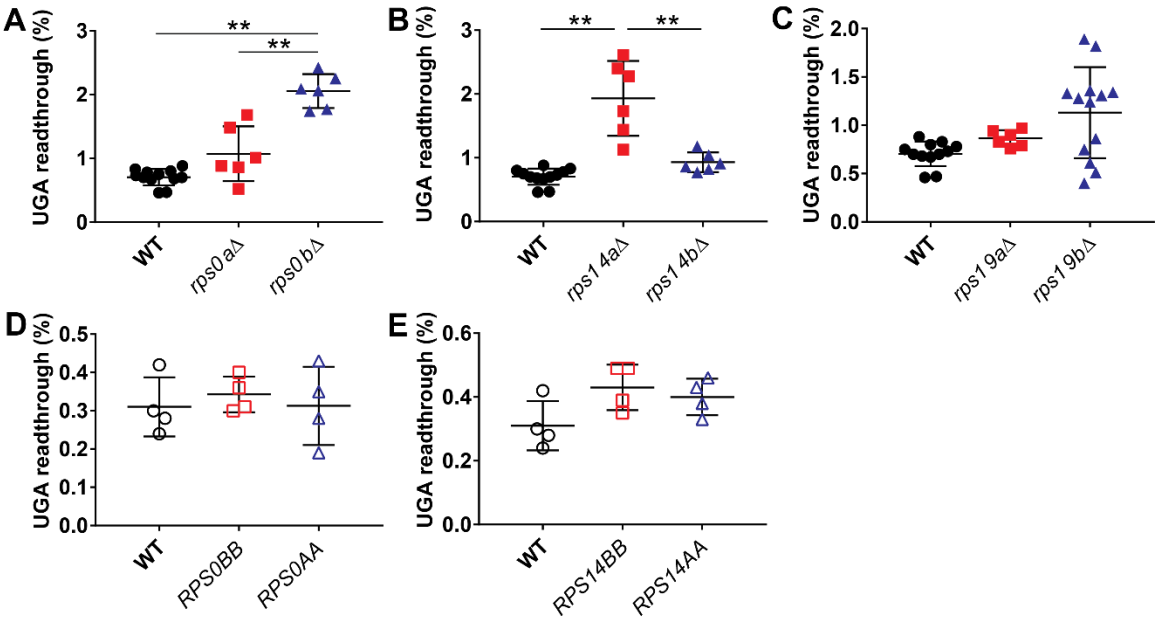

Figure 16. UGA stop codon readthrough in yeast models of haploinsufficiency

Rates of UGA stop codon readthrough in **(A)** *rps0Δ*, **(B)** *rps14Δ*, **(C)** *rps19Δ*, **(D)** *RPS0* duplication, and **(E)** *RPS14* duplication strains. Each point represents an experimental replicate performed in triplicate. A minimum of four biological replicates were assayed in triplicate for each combination of yeast strain and plasmid. One-way ANOVA was used to determine significance: ** $p<0.01$.

Missense suppression was assayed with reporters in which arginine 218 in the catalytic site of firefly luciferase was mutated to serine, by either a near-cognate (AGA → AGC) or non-cognate (AGA → TCT) mutation, rendering it catalytically inactive[138]. Near-cognate missense suppression rate was higher in *rps0aΔ* cells than in WT cells (**Figure 17A**). This increase was minimal and not considered biologically significant. No change in near-cognate missense suppression was observed in any of the other five ohnolog deletion strains (**Figure 17**).

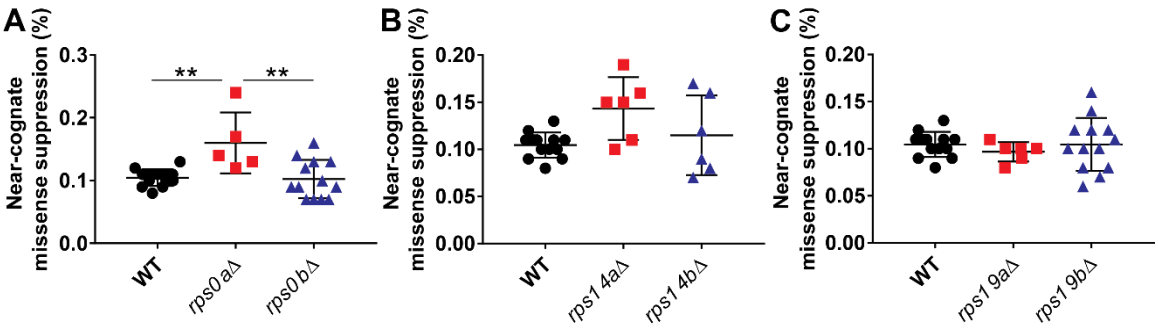

Figure 17. Near-cognate missense suppression in yeast models of haploinsufficiency

Rates of near-cognate missense suppression in **(A)** *rps0Δ*, **(B)** *rps14Δ*, and **(C)** *rps19Δ* strains. Each point represents an experimental replicate performed in triplicate. A minimum of five biological replicates were assayed in triplicate for each combination of yeast strain and plasmid. One-way ANOVA was used to determine significance: ** p<0.01.

The rate of non-cognate missense suppression was decreased in two cases (*rps14bΔ*, and *rps19bΔ*), and remained unchanged in all others (**Figure 18**). The observed differences were too small to be considered biologically significant.

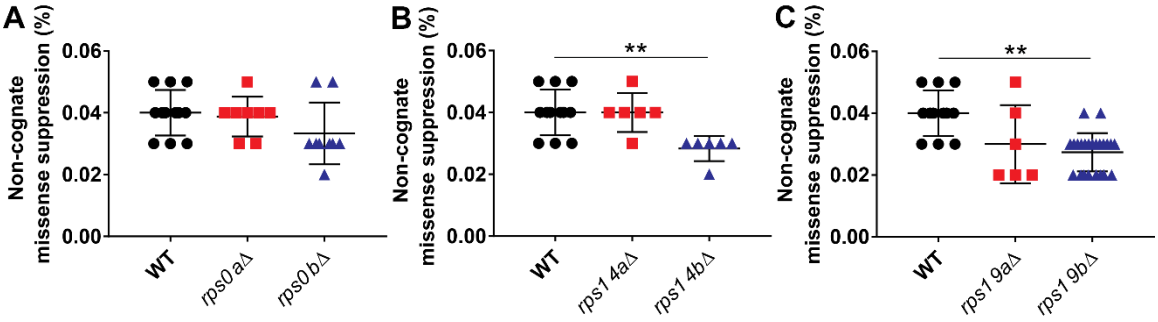

Figure 18. Non-cognate missense suppression in yeast models of haploinsufficiency

Rates of non-cognate missense suppression in **(A)** *rps0Δ*, **(B)** *rps14Δ*, and **(C)** *rps19Δ* strains. Each point represents an experimental replicate performed in triplicate. A minimum of six biological replicates were assayed in triplicate for each combination of yeast strain and plasmid. One-way ANOVA was used to determine significance: ** p<0.01.

DBA patient-derived lymphoblast cell lines (LCLs) display decreased UAG stop codon readthrough

Lymphoblast cell lines derived from two DBA patients harboring novel mutations in the *RPL9* gene were also used in this study: RPL9 L20P (C.I.), and RPL9 c.-2+1. These deidentified cell lines were obtained from Dr. Alyson MacInnes at the euroDBA consortium, who also provided us with three deidentified healthy control cell lines: F.T., NhnF, and NhnM. The cells (1.5 x 10^6 cells/transfection) were transfected with 1.5 µg of dual luciferase reporter plasmid by electroporation. The frameshift signal in PEG10 was used to monitor rates of -1 PRF[141,142], and that in OAZ1 was used to monitor rates of +1 PRF[109]. No changes in -1 PRF or +1 PRF were observed in either of the patients (**Figure 19**).

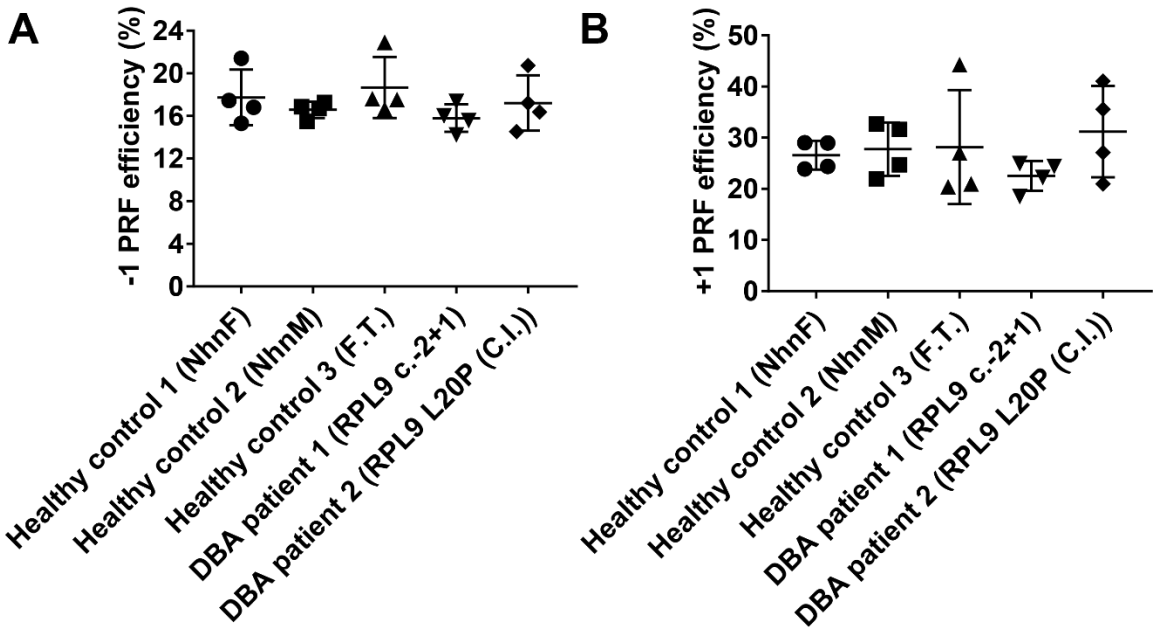

Figure 19. Rates of -1 and +1 PRF in DBA patient-derived LCLs
Rates of **(A)** -1 PRF promoted by PEG10, and **(B)** +1 PRF promoted by OAZ1 were measured in DBA patient-derived LCLs and healthy control cell lines. Each point represents an experimental replicate performed in triplicate. Four biological replicates were assayed in triplicate.

Fibroblasts from patients of another ribosomopathy, MacInnes Syndrome, showed differences in UAA stop codon readthrough[68]. Compared to healthy controls, DBA patient 1 carrying RPL9 c.-2+1 mutation displayed a decrease in UAG stop codon readthrough, while rates of UAA and UGA stop codon readthrough remained unchanged (**Figure 20**). Patient-derived cells tend to have lower *Renilla* and firefly luciferases activities than established commercial cell lines[68]. The firefly luciferase reads were at times below the lower threshold of linear range described in Promega's dual luciferase kit manual. However, stop codon readthrough levels in healthy controls are consistent with what was seen previously[68].

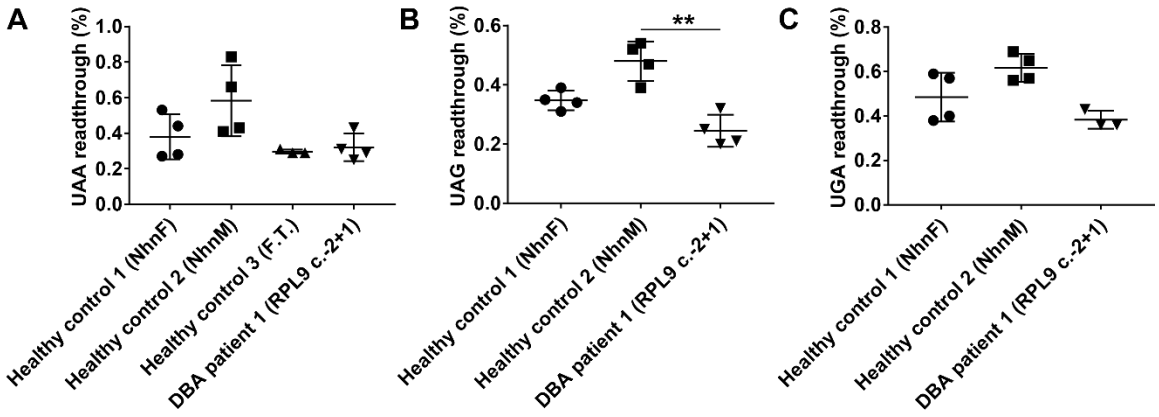

Figure 20. Rates of stop codon readthrough in DBA patient-derived LCLs
Rates of **(A)** UAA, **(B)** UAG, and **(C)** UGA stop codon readthrough were measured in DBA patient-derived LCLs and healthy control cell lines. Each point represents an experimental replicate performed in triplicate. Four biological replicates were assayed in triplicate. One-way ANOVA was used to determine significance: ** $p<0.01$.

X-DC yeast model cells show specific growth-related phenotype

Data from the yeast models of haploinsufficiency revealed translational fidelity defects, in a manner indicative of a gene dosage effect. This engendered the hypothesis that these cells may be stressed because defective ribosomes may be causing high levels of mistranslated, and perhaps misfolded proteins. We hypothesize that the same is the case in the X-DC cells, where translational fidelity defects have been shown in the yeast model (increase -1 PRF and stop codon recognition[154]).

The yeast model of X-DC, *cbf5-D95A*, has been qualitatively characterized as slow growing[66]. In order to quantify this phenotype, cell growth was monitored in 12-well plates, with 500 µl of YPAD media, and allowed to grow for 47 hours in a Synergy HT multi-well reader. These data were used to generate growth curves for each strain (**Figure 21**). This analysis revealed a

longer lag phase in the *cbf5-D95A* mutant cells (9 hours *vs.* 4 hours). The wild-type cells reached log-phase at hour 5, and stationary phase at 18 hours. Once cells reached log-phase growth, cell doubling times were determined. Under these conditions (samples in 500 µl YPAD in a 12-well plate inside Synergy HT chamber, kept stationary at 30°C, with 1 minute of shaking every hour just before each measurement was taken), doubling times were determined to be 2 hours 41 minutes (± 18 minutes) for the WT cells, and 4 hours 38 min (± 35 minutes) for the *cbf5-D95A* cells. Notably, the *cbf5-D95A* mutants remained alive in stationary phase for over 10 hours, while the wild-type cells began dying soon after diauxic shift.

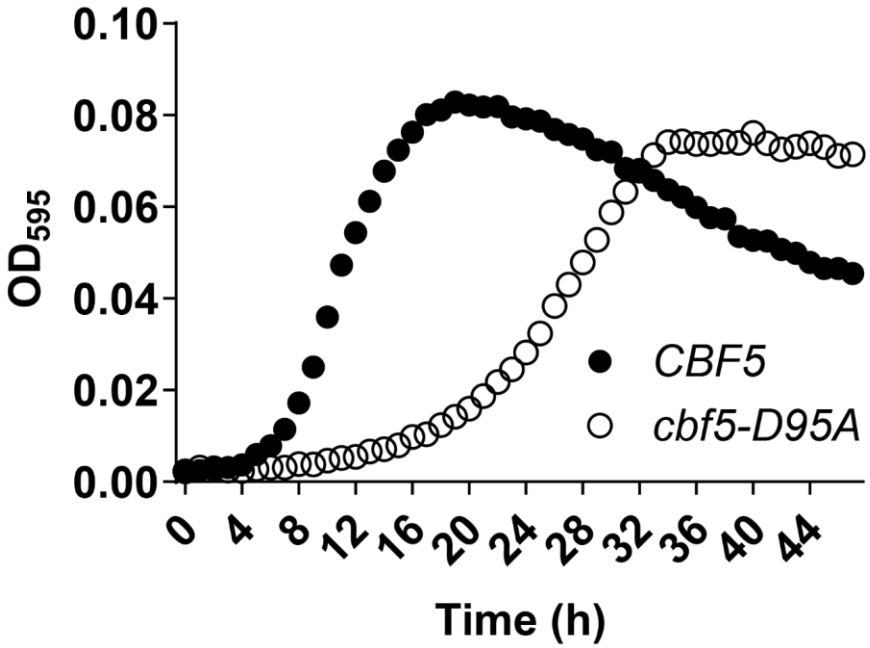

Figure 21. Growth curves for *CBF5* and *cbf5-D95A*

Samples were grown in 500 µl of YPAD media in 12-well plates in a Synergy HT plate reader. Chamber was kept at 30°C. Plate was stationary, with 1 minute of shaking prior to each OD_{595} measurement taken every hour. N = 10 biological replicates assayed in 4 independent experiments. OD_{595} measurements shown are background subtracted, and an average of each of the 10 biological replicates. Doubling times for each individual growth curve were calculated and averaged: WT: 2 h 41 min ± 18 min, *cbf5-D95A*: 4 h 38 min ± 35 min.

Cellular stress response is elevated in cbf5-D95A cells

While the *cbf5-D95A* allele is known to confer translational fidelity defects, the effects of reduced rRNA pseudouridylation on global gene expression remain uncharacterized. An RNA-Seq analysis was carried out on isogenic wild-type *CBF5* and *cbf5-D95A* yeast strains to address this. There were two goals for data analyses: 1) determine genes and pathways that are differentially expressed in *cbf5-D95A* cells, and 2) identify messages containing functional -1 PRF signals.

RNA was isolated from four biological replicates of each strain, and library preparation and Illumina sequencing was performed by the University of Maryland Next Generation Sequencing Core / IBBR DNA Sequencing Facility. RNA-Seq data were analyzed with the help of Dr. Ashton Trey Belew. The total number of reads generated from all libraries is displayed in Appendix 5 (**Figure 34**). Mapped sequencing data derived from all libraries were analyzed using a variety of methods, including principal component analysis (PCA) and hierarchical clustering to inspect the relationships between samples. The resulting PCA plot and heat maps (**Figure 35**) showed the expected clustering between biological replicates, and no outliers were identified. Following normalization, PCA plot analyses revealed that samples clustered by condition and that there was less variation in the *cbf5-D95A* samples (**Figure 22**).

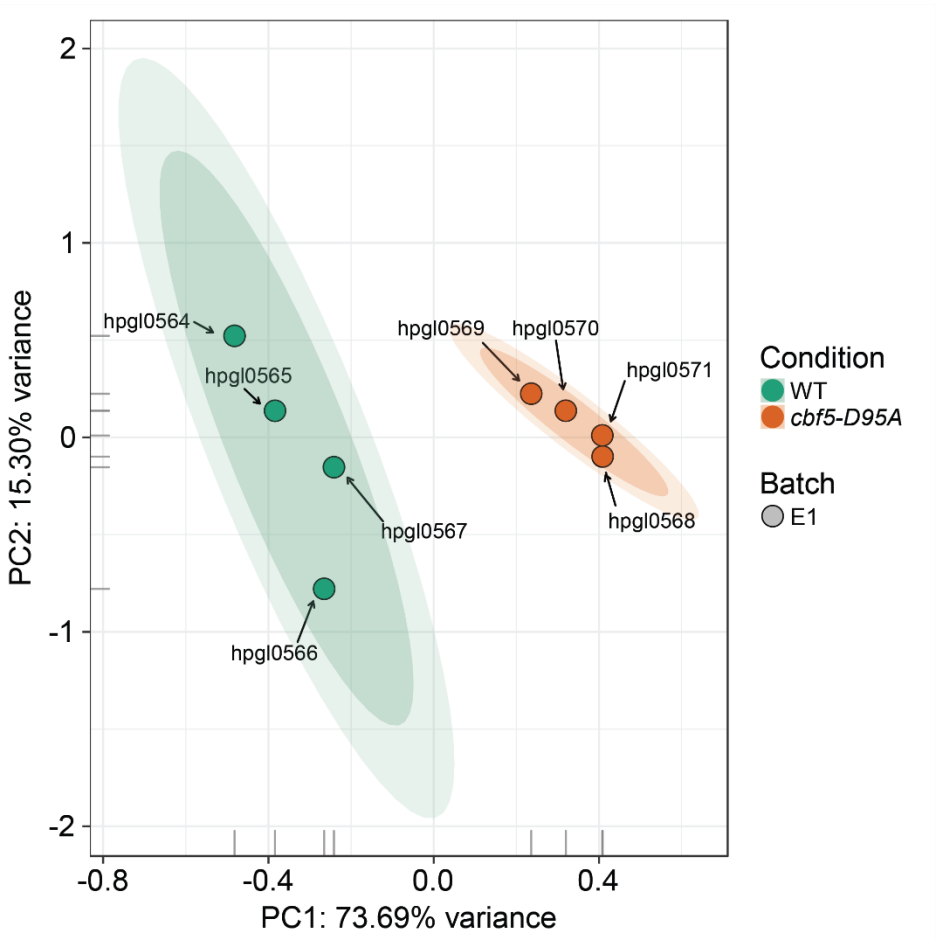

Figure 22. Principal component analyses plot of RNA-Seq data shows data clustering by condition

Principal Component Analyses (PCA) plot of RNA-Seq data generated from the libraries mapped to the *S. cerevisiae* genome following removal of rRNA/tRNA features. The data was $\log_2$(quantile(cpm(filter))) normalized and strong clustering by condition is evident in the plot. Each sample is color coded by condition/strain.

After application of a low count filter described in chapter 2 (1,280 genes removed, and 5,845 remaining), differential expression analyses were carried out. Adjusted *P* value < 0.05, and linear fold change ≥ 2, as determined by DEseq2, were selected as cut-off parameters to determine which messages were differentially expressed (DE). There were 241 upregulated messages,

and 478 downregulated messages in the *cbf5-D95A* cells. A table listing all messages and their differential expression can be found in Dataset E1_de_20180606.xlsx in the online repository.

A gene ontology (GO) enrichment analysis of differentially expressed (DE) genes in *cbf5-D95A* compared to isogenic wild-type cells was performed with gProfile:R. Summary tables containing the top 20 GO categories [biological processes (BP) and molecular functions (MF) only] enriched in *cbf5-D95A vs.* WT contrast, ranked by adjusted *P* value, are shown (**Table 2 and 3**). Tables listing all of the BP, MF, cellular components (CC), and KEGG pathways found to be enriched are available in Datasets E1_gprofiler_up_20180606.xlsx and E1_gprofiler_down_20180606.xlsx in the online repository. GO enrichment analyses revealed upregulation of 1) nucleotide metabolism (GO:0072524, GO:0046496, and GO:0019362), 2) oxidation-reduction [GO:0006733, GO:0055114, GO:0016491, GO:0006979 (response to oxidative stress, 12 of 122 are DE, adjusted *P* value = 1.63E-04), and GO:0034599 (cellular response to oxidative stress, 10 of 113 are DE, adjusted *P* value = 5.07E-03)], and 3) protein refolding (GO:0042026, GO:0051082 [unfolded protein binding, 9 of 83 are DE, adjusted *P* value = 7.03E-04), GO:0006457 (protein folding, 11 of 110 are DE, adjusted *P* value = 2.12E-02)] in the *cbf5-D95A* cells. Of note, (although not visible in **Table 2**), trehalose metabolism (GO:0070413, and GO:0005991) was also upregulated in *cbf5-D95A* cells.

Table 2. Top 20 gene ontology (GO) categories (biological processes, BP and metabolic function, MF) upregulated in *cbf5-D95A vs.* WT

	GO term	Adjusted *P* value	Number DE	Total number
GO:0072524	pyridine-containing compound metabolic process (BP)	2.48E-10	19	96
GO:0046496	nicotinamide nucleotide metabolic process (BP)	2.74E-09	17	83
GO:0019362	pyridine nucleotide metabolic process (BP)	3.37E-09	17	84
GO:0006733	oxidoreduction coenzyme metabolic process (BP)	3.72E-09	20	98
GO:0006732	coenzyme metabolic process (BP)	1.04E-08	26	182
GO:0016829	lyase activity (MF)	1.84E-08	19	107
GO:0051186	cofactor metabolic process (BP)	3.7E-08	28	223
GO:0055114	oxidation-reduction process (BP)	1.53E-07	43	451
GO:0032787	monocarboxylic acid metabolic process (BP)	9.34E-07	21	180
GO:0044281	small molecule metabolic process (BP)	9.93E-07	54	799
GO:0003824	catalytic activity (MF)	2.49E-06	116	2202
GO:0016491	oxidoreductase activity (MF)	5.05E-06	33	332
GO:0051156	glucose 6-phosphate metabolic process (BP)	6.35E-06	8	23
GO:0005975	carbohydrate metabolic process (BP)	6.37E-06	25	291
GO:0019752	carboxylic acid metabolic process (BP)	1.29E-05	33	426
GO:0006090	pyruvate metabolic process (BP)	1.70E-05	11	52

	GO term	Adjusted *P* value	Number DE	Total number
GO:0016054	organic acid catabolic process (BP)	2.36E-05	15	90
GO:0046395	carboxylic acid catabolic process (BP)	2.36E-05	15	90
GO:0043436	oxoacid metabolic process (BP)	3.20E-05	33	442
GO:0006082	organic acid metabolic process (BP)	3.39E-05	33	443
GO:0042026	protein refolding (BP)	3.51E-05	6	17

Cutoff for DE genes: fold change ≥ 2, adjusted *P* value cutoff of <0.05, by DEseq2. Number of DE genes and total number of genes in each of the top 20 GO terms are shown.

GO enrichment analyses revealed downregulation of amino acid biosynthesis (most GO terms listed in **Table 3**), and endoplasmic reticulum (ER) to Golgi vesicle-mediated transport (GO:0006888) in *cbf5-D95A* cells.

Table 3. Top 20 GO categories (BP and MF) downregulated in *cbf5-D95A vs.* WT

	GO term	Adjusted *P* value	Number DE	Total number
GO:0008652	cellular amino acid biosynthetic process (BP)	1.78E-06	30	133
GO:1901607	alpha-amino acid biosynthetic process (BP)	7.49E-06	28	125
GO:0000096	sulfur amino acid metabolic process (BP)	2.60E-05	16	49
GO:0016053	organic acid biosynthetic process (BP)	3.42E-05	35	193
GO:0046394	carboxylic acid biosynthetic process (BP)	3.42E-05	35	193

	GO term	Adjusted *P* value	Number DE	Total number
GO:1901605	alpha-amino acid metabolic process (BP)	1.70E-04	33	187
GO:0006555	methionine metabolic process (BP)	2.88E-04	14	44
GO:0006526	arginine biosynthetic process (BP)	2.99E-04	8	13
GO:0009086	methionine biosynthetic process (BP)	4.21E-04	13	39
GO:0006520	cellular amino acid metabolic process (BP)	5.10E-04	39	253
GO:0006888	ER to Golgi vesicle-mediated transport (BP)	5.14E-04	20	95
GO:0000097	sulfur amino acid biosynthetic process (BP)	5.89E-04	13	40
GO:0009070	serine family amino acid biosynthetic process (BP)	3.22E-03	10	27
GO:0009067	aspartate family amino acid biosynthetic process (BP)	5.73E-03	14	55
GO:0044283	small molecule biosynthetic process (BP)	5.87E-03	44	331
GO:0006525	arginine metabolic process (BP)	7.63E-03	8	18
GO:0009069	serine family amino acid metabolic process (BP)	2.08E-02	11	39
GO:0009066	aspartate family amino acid metabolic process (BP)	3.62E-02	15	72
GO:0031386	protein tag (MF)	4.66E-02	5	11
GO:0006534	cysteine metabolic process (BP)	4.74E-02	7	17

Cutoff for DE genes: fold change ≥ 2, adjusted *P* value cutoff of <0.05, by DEseq2. Number of DE genes and total number of genes in each of the top 20 GO terms are shown.

Thirty messages predicted to contain -1 PRF signals[101] were downregulated in the *cbf5-D95A* cells. Of these, only 9 of the predicted slippery sites were followed by computationally predicted strong pseudoknots. We hypothesize that messages with functional -1 PRF signals would be more normally targeted for NMD in wild-type cells, and thus further destabilized in the *cbf5-D95A* mutation (recall increased rates of -1 PRF and increased recognition of stop codons in *cbf5-D95A* cells[154]), and would be below detectable threshold.

UPF1, which encodes one of the key components of the NMD pathway[159], was deleted in the isogenic *cbf5-D95A* and WT strains in an effort to identify more messages with predicted -1 PRF signals that may be functional. It was anticipated that this would raise the abundance of the messages targeted for degradation through the NMD pathway increasing their levels above the threshold of detection. (The resulting strains, *CBF5 upf1Δ* and *cbf5-D95A upf1Δ*, will also be called *upf1Δ* and double mutant, respectively). A second RNA-Seq experiment was set up with two batches each with 2 biological replicates of the four strains: WT, *cbf5-D95A*, *upf1Δ*, and *cbf5-D95A upf1Δ*. RNA was isolated and libraries were prepared, sequenced and analyzed as described above. The total number of reads generated from all libraries is listed in Appendix 5 (**Figure 34**).

Mapped sequencing data derived from all libraries (first and second experiment) were analyzed using a variety of methods, including PCA and hierarchical clustering to inspect the relationships between samples and to identify potential outliers. The resulting PCA plot and heat maps (**Figure 23**) showed that samples cluster by batch, and that there is a nested effect visible within Experiment 2, Batch 1 (E2B1). Different patterns in gene expression were also visible in batch E2B1 when examining all samples in Integrative Genomics Viewer (IGV, representative images are shown in Appendix 5, **Figures 36 and 37**). Different surrogate variable analyses did not correct this, and batch E2B1 was considered an outlier and excluded from further analyses. The removed batch contained samples hpgl0774 through hpgl0781, resulting in a total of 6 samples of *CBF5 UPF1* (hpgl0564 through hpgl0567, hpgl0782, and hpgl0786), 6 samples of *cbf5-D95A UPF1* (hpgl0568 through hpgl0571, hpgl0783, and hpgl0787), 2 samples of *CBF5 upf1Δ* (hpgl0784, and hpgl0788), and 2 samples of *cbf5-D95A upf1Δ* (hpgl0785, and hpgl0789) for analyses. Following normalization and surrogate variable analysis, the hierarchical clustering (**Figure 24A**) and PCA plot of the remaining samples (**Figure 24B**) revealed that samples cluster by condition (i.e. genotype).

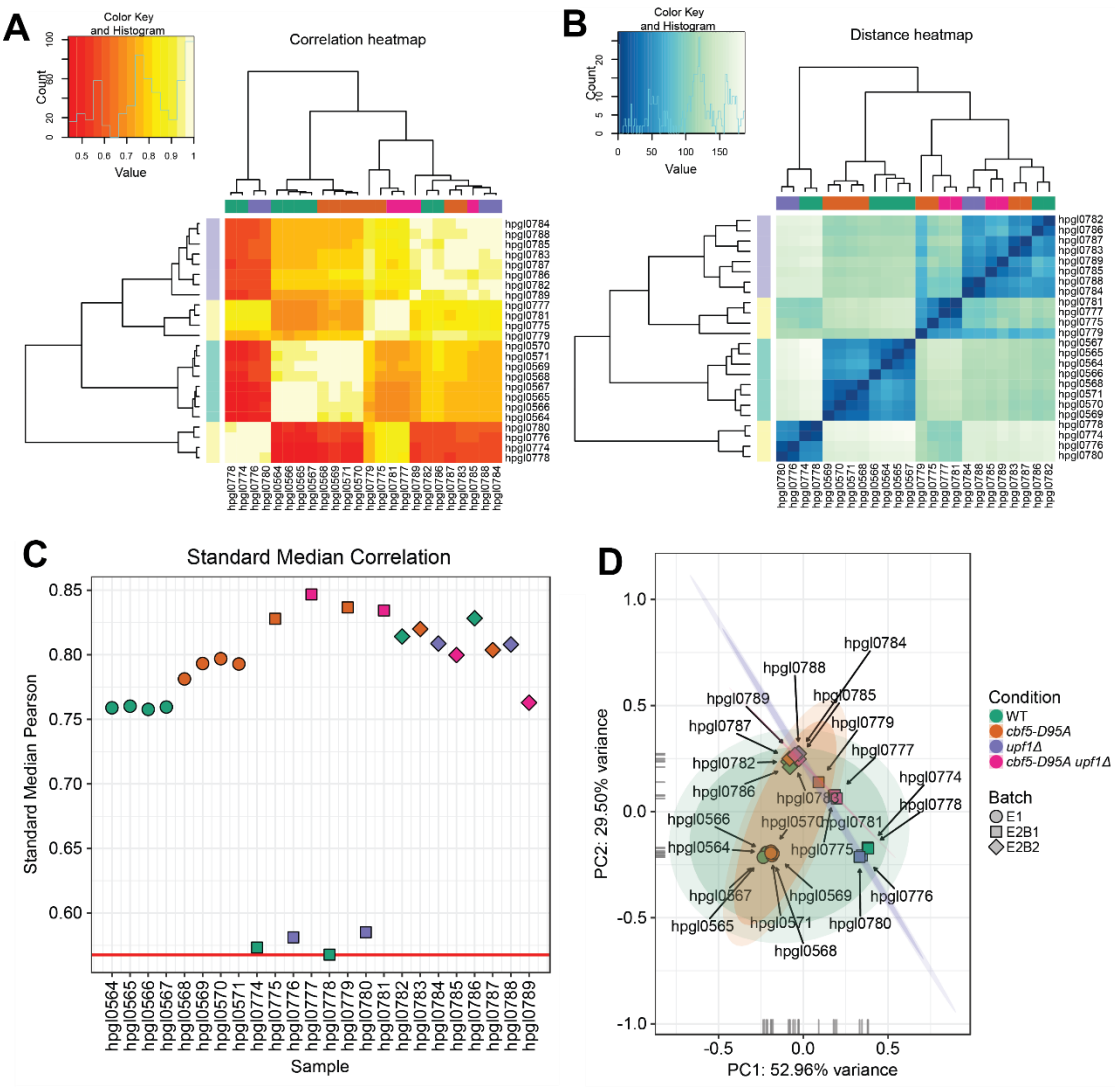

Figure 23. Quality control metrics suggesting the removal of batch E2B1

Hierarchical clustering analyses using **(A)** Pearson correlation and **(B)** Euclidean distances along with a **(C)** standard medium Pearson correlation between each sample and **(D)** Principal Component Analyses of the $\log_2$, cpm, quantile, and low-count filtered data (6,095 of 7,125 genes remained after applying low-count filter) suggested the removal of batch E2B1.

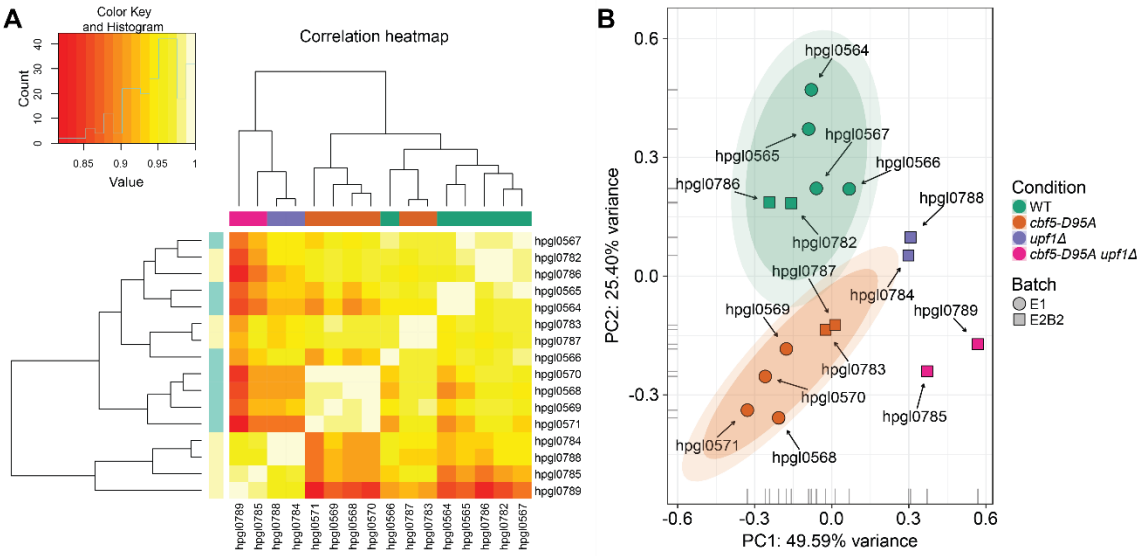

Figure 24. Global statistical assessment of biological replicates

(A) Heat-map and **(B)** PCA plots of RNA-Seq data generated from the libraries mapped to the *S. cerevisiae* genome following removal of rRNA/tRNA features. Once the outlier batch was removed and data passed through normalization and surrogate variable analysis, the clustering by condition became evident in both analyses. In both plots, each sample is color coded by condition.

The numbers of genes that emerged as differentially expressed (DE) with adjusted *P* value < 0.05, in pairwise contrasts of each genotype are shown in **Figure 25** (see Dataset E1E2_de_20180212.xlsx in online repository for the complete list). Full sets of enriched GO categories generated from analysis of DE genes in each pairwise contrast are available in Datasets E1E2_gprofiler_up_20180212.xlsx and E1E2_gprofiler_down_20180212.xlsx in the online repository. A summary table with the top 20 GO categories in *cbf5-D95A vs.* WT is below (**Table 4**), and revealed increased nucleotide metabolism (GO:0072524, GO:0019362, and GO:0046496),and response to oxidative stress (GO:0055114, GO:0006733, GO:0016491, GO:0016614), replicating the findings in the first set of samples (i.e. E1). A single GO category,

acid phosphatase activity (GO:0003993), was found to be downregulated in *cbf5-D95A* cells when all the RNA-Seq data was combined.

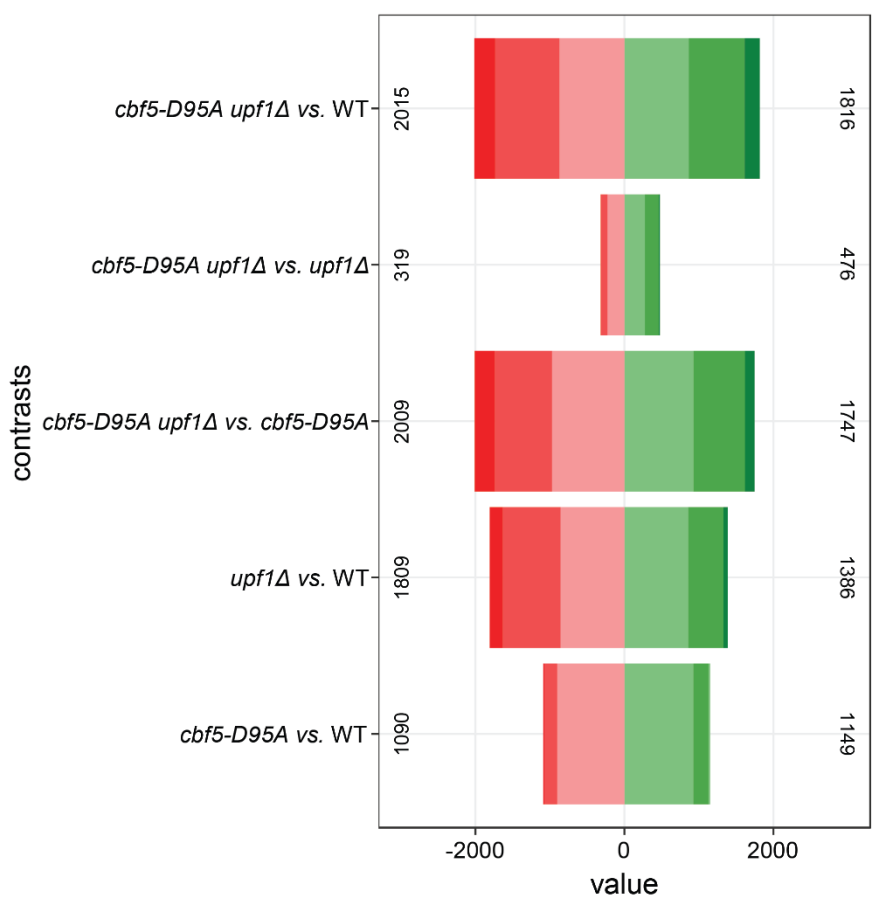

Figure 25. Differentially expressed genes with adjusted *P* value <0.05 in all pairwise contrasts

Red represents downregulated massages, and green represents upregulated messages. The lightest color represents genes for which the linear fold change ≤ 2, middle color is for messages that have 2 < linear fold change ≤ 4, and the darkest color represents messages with linear fold change > 4.

Table 4. Top 20 GO categories (BP and MF) enriched for *cbf5-D95A vs.* WT for combined data

	GO term	Adjusted *P* value	Number DE	Total number
***cbf5-D95A vs.* WT, up-regulated**				
GO:0072524	pyridine-containing compound metabolic process (BP)	1.24E-09	20	93
GO:0055114	oxidation-reduction process (BP)	1.44E-09	41	460
GO:0044282	small molecule catabolic process (BP)	3.18E-09	21	122
GO:0044712	single-organism catabolic process (BP)	5.60E-09	33	324
GO:0019362	pyridine nucleotide metabolic process (BP)	1.24E-08	18	82
GO:0046496	nicotinamide nucleotide metabolic process (BP)	1.24E-08	18	82
GO:0016829	lyase activity (MF)	2.30E-08	13	111
GO:0005975	carbohydrate metabolic process (BP)	1.62E-07	28	292
GO:0006733	oxidoreduction coenzyme metabolic process (BP)	2.03E-07	18	96
GO:0006089	lactate metabolic process (BP)	7.43E-07	4	11
GO:0032787	monocarboxylic acid metabolic process (BP)	9.14E-07	23	186
GO:0016836	hydro-lyase activity (MF)	2.07E-06	6	35
GO:0016491	oxidoreductase activity (MF)	2.90E-06	30	338
GO:0019172	glyoxalase III activity (MF)	6.35E-06	3	4
GO:0016835	carbon-oxygen lyase activity (MF)	1.02E-05	6	45
GO:0015291	secondary active transmembrane transporter activity (MF)	3.78E-05	16	107

	GO term	Adjusted *P* value	Number DE	Total number
GO:0015603	iron chelate transmembrane transporter activity (MF)	1.17E-04	5	6
GO:0042927	siderophore transporter activity (MF)	1.17E-04	5	6
GO:0015343	siderophore transmembrane transporter activity (MF)	1.17E-04	5	6
GO:0016614	oxidoreductase activity, acting on CH-OH group of donors (MF)	1.47E-04	13	83
***cbf5-D95A vs.* WT, down-regulated**				
GO:0003993	acid phosphatase activity (MF)	4.64E-02	4	9

Cutoff for DE genes: fold change ≥ 2, adjusted *P* value cutoff of <0.05, by DEseq2. Number of DE genes and total number of genes in each of the top 20 GO terms are shown.

Summary tables of GO enrichment analyses for the other contrasts are listed in Appendix 5 (**Tables 14-17**). The *upf1Δ vs.* WT contrast revealed upregulation of 1) cell cycle, 2) cell fate, 3) cellular transport and transport mechanisms, 4) control of cellular organization, and 5) energy generation (**Table 14** in Appendix 5). Downregulated GO categories for this contrast fall under the broad category of protein translation (**Table 14** in Appendix 5).

Analysis of *cbf5-D95A upf1Δ vs. cbf5-D95A* revealed upregulation of cell cycle and cellular transport categories, and downregulation of protein synthesis (**Table 15** in Appendix 5). Analysis of *cbf5-D95A upf1Δ vs. upf1Δ* revealed upregulation of oxidative stress response and cellular transport, and

downregulation of cell cycle and control of cellular organization (**Table 16** in Appendix 5).

Analysis of *cbf5-D95A upf1Δ vs.* WT revealed upregulation of cellular transport and control of cellular organization, and downregulation of protein synthesis and transcription (**Table 17** in Appendix 5).

In the dataset containing E1 and E2B2, there were only 3 predicted -1 PRF signal containing messages (CIT2, ADY3, and YOR365C) that were downregulated in the *cbf5-D95A vs.* WT cells. Of these only CIT2 has a strong predicted pseudoknot structure following the slippery site. None of the three messages were upregulated in *upf1Δ vs.* WT. Only YOR365C was upregulated in the double mutant *vs. cbf5-D95A*. However, YOR365C is described as a putative protein of unknown function in SGD. For these reasons, the identification and validation of functional -1 PRF signals was not pursued further.

cbf5-D95A cells have lower levels of ROS in post-diauxic phase

The RNA-Seq data indicated that the expression of genes involved in cellular response to oxidative stress is upregulated in *cbf5-D95A vs.* WT cells (**Table 2 and 4**)**.** Hydrogen peroxide (H_2O_2) exists in equilibrium inside and outside of the cell[143,144,160], and thus the amount of H_2O_2 outside of the cell can be measured as a proxy for the amount inside the cells[143,144,160]. H_2O_2 levels outside the cells were measured using an Amplex® Red Hydrogen Peroxide/Peroxidase assay kit (Invitrogen). Amplex® Red reacts with H_2O_2

outside of the cell to produce a fluorescent compound, resorufin, in the presence of horseradish peroxidase[161–164]. Using this kit, a trial experiment was carried out using WT cells at mid-log growth and a standard curve (varying concentrations of 0 to 5 µM H_2O_2). It was determined that the background (502 AU) was much lower than the other reads (highest fluorescence = 26,442 AU for 5 µM H_2O_2). However, it did not appear that the WT cells were secreting H_2O_2 at this growth phase, as the reads were very close to background (data not shown).

In order to obtain higher reads and compare the levels of H_2O_2 being secreted by WT and *cbf5-D95A* cells, the Amplex® Red kit was used when the cells reached the post-diauxic stage[143]. Cells were grown in the Synergy HT under the same conditions used for the growth curve experiments. Wild-type cells were collected at 22 hours, and *cbf5-D95A* cells at 42 hours. Different numbers of cells (2×10^7, 4×10^7, and 8×10^7) were resuspended in 1X reaction buffer and allowed to grow for 1 hour for the H_2O_2 levels to equilibrate. After loading the samples with Amplex® Red, cells were incubated in the dark for 30 minutes. Fluorescence was measured on a Promega GloMax Multi + Detection System using the green filter (absorbance: 525 nm and emission: 580-640 nm). Standard curves with varying concentrations of H_2O_2 (between 0 to 5 µM H_2O_2) were determined for each experiment. H_2O_2 concentrations were calculated using the standard curve from the same experiment. No statistically significance difference in concentration of H_2O_2 was found between the two strains when 2×10^7 and 4×10^7 cells were used. However, at 8×10^7 cells,

concentration of H_2O_2 in *cbf5-D95A* cells was about half of that in the WT cells (**Figure 26**).

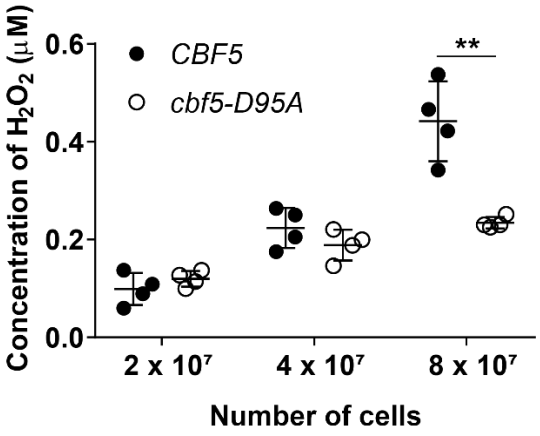

Figure 26. *cbf5-D95A* cells have lower reactive oxygen species levels at stationary phase

Samples were grown in 500 µl of YPAD media in 12-well plates in a Synergy HT plate reader. Chamber was kept at 30°C. Plate was stationary, with 1 minute of shaking prior to each OD_{595} measurement taken every hour. Wild-type cells were collected at 22 hours, and *cbf5-D95A* cells at 42 hours. Cells (2 x 10^7, 4 x 10^7, and 8 x 10^7) were resuspended in 1X reaction buffer, and allowed to grow for 1 hour shaking at 30°C. Samples were loaded with Amplex® Red and incubated for 30 minutes in the dark. Samples were assayed on a Promega GloMax Multi + Detection System using the blue filter (absorbance: 490 nm and emission: 510-570 nm). *N* = 4 biological replicates in independent experiments. Each dot represents a biological replicate. Mean and standard deviation are also shown. Statistical significance was calculated using a non-parametric one-way ANOVA. **, $p < 0.01$.

cbf5-D95A cells are pre-adapted to ER stress

Consistent with the finding of increased upregulation of genes involved in protein refolding (**Table 2**), and the downregulation of ER to Golgi transport (**Table 3**), defects in translational fidelity were predicted to increase the synthesis of defective proteins, and that accumulation of misfolded proteins in the ER should constitutively induce the unfolded protein response (UPR). High levels of UPR were predicted to render these cells more resistant (i.e. pre-

adapted) to other ER stressors. Tunicamycin, which prevents N-linked glycosylation of proteins in the ER, leads to the enhanced accumulation of misfolded proteins in the ER[165,166]. This leads to activation of IRE1 protein, which splices HAC1 mRNA. The spliced HAC1 message encodes a transcription factor that binds the unfolded protein response elements in the promoters of genes involved in UPR response. The sensitivity of cells to ER stress was assayed using tunicamycin in two different ways: 1) effects on yeast growth, and 2) effects on HAC1 mRNA splicing.

Yeast were grown in YPAD, back diluted and serial dilutions spotted on YPAD plates with or without 1 µg/ml tunicamycin. While the *cbf5-D95A* strain grew more slowly in YPAD media, these grew faster than the WT in media containing tunicamycin as compared to isogenic WT controls (**Figure 27**).

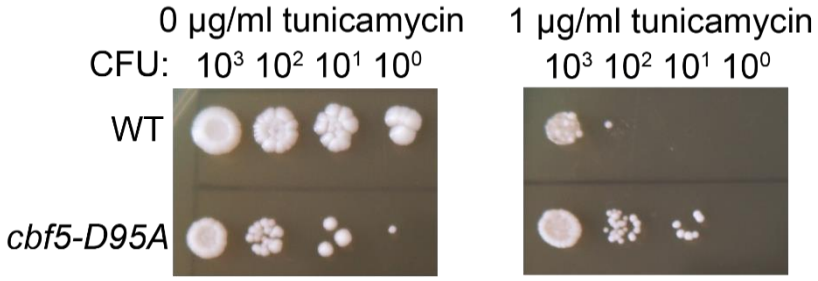

Figure 27. *cbf5-D95A* cells are less sensitive to ER stress than WT cells
Yeast was grown in YPAD liquid media, then backdiluted and spotted on YPAD plates with or without 1µg/ml tunicamycin. Three biological replicates were plated. Representative images shown.

The UPR is characterized by activation of Ire1p in yeast, through autophosphorylation in response to unfolded proteins[167–170]. The primary HAC1 transcript contains a 252 nucleotide intron ($HAC1^U$), which is spliced by Ire1p during UPR activation to produce the mature HAC1 mRNA ($HAC1^S$) [171]. $HAC1^S$

encodes a transcription factor which binds to the unfolded protein response element (UPRE) in the promoter of genes required for UPR response[171]. Although the HAC1 mRNA is always expressed in cells, Hac1p is only detected in UPR-activated cells; this could be due to 1) message not being translated, or 2) protein being degraded rapidly[171].The UPR response is similar in human cells, where the *HAC1* ortholog is *XBP1*[172,173].

To determine the effects of tunicamycin on HAC1 mRNA splicing, cells were treated with 1µg/ml tunicamycin for 1 hour, and RNA was extracted from 1 x 10^7 cells. cDNA was synthesized from 450 ng of RNA, and the HAC1 intron region was amplified. The basal level of expression of HAC1 mRNA was determined to be higher in the *cbf5-D95A* cells than in WT cells. Most of the HAC1 mRNA in WT cells treated with tunicamycin was spliced, while only about half was spliced in the *cbf5-D95A* cells (**Figure 28**).

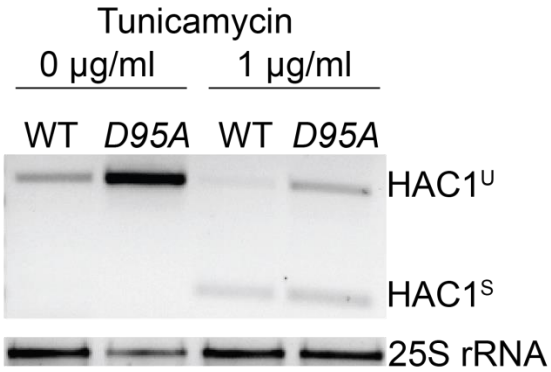

Figure 28. HAC1 mRNA splicing in *cbf5-D95A* cells as a result of ER stress
Yeast was grown in YPAD, back diluted and treated with 1µg/ml tunicamycin for 1 hour. RNA was isolated from 1 x 10^7 cells, and cDNA synthesized from 450 ng of RNA. Two µl of a 1:10 cDNA dilution were used as template for PCR reactions using primers to amplify the HAC1 intron region. PCR products were separated on a 1.5% agarose gel. A 111 bp product corresponds to spliced HAC1 mRNA ($HAC1^S$), and 363 bp product corresponds to unspliced HAC1 mRNA ($HAC1^U$). Five hundred ng of RNA were separated on a 1.5% agarose gel. Three biological replicates were treated and processed through the full protocol.

Yeast models of haploinsufficiency display varying sensitivities to ER stress

To determine if a similar pre-adaptation was present in pseudo-haploinsufficient yeast strains, the effects of tunicamycin on cell growth were determined in these cells. Control experiments were carried out with the isogenic ohnolog duplication strains.

Yeast cells were grown in liquid YPAD media, and after back dilution, serial dilutions were plated on YPAD plates with or without 1 µg/ml tunicamycin. *rps0bΔ* and *rps19bΔ* cells, which were slower-growing than WT cells on YPAD plates, grew faster than the WT strain in the presence of tunicamycin (**Figure 29A**, top and bottom panels). *rps14aΔ* cells, whose growth was similar to WT cells on YPAD plates, grew faster than the WT strain in the presence of

tunicamycin (**Figure 29A**, middle panel). *rps19aΔ* cells, whose growth was similar to WT on YPAD plates, grew slower than the WT strain in the presence of tunicamycin (**Figure 29A**, bottom panel). These data indicate that *rps0bΔ*, *rps14aΔ*, and *rps19bΔ* cells displayed decreased sensitivity to a second stressor. On the other hand, rps19a*Δ* cells displayed increased sensitivity to ER stressor. The experiment was repeated with the ohnolog duplication strains, as all changes in sensitivity to ER stress were rescued, and all strains grew at the same rate as the WT cells on the same plate (**Figure 29B**).

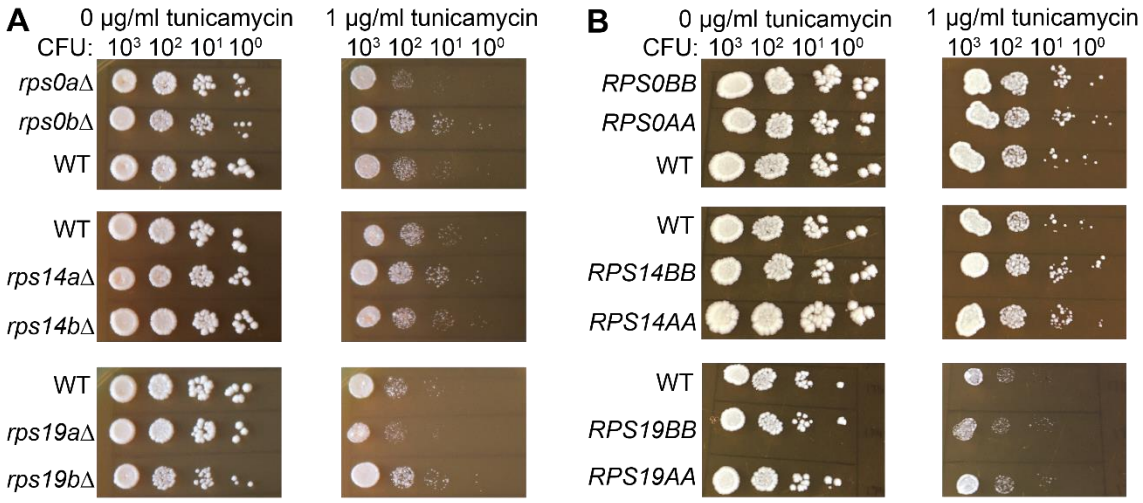

Figure 29. Sensitivity of yeast models of haploinsufficiency to ER stress
Dilution spot assays of yeast ohnolog deletion and duplication strains in YPAD plates with or without 1 µg/ml tunicamycin. Three biological replicates were plated. Representative images shown.

Discussion

Prior studies showed changes in translational fidelity in X-DC patients and yeast and mouse models[100,154]. In this work, the translational fidelity

profiles of DBA patient-derived cells (**Figure 19 and 20**) and yeast models of haploinsufficiency (**Figures 12-18**) were monitored to test the hypothesis that ribosomopathies are generally associated with translational fidelity defects. Interestingly, while gene-specific differences changes in translational fidelity were observed in many of the pseudo-haploinsufficient yeast strains, these were all rescued in the control ohnolog duplication strains (**Figures 12, 15, and 16**). These observations are consistent with a gene dosage, rather than a specialized ribosome model.

Quantitative analysis of the yeast X-DC model growth suggested that *cbf5-D95A* cells may be pre-adapted to stress (**Figure 21**). GO analyses of RNA-seq data revealed that *cbf5-D95A* cells have upregulated nucleotide biosynthesis, response to oxidative stress, protein refolding, and trehalose metabolism (**Tables 2 and 4**). The same cells displayed downregulated amino acid biosynthesis and ER to Golgi vesicle-mediated transport than WT cells (**Table 3**). We hypothesize that these changes may be due to the intrinsic instability of mutant ribosomes. Ribosome biosynthesis accounts for ~80% of the metabolic load in actively growing yeast cells[174]. Enhanced ribosome turnover would further increase the demands on cellular metabolism. This would necessitate increased energy consumption to produce the increased amounts of ATP and GTP required for ribosome biosynthesis, hydrolysis of which would result in increased reactive oxygen species (ROS), resulting in upregulation of response to oxidative stress. Increased rates of ribosome biosynthesis would also necessitate upregulation of nucleotide biosynthesis to

meet the demands for the synthesis of new rRNAs. In addition, decreased translational fidelity is predicted to increase the fraction of misfolded proteins, as reflected in the upregulation of protein refolding machinery, and trehalose is associated with upregulated stress response[175]. In contrast, the unfolded protein response is localized in the endoplasmic reticulum: increased levels of misfolded proteins is predicted to increase the flux of these proteins to the proteasome, and away from the Golgi. Furthermore, increased rates of proteosomal amino acid scavenging would be expected to provide negative feedback on the amino acid biosynthetic machinery. A future experiment will directly address the hypothesis that mutant ribosomes are unstable by measuring ribosome half-lives in isogenic wild-type and *cbf5-D95A* cells.

Follow-up studies determined that *cbf5-D95A* stationary phase cells have lower ROS levels than WT cells (**Figure 26**). This observation is consistent with the longer plateau of the *cbf5-D95A* cells upon reaching stationary phase (**Figure 21**). These results support the hypothesis that cells carrying this mutation may be pre-adapted to stress[143].

Assays monitoring a second type of stress, ER stress induced by tunicamycin, revealed that *cbf5-D95A* cells were less sensitive than WT cells, as shown by growth in plates containing tunicamycin (**Figure 27**). It was determined that *cbf5-D95A* cells have increased basal expression of HAC1 mRNA, and that after tunicamycin treatment these cells display approximately the same amount of spliced HAC1 mRNA as the WT cells, also supporting the pre-adaptation model (**Figure 28**).

Ohnolog-deletion specific effects were observed with regard to ER stress sensitivity monitored by growth in the presence of tunicamycin in the pseudo-haploinsufficient yeast models. This experiment was repeated with the control ohnolog duplication strains, and differences observed in ohnolog deletion strains were rescued (**Figure 29**). This supports the gene dosage model to explain ribosomopathies.

Taken as a whole, the data presented here points to the metabolic imbalance model[149] (and not specialized ribosomes[146]) as the explanation for the translational fidelity defects and differences in sensitivity to ER stress observed in the pseudo-haploinsufficient yeast strains. The caveats are that this can only be extended to yeast growing in rich media, and further studies are required to determine if this finding holds true in human cells. It appears that there is a pre-adaptation of *cbf5-D95A* cells to handle other stresses better as a result of the mutation they carry. A longer plateau upon reaching stationary phase in growth curve analysis, lower ROS levels, and decreased sensitivity to ER stress observed in *cbf5-D95A* cells all support this hypothesis.

Chapter 4: The clinical presentation of MacInnes Syndrome, a novel ribosomopathy due to mutations in ribosomal protein uS12, is partly due to translational fidelity defects

Introduction

A novel ribosomopathy involving uS12 was recently identified by our collaborator, Dr. Alyson MacInnes, at the euroDBA in the Netherlands. Two unrelated patients were identified with mutations in the *RPS23* gene, encoding uS12-R67K and uS12-F120I[68]. The patients symptoms include dysmorphic features such as short stature, microcephaly, flat back of the skull, simian palmar creases, epicanthic eye folds, long eyelashes, fetal finger pads, and hearing loss[68]. The patient carrying the uS12-R67K mutation was additionally diagnosed with intellectual disability and autism spectrum disorder[68]. While some of these symptoms are similar to those presented by X-DC and DBA patients, these two patients did not present with anemia or any other hematologic symptoms[68]. OMIM named this syndrome Brachycephaly, trichomegaly, and developmental delay (BTDD, OMIM #617412) or MacInnes Syndrome (MCINS)[176], after the publication of this project.

Ribosomal protein uS12 (encoded by *RPS23* gene) is part of the small ribosomal subunit and lies within the decoding center[68,177]. This protein is in contact with the minor groove of the D stem of aminoacyl-tRNAs, and helps

the ribosome discriminate among aminoacyl-tRNAs[177–180]. Residue R67 lies in the PNSA loop, and F120I lies in the PGVRY loop, both highly conserved[68,181–183]. Arginine 67 forms two polar contacts with guanosine 67 in 18S rRNA, which are predicted by PyMOL to be disrupted in the R67K mutant[68]. Phenylalanine 120, on the other hand, is predicted to interact with phenylalanine 41 in uS12 by pi-pi stacking, which would not be possible with the F120I mutation[68].

In humans, uS12 is post-translationally hydroxylated at proline-62 by OGFOD1, 2-oxoglutarate and iron dependent oxygenase domain containing protein 1[184]. This residue is located in a loop that protrudes into the decoding center and is conserved through yeast[184,185]. It was determined that >95% of uS12 proteins in the ribosomes are hydroxylated[184]. In yeast, there are 2 gene ohnologs (*RS23A* and *RS23B*), which encode the same protein, uS12[49]. Proline-64 is post-translationally dihydroxylated in yeast uS12[185]. In this case, hydroxylation reactions are catalyzed by Tpa1p, the yeast ortholog of OGFOD1[185]. Strains harboring mutations at P64 are not viable and those with mutations in nearby residues have growth defects[185]. The effect of uS12 hydroxylation on stop codon readthrough depends on the context/sequence, i.e. decreased accuracy for UAA stop codon and increased accuracy for UGA stop codon for cells in which *TPA1* had been deleted[185]. *uS12-K62R* cells displayed increased UAA stop codon readthrough[185]. In a separate study, the *uS12-K62R* cells were found to have increased paromomycin sensitivity and increased nonsense suppression, which the authors suggest may be due to decreased affinity of the ribosome for the release factor[182]. Independently, a

third study also found that yeast cells carrying uS12-K62R displayed increased translation error frequency, which they calculated by taking the ratio of incorporated [^{3}H] leucine to the sum of incorporated [^{3}H] leucine and [^{3}H] phenylalanine in an *in vitro* translation of poly (U) mRNA templates[183].

As part of an international collaboration to study the effects of the uS12 mutations associated with the newly identified MacInnes Syndrome, our contribution consisted of determining the effects of the uS12-R67K and uS12-F120I mutations on translational fidelity. To answer this question, both yeast model and patient-derived fibroblasts were used.

The laboratory of Dr. Susan Baserga, at Yale University, kindly provided us with a yeast model strain (*rps23a-R69K*), an isogenic *WT,* and an *rps23a-K62R* strain as a control. To develop this set of strains, the endogenous *RPS23B* gene was deleted and the endogenous *RS23A* was placed under the control of a galactose-inducible promoter. The resulting yeast strain was transformed with plasmids containing different versions of *RPS23A*: wild-type, *K62R* (control mutation which, as described above, leads to translational fidelity defects[182,183,185]), and *R69K* (model of patient mutation). By first growing the cells in galactose/raffinose medium, where both the endogenous and plasmid-borne copies of *RPS23A* are expressed, a large amount of cells can be obtained. Then, 24 hours prior to the experiment, replacement with dextrose medium allows depletion of the endogenous uS12, so that the assays reflect the result of the plasmid-borne copies. Deidentified fibroblasts derived from

both patients (RPS23-R67K and RPS23-F120I) and two healthy controls (C109 and 9E0872) were kindly provided by Dr. MacInnes.

Results

The yeast model of MacInnes Syndrome displays translational fidelity defects

Given that ribosomopathies are due to mutations that affect ribosome biogenesis, it is logical to assay the ribosome's translational accuracy. To determine the translational fidelity profile of the yeast model of MacInnes Syndrome, assays were carried out with yeast transformed with dual luciferase reporters specifically designed to measure rates of -1 PRF, +1 PRF, stop codon readthrough, and missense suppression. In addition to the *rps23a-R69K* mutant that mimics one of the patient's mutations, the *rps23a-K62R* mutant was also used as a control, since it had been previously shown to have translational fidelity defects[182,183,185].

Both *rps23a-K62R* and *rps23a-R69K* cells were shown to have higher rates of -1 PRF promoted by the *STN1* frameshift signal than the WT cells (**Figure 30A**). On the other hand, *rps23a-K62R* cells had lower rates of -1 PRF promoted by the L-A frameshift signal than the WT cells (**Figure 30A**). The rate of UAA stop codon readthrough was increased in *rps23a-K62R* cells, as observed previously[185] (**Figure 30B**). *rps23a-R69K* cells displayed higher rates of UAA and UAG stop codon readthrough than WT cells (**Figure 30B**). Missense suppression was assayed with reporters in which arginine 218 in the catalytic site of firefly luciferase was mutated to serine, by either a near-cognate

(AGA → AGC) or non-cognate (AGA → TCT) mutation, rendering it catalytically inactive[138]. *rps23a-K62R* cells displayed higher rates of both non-cognate, and near-cognate missense suppression than *WT* cells, as observed previously[183] (**Figure 30C**). *rps23a-R69K* cells had higher rates of non-cognate missense suppression than the *WT* cells, while rates of near-cognate missense suppression remained unchanged (**Figure 30C**). The rate of +1 PRF was higher than *WT* in *rps23a-K62R*, while it remained unchanged in *rps23a-R69K* (**Figure 30D**).

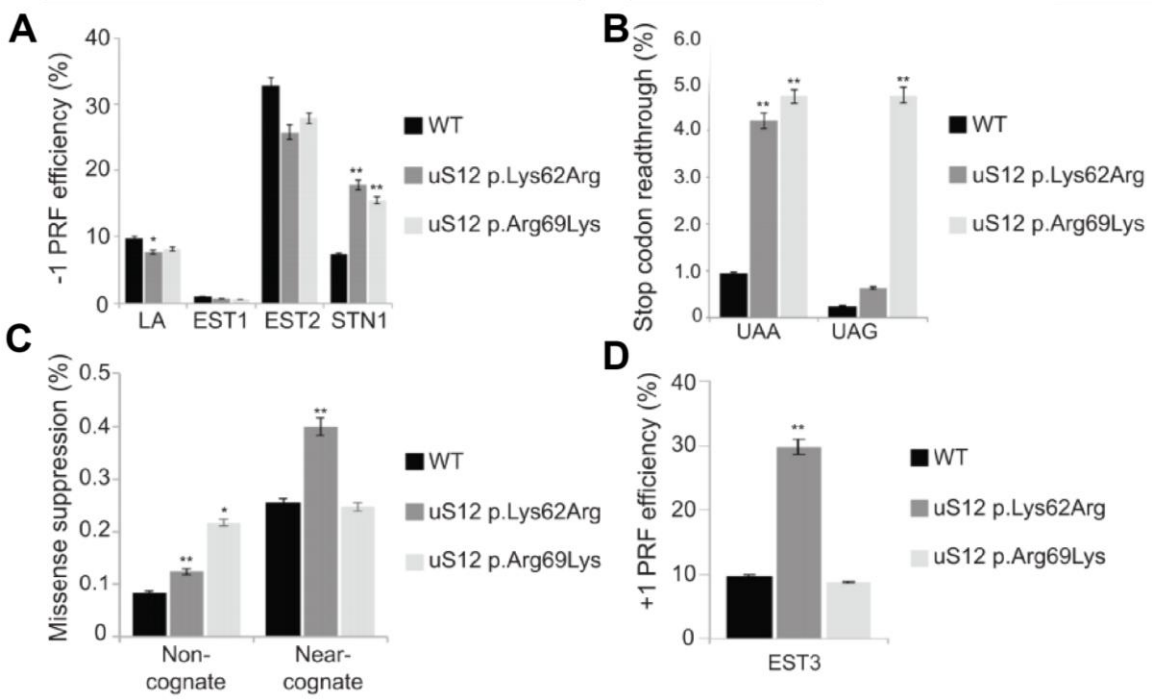

Figure 30. Translational fidelity defects in the yeast model of MacInnes Syndrome.

Rates of **(A)** -1 PRF, **(B)** stop codon readthrough, **(C)** missense suppression, and **(D)** +1 PRF in the yeast model of MacInnes Syndrome (*rps23a-R69K*) and the control strain (*rps23a-K62R*) were determined by dual luciferase assays. A minimum of seven biological replicates were assayed in triplicate. Student's t-test was used to determine statistically significant differences[122]: * $p<0.05$, and ** $p<0.01$. Figure first published in Paolini et al., 2017[68].

Patient-derived fibroblasts display increased rates of UAA stop codon readthrough

Translational fidelity was also assayed in fibroblasts derived from both MacInnes Syndrome patients (uS12-R67K and uS12-F120I) and two healthy controls (C109 and 9E0872), which were kindly provided by Dr. MacInnes. Fibroblasts were transfected with dual luciferase reporters by electroporation. Rates of UAA stop codon readthrough were higher in both uS12-R67K and uS12-F120I patient fibroblasts than in healthy control fibroblasts (**Figure 31**). These results are congruent with the increased UAA stop codon readthrough observed in yeast cells carrying the *rps23a-R69K* mutation (**Figure 30B**).

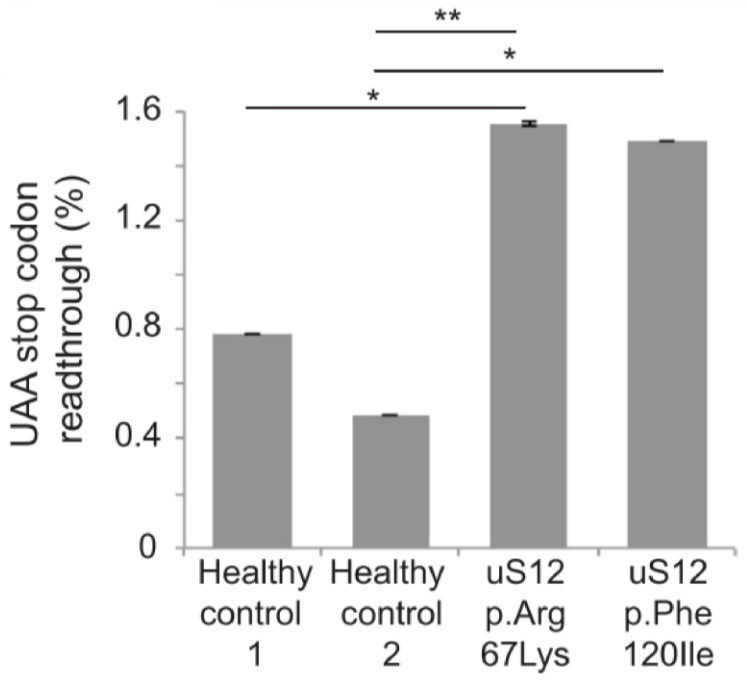

Figure 31. UAA stop codon readthrough in fibroblasts derived from the two MacInnes Syndrome patients

Rates of UAA stop codon readthrough were assayed by dual luciferase assays in fibroblasts derived from the two MacInnes Syndrome patients, and two healthy controls. A minimum of three biological replicates were assayed in triplicate. Student's t-test was used to determine statistical significance[122]: * $p<0.05$, and ** $p<0.01$. Figure first published in Paolini et al., 2017[68].

The yeast model of MacInnes Syndrome displays lower sensitivity to ER stress than WT cells

The sensitivity of cells to ER stress was assayed in two different ways. To determine the effects of tunicamycin, an ER stressor, on yeast growth, *rps23a-K62R* and *rps23a-R69K* cells were cultured alongside the *WT* cells in –trp media containing galactose and raffinose. Twenty-four hours before the cultures were back diluted, and spotted in YPAD and YPAD with 1 µg/ml tunicamycin plates, the media was changed to –trp media containing dextrose,

to ensure no endogenous uS12 was present, as described above. Samples were incubated at 30°C and photographed daily. The WT cells grew faster than both *rps23a-K62R* and *rps23a-R69K* mutants in the media without tunicamycin (**Figure 32**, middle left). The two mutants had similar growth rates (**Figure 32**, top and bottom left). On the plates treated with tunicamycin, *rps23a-R69K* cells grew faster than the WT cells, indicating decreased sensitivity to tunicamycin and ER stress (**Figure 32**, middle and bottom right). *Rps23a-K62R* cells were severely sensitive to tunicamycin and barely grew on the first dilution spot (**Figure 32**, top right).

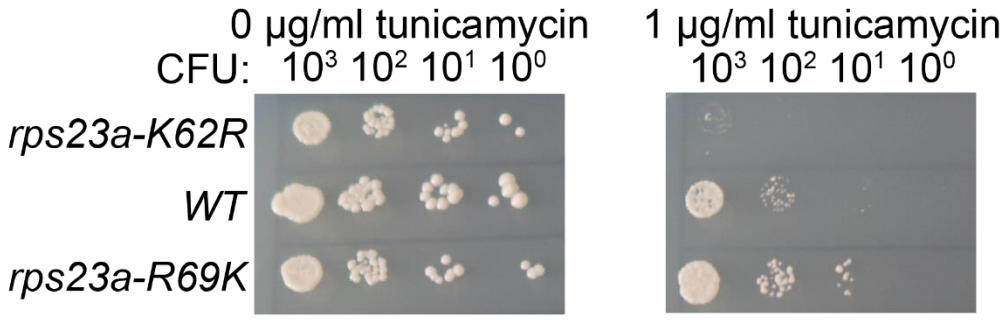

Figure 32. *rps23a-R69K* cells displayed decreased sensitivity to ER stress
Yeast was grown in –trp media containing galactose and raffinose. Twenty-four hours before the experiment, media was switched to –trp media containing dextrose, to ensure expression of the mutant *rps23a*. Yeast was backdiluted, and serial dilutions were spotted on –trp media containing dextrose with or without 1µg/ml tunicamycin. Three biological replicates were assayed.

As described earlier, the unfolded protein response is activated through activation of IRE1, which splices HAC1 mRNA in the presence of ER stress[167,168,171]. *rps23a-K62R* and *rps23a-R69K* cells were cultured in –trp media with galactose and raffinose, and media was changed to –trp with dextrose 24 hours prior to experiment. Yeast was backdiluted, and then treated

with 1 µg/ml tunicamycin for 1 hour. RNA was isolated from 1 x 10^7 cells, and cDNA synthesized from 450 ng of RNA (due to limitation in reaction volume). HAC1 mRNA splicing status was determined by PCR with primers designed to amplify the HAC1 intron region. As a loading control, 500 ng of RNA were loaded on an agarose gel for separation of rRNA. In untreated samples, *RPS23A-R69K* had the highest basal levels of unspliced HAC1 mRNA (**Figure 33**, lane 3). After tunicamycin treatment, the WT and *rps23a-R69K* cells had a low level of spliced HAC1 mRNA, while about 50% of HAC1 mRNA in *rps23a-K62R* cells was spliced (**Figure 33**, lanes 4-6).

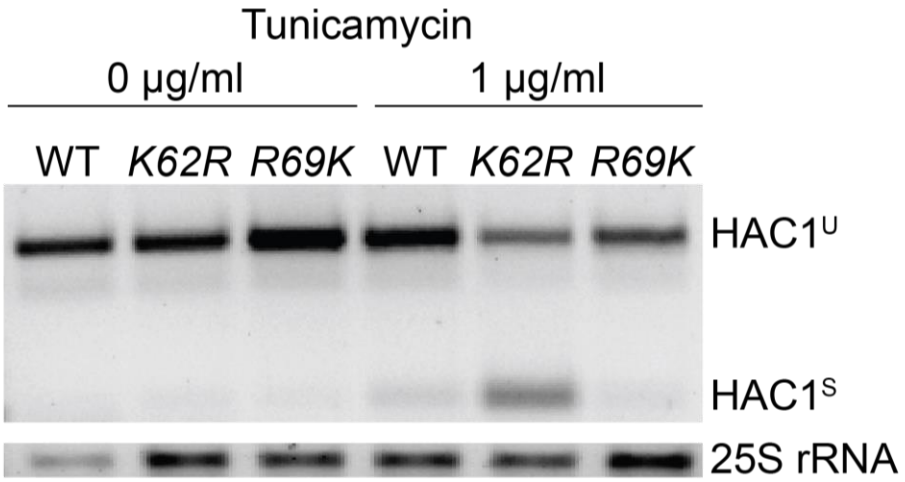

Figure 33. HAC1 mRNA splicing in *rps23a* mutant cells as a result of ER stress

Yeast was grown in –trp media containing galactose and raffinose. Twenty-four hours before the experiment, media was switched to –trp media containing dextrose, to ensure expression of the mutant *rps23a*. Cells were treated with 1µg/ml tunicamycin for 1 hour, and RNA was isolated from 1 x 10^7 cells. cDNA was synthesized from 450 ng of RNA, and the HAC1 intron region was amplified by PCR. Twenty-five µl of the PCR products were separated on a 1.5% agarose gel. A 111 bp product is expected for spliced HAC1, and 363 bp product is expected for unspliced HAC1. Five hundred ng of RNA were separated on a native 1.5% agarose gel. Three biological replicates were treated and processed through the full protocol.

Discussion

As part of this project, it was determined that the patient cells have ribosome biogenesis defects. There is an accumulation of 18S-E pre-rRNA in cells carrying the uS12-R67K mutation, suggesting that one of the final steps in maturation of pre-rRNA is disrupted, as is the case with DBA patients with mutations in RPS10, RPS26, RPL5, or RPL11 (encoding ribosomal proteins eS10, eS26, uL18, and uL5, respectively)[27,30,49,68]. Polysome profiles showed a decrease in the 40S subunit peak in uS12-R67K fibroblasts and LCL, which could not be counteracted by the increase of uS12 mRNA transcription observed in the mutant fibroblasts[68]. The decrease in 40S subunit peak is similar to what was seen in DBA patient cells with mutations RPS19 (encoding ribosomal protein eS19)[49,71,72]. Interestingly, examination of polysome fractions showed that only 10% of translating ribosomes carry the R67K mutation[68], suggesting there may be a mechanism to exclude mutant uS12 similar to what was observed in *E. coli*[186].

Since the R67K mutation occurs in close proximity to the P-62 residue that is hydroxylated in uS12, hydroxylation state of these mutant proteins was determined. While hydroxylation of P-62 by OGFOD1 is reduced in uS12-R67K LCL, there is no change in the interaction between uS12 and OGFOD1[68]. On the other hand, interaction between uS12-F120I and OGFOD1 is disturbed, in addition to the reduction in hydroxylation of P-62[68].

When cells are exposed to environmental stress, cytoplasmic stress granules form and sequester pre-initiation complexes, suppressing translation

of mRNAs not required for stress response[187,188]. Deregulated stress granule formation has been associated with pathologies such as neuronal dysfunction and degeneration[189]. Patient fibroblasts were exposed to arsenite to induce oxidative stress and induce formation of stress granules as a result. The cells carrying the R67K and F120I mutations in uS12 developed more stress granules than the healthy controls, suggesting that patient cells are more sensitive to oxidative stress[68]. It is known that pre-initiation complexes requiring repair are recruited to stress granules in the presence of arsenite[190], which could explain the increase in stress granules in the patient cells.

It has been shown that increased oxidative stress levels or reduced levels of OGFOD1 can lead to changes in the fidelity of protein translation[184,191]. Changes in translational recoding were confirmed, as described in our contribution to this project. The yeast model of MacInnes syndrome displayed an increase in -1 PRF stimulated by the *STN1* frameshift signal, and in non-cognate missense suppression. These yeast *rps23a-R67K* cells also showed an increase in UAA and UAG stop codon readthrough. Fibroblasts derived from both patients also displayed increase UAA stop codon readthrough when compared to two healthy controls. It is worth noting that +1 PRF is caused by slipping of the peptidyl-tRNA, while -1 PRF is driven by slippage of both the peptidyl- and aminoacyl-tRNAs[99,107]. Missense and nonsense suppression rely only on the A-site of the ribosome. These details taken together with the translational fidelity data suggest that the uS12 mutants are most likely affecting the A-site, but not the P-site function.

This study uncovered two patients with similar phenotypic presentation carrying two different mutations in conserved regions of uS12, the PNSA and PGVRY domains. The uS12-R67K mutation was shown to affect a later step in pre-rRNA maturation, and both mutations impair OGFOD1 hydroxylation of residue P-62 in uS12 and increase sensitivity of the cells to oxidative stress. This, in turn leads to the variations in translational fidelity observed in the fibroblasts derived from the two patients and in the yeast model of MacInnes Syndrome. The low percentage of mutant uS12 found in the polysome fractions of the polysome profile obtained from uS12-R67K LCL suggests that there may be a mechanism to prevent ribosomes carrying the mutated uS12 from entering the pool of actively translating ribosomes.

Chapter 5: Conclusions and future directions

The ribosome is central to the process of translating mRNAs to proteins: it is critical that it maintains proper reading frame and correct decoding of codons. Ribosomopathies are diseases in which mutations of ribosomal proteins, or of ribosome biogenesis factors, lead to defects in ribosome biogenesis. While it has been shown that cells in ribosomopathy patients and models have ribosome biogenesis defects, the ribosome function in the patient cells has not been extensively studied. Here, we monitored translational fidelity in yeast models of ribosomopathies, as well as cells derived from MacInnes Syndrome patients and from DBA patients carrying two novel mutations in *RPL9* (uL6). An RNA-seq experiment was carried out with the yeast X-DC model, and led us to further explore the consequences of ribosomopathological mutations on oxidative and ER stress.

As was described in chapter 1, most ribosomopathy patients present with anemia, and a unique set of symptoms dependent on which specific disorder they have. Two major models have been proposed to explain how the mutations cause the disease. First, specialized ribosomes have been proposed as a solution[146,147]. Supporters of this model list the unique sets of symptoms as an indication of this[20,29]. They suggest that ribosomal proteins, as part of the ribosome, have unique functions in different tissues, with Rpl38 and regulation of Hox mRNA translation given as an example [148,192–195]. An alternative model suggests that ribosomopathies are due to metabolic imbalance[149–151]. Supporters of this theory argue that mutations in ribosomal proteins lead to a

lower concentration of ribosomes in the cells, which can affect translation of messages depending on rates of translation initiation[149,152]. Supporting evidence includes translation of *GATA1*, which is mutated in some DBA patients[43,148,153].

We determined the translational fidelity profile of pseudo-haploinsufficient yeast models of three ribosomopathies. While different assays of translational fidelity revealed ohnolog-specific effects, ribosomal protein ohnolog duplication corrected the defects seen in the model yeast strains (**Figures 12, 15, 16**). These data suggest gene dosage and support the metabolic imbalance model. Consistent with this, yeast ribosomal protein ohnologs have been shown to be expressed at different levels, which may explain our initial observations[196–199]. We hasten to add however, that the observations and conclusions made here are limited to laboratory yeast growing in glucose and nitrogen source rich medium, and thus merely represent a starting point down the path to more detailed investigations. Ribosome specialization may be operative in yeast under different nutrient conditions, during sporulation (a model of differentiation), or in wild-source diploid yeast strains. Furthermore, additional research is required to address this question in higher eukaryotes, where cell type and development of the organism may require the proposed “specialized” ribosomes.

It has been shown that translational fidelity defects can protect bacterial cells against oxidative stress[200]. Fan et al. used bacterial strains carrying mutations that either increased (*rpsD**) or decreased (*rpsL**) UAG stop codon

readthrough[200]. Protein synthesis rate was not affected in either mutant. An RNA-seq experiment revealed upregulation of antioxidant genes [including *katE* (catalase that scavenges H_2O_2) and *osmC* (reduces hydroperoxide)] in *rpsD**, and downregulation of these same genes in *rpsL**. Upon treatment of the cells with 5 mM H_2O_2, which kills the WT cells, *rpsD** cells had increased survival rate, while *rpsL** cells were more sensitive. Deletion of *KatE* and *OsmC* in the *rpsD** cells increased sensitivity of the cells to treatment with H_2O_2. *katE* and *osmC* are regulated by *rpoS*, a factor controlling general stress response. Deleting *rpoS* in either the WT or *rpsD** cells led to the highest sensitivity to H_2O_2. Overexpression of KatE and RpoS protected WT and *rpsD** cells against H_2O_2. Western bot analysis showed that RpoS was increased in *rpsD** cells and decreased in *rpsL** cells. Canavanine, a structural analog of arginine, is misincorporated during protein synthesis if present in the environment. Addition of canavanine increased protection of WT cells to H_2O_2. These results suggest that mistranslation upregulates general stress response, which in turn is adaptive to oxidative stress conditions in *E. coli*. A similar effect was observed in *cbf5-D95A* cells, which have translational fidelity defects[100,154], and reduced levels of reactive oxygen species (**Figure 26**).

Growth curve analysis showed *cbf5-D95A* cells living longer than the WT cells upon reaching stationary phase, suggesting that they may be pre-adapted to some stressors (**Figure 21**). RNA-seq analyses revealed upregulation of nucleotide metabolism, response to oxidative stress, protein refolding/unfolded protein response, and trehalose metabolism in *cbf5-D95A*

cells (**Table 2 and 4**). We hypothesize that increased nucleotide metabolism is due to increased ribosome biosynthesis in *cbf5-D95A* cells. This is an energy intensive process, and production of ATP in the mitochondria creates oxidative free radicals. The cells then upregulate oxidative stress response genes to lower reactive oxygen species. We posit that decreased translational fidelity is leading to defective proteins, triggering the unfolded protein response. Trehalose is synthesized by yeast as a response to stress, and has been shown to increase lifespan not only in yeast, but also in *Caenorhabditis elegans* and *Drosophila melanogaster*[201–204]. Our results are consistent with previous studies showing that zebrafish models of DBA and 5q- Syndrome (*RPS19* and *RPS14* deficiency, respectively) displayed upregulation of stress response [205,206].

Amino acid biosynthesis and ER to Golgi vesicle-mediated transport were downregulated in *cbf5-D95A* cells (**Table 3**). We hypothesize this is due to these cells having lower translational capacity, and as such having decreased need for amino acid biosynthesis. These results are consistent with those found in ribosomopathy patients. Amino acid biosynthesis was downregulated in *RPS19*-deficient DBA patient-derived fibroblasts and LCLs[207,208].

Based on the available data, we hypothesized that the *cbf5-D95A* cells contain ribosomes with translational fidelity defects and are synthesizing defective proteins[66,100,154]. These proteins are likely not processed correctly in the endoplasmic reticulum (ER), leading to their retention within this organelle.

This explanation fits with the downregulation of ER to Golgi transport seen in the *cbf5-D95A* cells (**Table 3**) and upregulation of protein folding (**Table 2**).

The sensitivity of yeast ribosomopathy models to tunicamycin, an ER stressor, was studied. X-DC and MacInnes Syndrome models were less sensitive to tunicamycin and had increased basal expression of HAC1 mRNA (**Figures 27, 28, 32, and 33**). Models of ICA and 5q- Syndrome were also less sensitive than WT cells when growing in the presence of tunicamycin (**Figure 29A**). The yeast models of DBA, i.e. *rps19aΔ* and *rps19bΔ*, had an increase and a decrease in tunicamycin sensitivity, respectively (**Figure 29A**). As discussed above, the difference in phenotype may be due to differences in ohnolog expression[196–199].

We hypothesize that the *cbf5-D95A* ribosomes have greater turnover rates, due to defective function. Ribosome biosynthesis is an energetically expensive process[174]. Increased mitochondrial function to produce sufficient ATP to supply to this process may be resulting in the upregulation of genes involved in the response to oxidative stress (**Table 2 and 4**). To test the ribosome turnover hypothesis, future work will include measuring ribosome half-life taking into account doubling time of the cells. If ribosome turnover is increased in *cbf5*-D95A cells, a glucose consumption assay will follow this experiment. We hypothesize that cells harboring the *cbf5-D95A* mutation will have increased glucose consumption due to increased rates of ribosome synthesis.

Appendix 1: Yeast strains

Table 5. Yeast strains used in this study

Strain	Genotype/Description
yJD1524	*ade2-1 can1-100 his3-11 leu2-3, 112 trp1-1 ura3-1 cbf5::TRP1 + CBF5 on pRS313*
yJD1525	*ade2-1 can1-100 his3-11 leu2-3, 112 trp1-1 ura3-1 cbf5::TRP1 + CBF5 D95A on pRS313*
yJD1745	*ade2-1 can1-100 his3-11 leu2-3, 112 trp1-1 ura3-1 cbf5::TRP1 upf1::LEU2 + CBF5 on pRS313*
yJD1746	*ade2-1 can1-100 his3-11 leu2-3, 112 trp1-1 ura3-1 cbf5::TRP1 upf1::LEU2 + CBF5 D95A on pRS313*
yJD1728	*MATa ura3-52 lys2-801_amber ade2-101_ochre trp1-Δ63 his3-Δ200 leu2-Δ1 transformed with p424GPD empty vector* (strain has RPS23B deleted and RPS23A under gal-inducible promoter kindly provided by Dr. Susan Baserga, Yale University)
yJD1729	*MATa ura3-52 lys2-801_amber ade2-101_ochre trp1-Δ63 his3-Δ200 leu2-Δ1 (YPH499) transformed with p424GPD RPS23A-WT* (strain has RPS23B deleted and RPS23A under gal-inducible promoter kindly provided by Dr. Susan Baserga, Yale University)
yJD1730	*MATa ura3-52 lys2-801_amber ade2-101_ochre trp1-Δ63 his3-Δ200 leu2-Δ1 (YPH499) transformed with p424GPD RPS23A-K62R* (strain has RPS23B deleted and RPS23A under gal-inducible promoter kindly provided by Dr. Susan Baserga, Yale University)
yJD1731	*MATa ura3-52 lys2-801_amber ade2-101_ochre trp1-Δ63 his3-Δ200 leu2-Δ1 (YPH499) transformed with p424GPD RPS23A-R69K* (strain has RPS23B deleted and RPS23A under gal-inducible promoter kindly provided by Dr. Susan Baserga, Yale University)
yJD1753	*MATa his3Δ1 leu2Δ0 met15Δ0 ura3Δ0* (BY4741, isogenic WT for 6 strains below. Dharmacon, cat # YSC1048)
yJD1754	*MATa his3Δ1 leu2Δ0 met15Δ0 ura3Δ0 ygr214w::KANr* (*rps0aΔ*. Dharmacon, cat #YSC6273-201936399)
yJD1756	*MATa his3Δ1 leu2Δ0 met15Δ0 ura3Δ0 ylr048w::KANr* (*rps0bΔ*. Dharmacon, cat #YSC6273-201928941)
yJD1757	*MATa his3Δ1 leu2Δ0 met15Δ0 ura3Δ0 ycr031c::KANr*

Strain	Genotype/Description
	(*rps14aΔ*. Dharmacon, cat #YSC6273-201937084)
yJD1758	*MATa his3Δ1 leu2Δ0 met15Δ0 ura3Δ0 yjl191w::KANr* (*rps14bΔ*. Dharmacon, cat #YSC6273-201919008, CloneId:1234)
yJD1759	*MATa his3Δ1 leu2Δ0 met15Δ0 ura3Δ0 yol121c::KANr* (*rps19aΔ*. Dharmacon, cat #YSC6273-201937499)
yJD1760	*MATa his3Δ1 leu2Δ0 met15Δ0 ura3Δ0 ynl302c::KANr* (*rps19bΔ*. Dharmacon, cat #YSC6273-201918337, CloneId:1142)
yJD1732	*Mat a ura3Δ0 lys2Δ0 leu2Δ0 his3Δ200* (JPY10H3, isogenic WT for 6 strains below. Kindly provided by Sherif Abou Elela's lab at Sherbrooke University)
yJD1739	*Mat a ura3Δ0 lys2Δ0 leu2Δ0 his3Δ200 rps0a::RPS0B* (*RPS0BB*, MGY628. Kindly provided by Sherif Abou Elela's lab at Sherbrooke University)
yJD1740	*Mat a ura3Δ0 lys2Δ0 leu2Δ0 his3Δ200 rps0b::RPS0A* (*RPS0AA*, MGY629. Kindly provided by Sherif Abou Elela's lab at Sherbrooke University)
yJD1741	*Mat a ura3Δ0 lys2Δ0 leu2Δ0 his3Δ200 rps14a::RPS14B* (*RPS14BB*, MGY630. Kindly provided by Sherif Abou Elela's lab at Sherbrooke University)
yJD1742	*Mat a ura3Δ0 lys2Δ0 leu2Δ0 his3Δ200 rps14b::RPS14A* (*RPS14AA*, MGY631. Kindly provided by Sherif Abou Elela's lab at Sherbrooke University)
yJD1743	Mat a ura3Δ0 lys2Δ0 leu2Δ0 his3Δ200 rps19a::RPS19B (*RPS19BB*, MGY632. Kindly provided by Sherif Abou Elela's lab at Sherbrooke University)
yJD1744	*Mat a ura3Δ0 lys2Δ0 leu2Δ0 his3Δ200 rps19b::RPS19A* (*RPS19AA*, MGY633. *Kindly provided by Sherif Abou Elela's lab at Sherbrooke University)*

Appendix 2: Plasmids

Table 6. Plasmids used in this study

Plasmids	Description	Usage
pJD375	pYDL-Readthrough	Yeast DL assays
pJD376	pYDL-LA	Yeast DL assays
pJD377	pYDL-Ty1/EST3	Yeast DL assays
pJD431	pYDL-UAA	Yeast DL assays
pJD432	pYDL-UAG	Yeast DL assays
pJD433	pYDL-UGA	Yeast DL assays
pJD642	pYDL-non-cognate missense suppression	Yeast DL assays
pJD643	pYDL-near-cognate missense suppression	Yeast DL assays
pJD1018	pYDL-EST2	Yeast DL assays
pJD1039	pYDL-STN1	Yeast DL assays
pJD1041	pYDL-EST1	Yeast DL assays
pJD2257	pSGDmod-Readthrough	DL assay – DBA LCLs
pJD2337	pSGDmod-PEG10	DL assay – DBA LCLs
pJD2349	pSGDmod-OAZ1	DL assay – DBA LCLs
pJD2443	pSGDmod-UAA	DL assay – DBA LCLs
pJD2444	pSGDmod-UGA	DL assay – DBA LCLs
pJD2445	pSGDmod-UAG	DL assay – DBA LCLs
pJD1521	pUG73 – Hegemann's plasmid for yeast KO with LEU2 marker	Yeast *upf1* deletion
pJD2044	pHDL-fullCMV-control	DL assay – MacInnes Syndrome fibroblasts
pJD2046	pHDL-fullCMV-UAA	DL assay – MacInnes Syndrome fibroblasts
pJD175f	pHDL-SV40-control	Cloning
pJD1643	pHDL-SV40-UAA	Cloning
pJD2256	pSGDmod-HIV	Cloning
pCDNA3.1(+)	Contains CMV promoter/enhancer	Cloning

Appendix 3: Cell lines

Table 7. Cell lines used in this study

Cell line name	Description	Clinical phenotype
NhnF	Control LCL	Healthy
NhnM	Control LCL	Healthy
F.T.	Control LCL	Healthy
RPL9 c.-2+1	Chr4(GRCh37):g.39460510C>G	DBA
RPL9 L20P (C.I.)	uL6 L20P (c.59C>T)	Cervical carcinoma, suspected DBA
C109	Control fibroblast line	Healthy
9E0872	Control fibroblast line	Healthy
uS12 p.Arg67Lys	uS12 R67K	MacInnes Syndrome
uS12 p.Phe120Ile	uS12 F120I	MacInnes Syndrome

All cell lines were kindly provided by Dr. Alyson MacInnes, at European Diamond Blackfan Anemia Foundation (euroDBA). Cell lines were deidentified by provider.

Appendix 4: Oligonucleotides

Table 8. Oligonucleotides used for sequencing

Primers	Reference number	Sequence
DL_MCS seqng	147105020	CGTACGTGATGTTCACC
yCBF5_seqng Fwd	128146839	GGAGGATTTCGTTATTAAGCCTGA
yCBF5_seqng Rev	12814684	CAAACCCCATCTTCTTGGGTATAA
yCBF5_5p_sqcng_fwd	130246582	TCAAAGGAGGATTTCGTTATTAAGC
DL_Pro1	150855014	GCTGTAATTGAACTGGGAGTGGAC
DL_Pro2	150855015	CCACTGCGGACCAGTTATCATC
Renilla_seq_f1	158697105	GTTTCCTCGTCATTGTTCTCG
Renilla_seq_f2	158697106	GGTATGGGCAAATCAGGCAA
Renilla_seq_f3	158697107	CGTCGTCCAACATTATCATGGC
Renilla_seq_f4	158697108	GCAAGAAGATGCACCTGATGAAATG
Firefly_seq_f1	158697109	TCGCAGCCTACCGTAGT
Firefly_seq_f2	158697110	CATTCTTCGCCAAAAGCACTCT
Firefly_seq_f3	158697111	AACATCTTCGACGCGGG
Firefly_seq_r1	158697112	GGCGTGAATGTAAGCGTG
Firefly_seq_r2	158697113	GGTCCTCTGACACATAATTCGC
Firefly_seq_r3	158697114	CATGCGAGAATCTGACGCAG
Firefly_seq_r4	158697115	CACCTCGATATGTGCATCTGTA
Renilla_seq_r1	158697116	GTACAACGTCAGGTTTACCACC
Renilla_seq_r2	158697117	AATAAGAAGAGGCCGCGT
ADH1_promoter_seq_f1	163946558	TCAAGGAGCATGAAGGCAAAAGAC
ADH1_promoter_seq_f2	163946559	CCTTTTGTTGTTTCCGGGTGTA
pJD375_seq_f1	163946560	GGCGTTACCCAACTTAATCG
pJD375_seq_f2	163946561	CGTTTACAATTTCCTGATGCGG
pJD375_seq_f3	163946562	TCTGCCCATTCTGCTATTCTG
pJD375_seq_f4	163946563	CAGACAAGCTGTGACCGT
pJD375_seq_f5	163946564	TAGCAXGTGATGAAAAGGACCC
pJD375_seq_f6	163946565	ATCATGTAACTCGCCTGGATCG
pJD375_seq_f7	163946566	GCGTAATCTGCTGCTTGC
pJD375_seq_f8	163946567	GCGTCGATTTTTGTGATGCTC
pJD375_seq_r1	163946568	GTCTAGGGCTACAGTATTAGTTCG

Primers	Reference number	Sequence
pJD375_seq_r2	163946569	GTTGTCGTGGTCGTCATCAT
pJD375_seq_r3	163946570	AATTGCGTTGCGCTCACTGC
pJD375_seq_r4	163946571	GGATTAGCAGAGCGAGGTAT
pJD375_seq_r5	163946572	GAAGTGGTCCTGCAACTTTATCC
pJD375_seq_r6	163946573	GGCGACACGGAAATGTTGAA
pJD375_seq_r7	163946574	GATACGAGGCGCGTGTAAGT
pJD375_seq_r8	163946575	GTGTGCTTCATTGGATGTTCG
pJD375_seq_r9	163946576	ATGCTAAGGTAGAGGGTG
pJD375_seq_r10	163946577	CGTGGCGAGAAAGGAAGGGA
SGDluc-F4	159513400	AAGATGTTCATCGAGTCCGACC
SGDluc-R5	159513414	CGCTTCATAGCTTCTGCCAGC

All oligonucleotides on this list were obtained from IDT.

Table 9. Oligonucleotides used for *UPF1* deletion in yeast (LEU2 marker)

Primers	Reference number	Sequence
OL5’ for KO yUPF1	124892333	CATAGTTAGTTACTATCCACTCA ATAATATTAAACGAGTGAATGCC AGCTGAAGCTTCGTACGC
OL3’ for KO yUPF1	124892334	GTAAAGAGTATTCATTAGAAGTA CAATGGTAGCCCTATTTGGTTGG CATAGGCCACTAGTGGATCTG
Oligo A for KO yUPF1 v2	138930282	CGCCATCAAATCTAAGAAGAGAA TCCTTTTCGCTTCTTTC
Oligo B for KO yUPF1	133698646	CGGTATCCCCTAAGTCAGAATCT GGATGTAAAG
Oligo C for KO yUPF1	133698647	CGGCCAATGAACGCTCAATTTAA CGTAGAATCTG
Oligo D for KO yUPF1 v2	138930283	CGAGAGAGAAAAGAGGAGTTCT AAGTAACGATATTTTACAACTGA GATAAGTAC
Oligo B-M for KO yUPF1 (LEU2 marker)	138576612	AGTTATCCTTGGATTTGG
Oligo C-M for KO yUPF1 (LEU2 marker)	138576613	ATCTCATGGATGATATCC

All oligonucleotides on this list were obtained from IDT.

Table 10. Oligonucleotides used for cloning experiments

Primers	Sequence
BamSalKilT	GATCAACTGCAGTCT
BamSalKilB	TCGAAGACTGCAGTT
Alphahelixspacer-T2	TCGACCGAAGCAGCCGCTAAAGAGGCTGCGGCAAAAGCTG
Alphahelixspacer-B2	GATCCAGCTTTTGCCGCAGCCTCTTTAGCGGCTGCTTCGG
AHS-TAA-T2a	TCGACCGAAGCAGCCTAAAAAGAGGCTGCGGCAAAAGCTG
AHS-TAA-B2	GATCCAGCTTTTGCCGCAGCCTCTTTTTAGGCTGCTTCGG
AHS-TAG-T2a	TCGACCGAAGCAGCCTAGAAAGAGGCTGCGGCAAAAGCTG
AHS-TAG-B2	GATCCAGCTTTTGCCGCAGCCTCTTTCTAGGCTGCTTCGG
AHS-TGA-T2a	TCGACCGAAGCAGCCTGAAAAGAGGCTGCGGCAAAAGCTG
AHS-TGA-B2	GATCCAGCTTTTGCCGCAGCCTCTTTTCAGGCTGCTTCGG
CMVprom-forward	ACTGTCGGTACCCAGATATACGCGTTGACATTGATTATTGAC
CMVprom-reverse	ACTGTCCTGCAGGCCAGTAAGCAGTGGGTTCTCTAG

Oligonucleotides on this list were obtained from IDT or Genewiz.

Table 11. Gene fragments used for cloning

Gene Fragments	Sequence
Gene fragment for HIV -1 PRF insertion into pSGDluc modified vector	GAGCTTCGTGGAGCGCGTGCTGAAGAACGA GCAGTATTTCTACACCTCGAGAGAAGCCAGA CACAAACAGAAAATTGTGGCACCGGTGAAA CAGACTTTGAATTTTGACCTTCTTAAGCTGG CGGGAGACGTCGAGTCCAACCCCGGGCCC TCGTCGACTTTTTTAGGGAAGATCTGGCCTT CCCACAAGGGGAGGCCAGGGAATTTTCTTC CGAGCTCGAAGACGCCAAAAACATAAAGAA AGGCCCGGCGCCATTCTATCCTCTAGAGGA TGGAACCGCTGGAGAGCAACTGCATAAGGC TGGATCCGAGGCACGGCATAAGCAAAAGAT CGTAGCCCCAGTAAAGCAAACACTCAACTTC GATCTACTCAAACTCGCAGGTGATGTGGAAT CTAATCCAGGACCTTTCGGATCTGCCACCAT TGAAGATGCCAAAAACATTAAGAAGGGCCCA GCGCCATTCTACCCACTCGAAGACGGGACC GCCGGCGAGC
Gene fragment for PEG10insertion into pSGDluc modified vector	GTCGAGTCCAACCCCGGGCCCTCGTCGACC AAAGTCTTCGCCGGCGGGAAACTCCCCGGC CCCGCTGTAGAGGGACCTTCAGCGACCGGG CCAGAAATAATAAGGTCCCCGGATCCGAGG CACGGCATAAGCAAAAGATCGT
Gene fragment for OAZ1 +1 PRF insertion into pSGDluc modified vector	GAGACGTCGAGTCCAACCCCGGGCCCTCGT CGACCAGGGTCTCCCTCCACTGCTGTAGTA ACCCGGGTCCGGGGCCTCGGTGGTGCTCC TGATGCCCCTCACCCACCCCTGAAGATCCC AGGTGGGCGAGGGAATAGTCAGAGGGATCA CAATCTTTCAGGATCCGAGGCACGGCATAA GCAAAAGATCG

All gene fragments on this list were obtained from Genewiz.

Table 12. Oligonucleotides used for checking HAC1 mRNA splicing status

Primers	Reference number	Sequence
HAC1_fwd_splicing	189869741	GGAAACAGTCTACCCTTTGACAAT
HAC1_rev_splicing	189869742	TCATGAAGTGATGAAGAAATCATTC

Both oligonucleotides on this list were obtained from IDT.

Appendix 5: *CBF5* RNA-Seq supplementary data

An RNA-Seq experiment was carried out with isogenic WT and *cbf5-D95A* yeast cells to 1) determine the effects of reduced pseudouridylation of yeast rRNA on gene expression, and 2) identify messages containing functional -1 PRF signals. RNA-Seq data analysis is described in chapter 3, and in more detail in Materials and Methods (chapter 2). Sets of differentially expressed genes and pathways are contained within this dissertation and in an online repository at https://github.com/cmsvieira/scerevisiae_cbf5.

A small number of messages with predicted -1 PRF had low abundance in the c*bf5-D95A c*ells. In an effort to rescue the abundance of -1 PRF-containing messages, *UPF1* (involved in NMD pathway) was deleted from the *CBF5* and *cbf5-D95A* strains. The RNA-Seq experiment was then repeated with *CBF5*, *cbf5-D95A, upf1Δ* and *cbf5-D95A upf1Δ*. As before, data analysis is described in chapter 3, and in more detail in Materials and Methods (chapter 2).

The purpose of this appendix is to include supplementary data relating to the RNA-Seq experiments described in chapter 3.

SRA accessions

Sequencing data have been submitted to Genbank, with Bioproject accession number PRJNA475276, for project SRP150277. Biosample accession for each sample is listed in **Table 13**.

Table 13. Genbank accession numbers for RNA-Seq data

Biosample accession	Library ID	Title
SAMN09384240	HPGL0564	CBF5 UPF1.E1.1
SAMN09384241	HPGL0565	CBF5 UPF1.E1.2
SAMN09384242	HPGL0566	CBF5 UPF1.E1.3
SAMN09384243	HPGL0567	CBF5 UPF1.E1.4
SAMN09384244	HPGL0568	cbf5-D95A UPF1.E1.1
SAMN09384245	HPGL0569	cbf5-D95A UPF1.E1.2
SAMN09384246	HPGL0570	cbf5-D95A UPF1.E1.3
SAMN09384247	HPGL0571	cbf5-D95A UPF1.E1.4
SAMN09384248	HPGL0774	CBF5 UPF1.E2B1.1
SAMN09384249	HPGL0775	cbf5-D95A UPF1.E2B1.1
SAMN09384250	HPGL0776	CBF5 upf1delta.E2B1.1
SAMN09384251	HPGL0777	cbf5-D95A upf1delta.E2B1.1
SAMN09384252	HPGL0778	CBF5 UPF1.E2B1.2
SAMN09384253	HPGL0779	cbf5-D95A UPF1.E2B1.2
SAMN09384254	HPGL0780	CBF5 upf1delta.E2B1.2
SAMN09384255	HPGL0781	cbf5-D95A upf1delta.E2B1.2
SAMN09384256	HPGL0782	CBF5 UPF1.E2B2.1
SAMN09384257	HPGL0783	cbf5-D95A UPF1.E2B2.1
SAMN09384258	HPGL0784	CBF5 upf1delta.E2B2.1
SAMN09384259	HPGL0785	cbf5-D95A upf1delta.E2B2.1
SAMN09384260	HPGL0786	CBF5 UPF1.E2B2.2
SAMN09384261	HPGL0787	cbf5-D95A UPF1.E2B2.2
SAMN09384262	HPGL0788	CBF5 upf1delta.E2B2.2
SAMN09384263	HPGL0789	cbf5-D95A upf1delta.E2B2.2

Quality control metrics

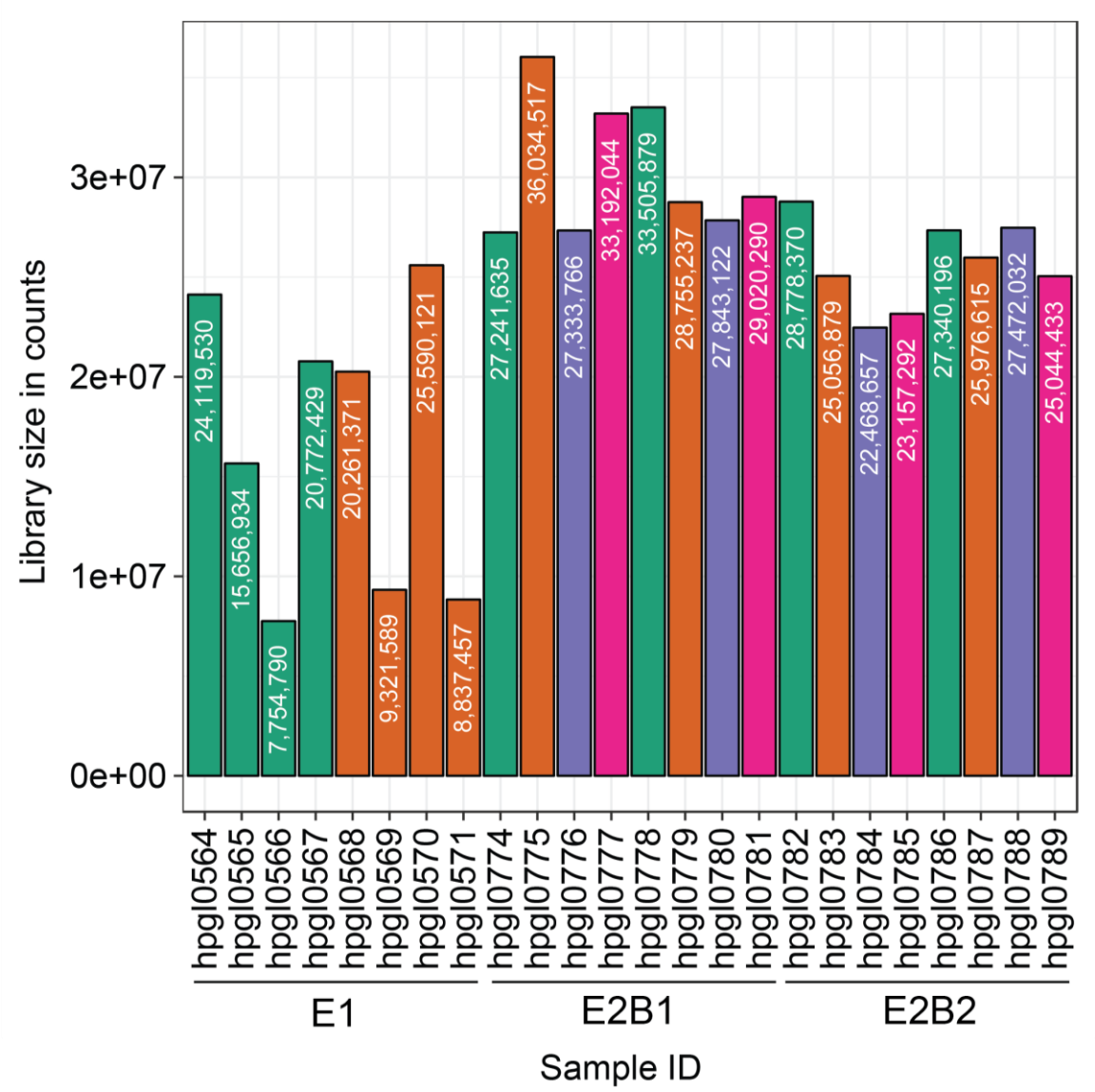

Figure 34. Library sizes for all samples in RNA-seq experiments
Raw library sizes were plotted to check sequencing depths for all samples.

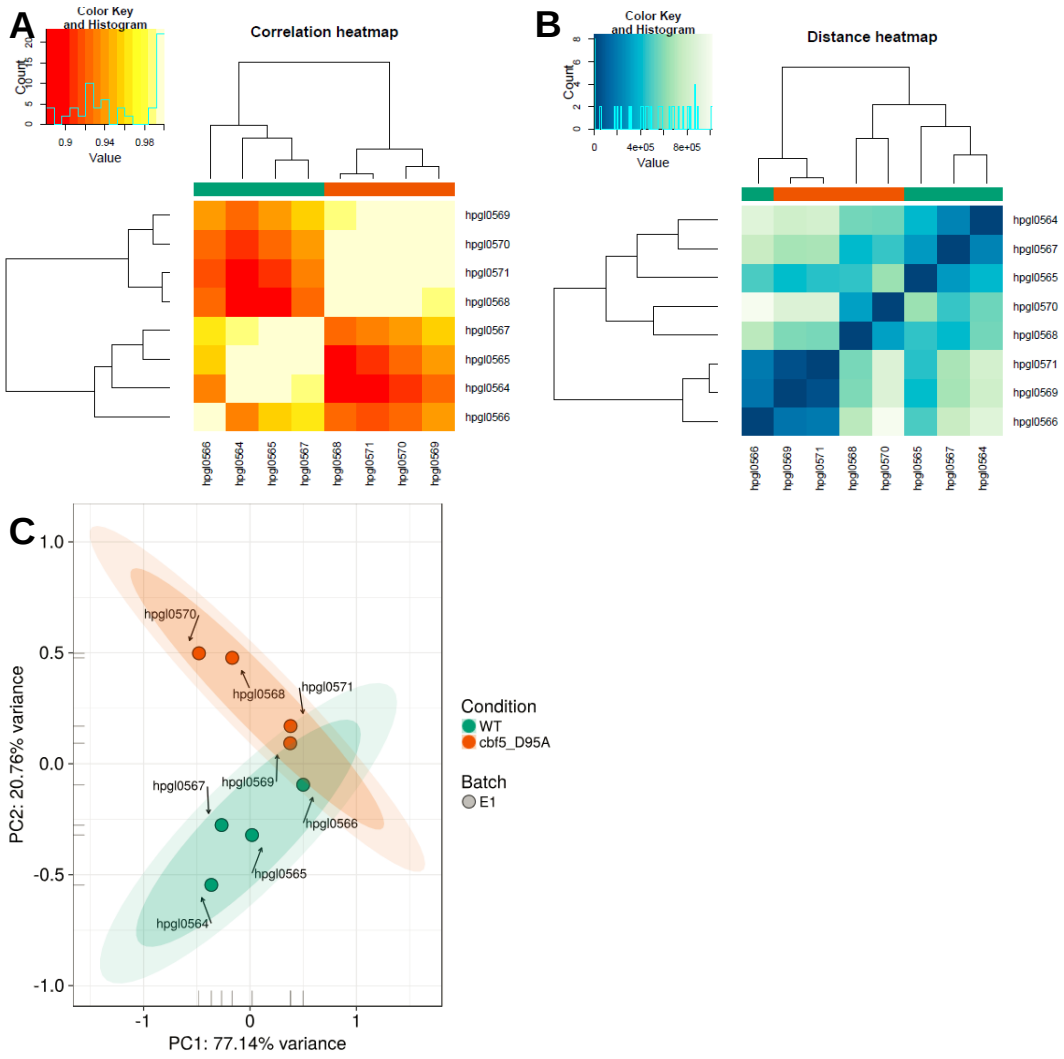

Figure 35. Quality control metrics reveal no outliers in E1

Hierarchical clustering analyses using **(A)** Pearson correlation and **(B)** Euclidean distances along with a **(C)** Principal Component Analyses of the log_2, cpm, quantile, and low-count filtered data suggested no outliers were present.

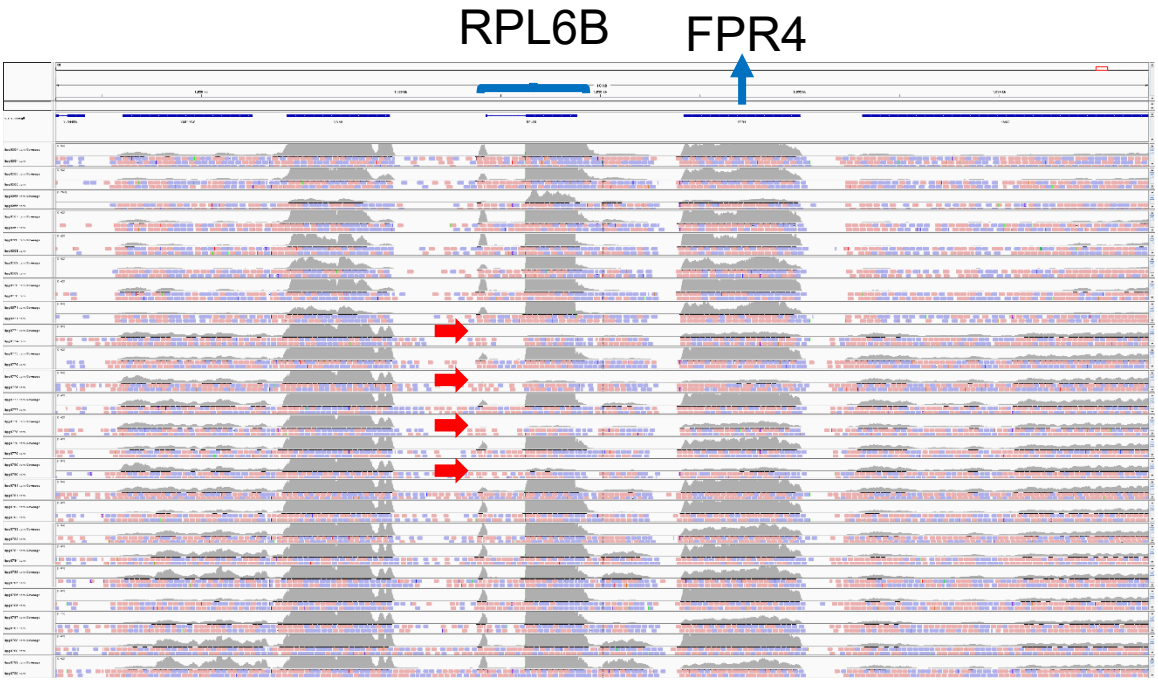

Figure 36. Screenshot from Integrated Genomics Viewer (IGV) displaying peculiar pattern of E2B1 in a region of chromosome XII

Genes in this region of chromosome XII and sample IDs are labeled. Red arrows point at samples hpgl0774, hpgl0776, hpgl0778, and hpgl0780 (from top to bottom arrow), part of batch E2B1.

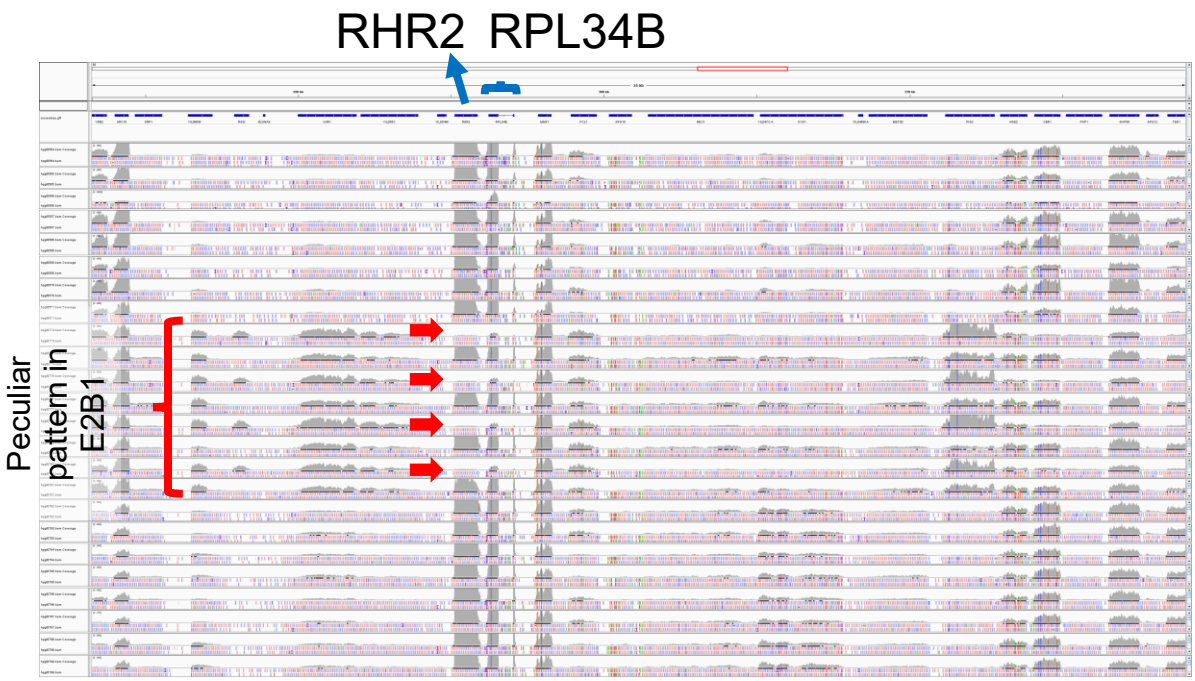

Figure 37. Screenshot from Integrated Genomics Viewer (IGV) displaying peculiar pattern of E2B1 in a region of chromosome IX

Genes in this region of chromosome IX and sample IDs are labeled. Red arrows point at samples hpgl0774, hpgl0776, hpgl0778, and hpgl0780 (from top to bottom arrow), part of batch E2B1.

Gene Ontology (GO) Analyses

A set of differentially expressed genes (fold-change ≥ 2, adjusted *P* value < 0.05) in each contrast was created, and gene ontology (GO) analyses were carried out. Each table below has up to top 10 biological processes (BP) and 10 molecular functions (MF) GO terms found in the analysis of each contrast. Tables 14 through 17 below are discussed within chapter 3. Complete results of the analyses can be found in Datasets E1E2_gprofiler_up_20180212.xlsx and E1E2_gprofiler_down_20180212.xlsx in the online repository.

Table 14. Top 20 gene ontology (GO) categories (biological processes, BP and metabolic functions, MF) enriched for *upf1Δ vs.* WT

	GO term	Adjusted *P* value	Number DE	Total number
***upf1Δ vs.* WT, up-regulated**				
GO:0022857	transmembrane transporter activity (MF)	5.96E-08	57	350
GO:0051321	meiotic cell cycle (BP)	7.34E-08	1751	308
GO:0048646	anatomical structure formation involved in morphogenesis (BP)	3.54E-07	36	181
GO:0030435	sporulation resulting in formation of a cellular spore (BP)	4.60E-07	35	174
GO:0044702	single organism reproductive process (BP)	5.21E-07	54	355
GO:0043834	sporulation (BP)	7.52E-07	35	177
GO:0005215	transporter activity (MF)	9.20E-07	63	436
GO:0022804	active transmembrane transporter activity (MF)	1.03E-06	33	170
GO:1903046	meiotic cell cycle process (BP)	2.03E-06	44	267
GO:0048856	anatomical structure development (BP)	5.80E-06	38	218
GO:0009653	anatomical structure morphogenesis (BP)	5.80E-06	38	218
GO:0055085	transmembrane transport (BP)	9.86E-06	63	462
GO:0030154	cell differentiation (BP)	1.03E-05	37	213
GO:0015291	secondary active transmembrane transporter activity (MF)	3.35E-05	21	107
GO:0052851	ferric-chelate reductase (NADPH) activity (MF)	4.79E-05	5	7
GO:0090484	drug transporter activity (MF)	7.58E-05	12	28

	GO term	Adjusted *P* value	Number DE	Total number
GO:0016723	oxidoreductase activity, oxidizing metal ions, NAD or NADP as acceptor (MF)	1.26E-04	5	8
GO:0000293	ferric-chelate reductase activity (MF)	1.26E-04	5	8
GO:0015293	symporter activity (MF)	3.51E-04	12	46
GO:1901476	carbohydrate transporter activity (MF)	1.05E-03	10	34
***upf1Δ vs.* WT, down-regulated**				
GO:0003735	structural constituent of ribosome (MF)	1.45E-76	146	233
GO:0005198	structural molecule activity (MF)	2.66E-51	168	396
GO:0002181	cytoplasmic translation (BP)	5.62E-38	100	202
GO:0006518	peptide metabolic process (BP)	6.05E-16	177	814
GO:0043603	cellular amide metabolic process (BP)	3.57E-15	181	880
GO:0043043	peptide biosynthetic process (BP)	1.04E-14	168	776
GO:0006412	translation (BP)	1.47E-14	167	772
GO:0043604	amide biosynthetic process (BP)	2.23E-14	174	821
GO:0033108	mitochondrial respiratory chain complex assembly (BP)	1.48E-11	25	39
GO:1901566	organonitrogen compound biosynthetic process (BP)	2.30E-11	231	1274
GO:0007005	mitochondrion organization (BP)	1.37E-10	76	273
GO:0065003	macromolecular complex assembly (BP)	2.02E-09	121	609

	GO term	Adjusted *P* value	Number DE	Total number
GO:0015078	hydrogen ion transmembrane transporter activity (MF)	7.00E-06	24	62
GO:0015077	monovalent inorganic cation transmembrane transporter activity (MF)	1.78E-05	26	74
GO:0009055	electron carrier activity (MF)	2.57E-04	21	55
GO:0019843	rRNA binding (MF)	4.78E-04	38	145
GO:0046982	protein heterodimerization activity (MF)	5.57E-03	12	35
GO:0044769	ATPase activity, coupled to transmembrane movement of ions, rotational mechanism (MF)	2.45E-02	10	21
GO:0008144	drug binding (MF)	4.85E-02	5	6

Cutoff for DE genes: fold change ≥ 2, adjusted *P* value cutoff of <0.05, by DEseq2. Number of DE genes and total number of genes in each of the top 20 GO terms are shown.

Table 15. Top 20 GO categories (BP and MF) enriched for *cbf5-D95A upf1Δ vs. cbf5-D95A*

	GO term	Adjusted *P* value	Number DE	Total number
***cbf5-D95A upf1Δ vs. cbf5-D95A*, up-regulated**				
GO:0051321	meiotic cell cycle (BP)	7.56E-10	59	308
GO:0044702	single organism reproductive process (BP)	4.14E-09	63	355
GO:1903046	meiotic cell cycle process (BP)	1.22E-07	50	267
GO:0000003	reproduction (BP)	6.90E-07	74	500
GO:0022414	reproductive process (BP)	9.73E-07	72	484

	GO term	Adjusted *P* value	Number DE	Total number
GO:0022857	transmembrane transporter activity (MF)	3.47E-06	53	350
GO:0035825	reciprocal DNA recombination (BP)	7.04E-06	20	68
GO:0007131	reciprocal meiotic recombination (BP)	7.04E-06	20	68
GO:0048646	anatomical structure formation involved in morphogenesis (BP)	2.32E-05	35	181
GO:0005215	transporter activity (MF)	2.46E-05	82	436
GO:0030435	sporulation resulting in formation of a cellular spore (BP)	2.84E-05	34	174
GO:0022804	active transmembrane transporter activity (MF)	4.03E-05	40	170
GO:0043934	sporulation (BP)	4.43E-05	34	177
GO:1901476	carbohydrate transporter activity (MF)	7.55E-04	14	34
GO:0015144	carbohydrate transmembrane transporter activity (MF)	7.55E-04	14	34
GO:0016723	oxidoreductase activity, oxidizing metal ions, NAD or NADP as acceptor (MF)	1.53E-03	6	8
GO:0000293	ferric-chelate reductase activity (MF)	1.53E-03	6	8
GO:0052851	ferric-chelate reductase (NADPH) activity (MF)	3.09E-03	4	7
GO:0015291	secondary active transmembrane transporter activity (MF)	4.90E-03	26	107
GO:0090484	drug transporter activity (MF)	6.28E-03	10	28

	GO term	Adjusted *P* value	Number DE	Total number
***cbf5-D95A upf1Δ vs. cbf5-D95A*, down-regulated**				
GO:0003735	structural constituent of ribosome (MF)	7.32E-48	125	233
GO:0005198	structural molecule activity (MF)	6.32E-33	152	396
GO:0032543	mitochondrial translation (BP)	1.61E-32	89	168
GO:0043933	macromolecular complex subunit organization (BP)	4.36E-12	169	718
GO:0034622	cellular macromolecular complex assembly (BP)	6.37E-12	140	557
GO:0065003	macromolecular complex assembly (BP)	8.62E-12	149	609
GO:0043043	peptide biosynthetic process (BP)	7.20E-10	171	776
GO:0006412	translation (BP)	9.16E-10	170	772
GO:0006518	peptide metabolic process (BP)	1.83E-09	176	814
GO:0007005	mitochondrion organization (BP)	4.05E-09	80	273
GO:0043604	amide biosynthetic process (BP)	4.07E-09	176	821
GO:0017004	cytochrome complex assembly (BP)	3.28E-08	22	36
GO:0005515	protein binding (MF)	2.71E-07	123	808
GO:0044877	macromolecular complex binding (MF)	3.31E-06	39	128
GO:0016209	antioxidant activity (MF)	3.97E-05	17	35
GO:0046982	protein heterodimerization activity (MF)	2.19E-04	12	35
GO:0016684	oxidoreductase activity, acting on peroxide as acceptor (MF)	2.23E-04	11	17
GO:0004601	peroxidase activity (MF)	2.23E-04	11	17

	GO term	Adjusted *P* value	Number DE	Total number
GO:0046983	protein dimerization activity (MF)	2.87E-04	24	75
GO:0043022	ribosome binding (MF)	3.82E-04	14	28

Cutoff for DE genes: fold change ≥ 2, adjusted *P* value cutoff of <0.05, by DEseq2. Number of DE genes and total number of genes in each of the top 20 GO terms are shown.

Table 16. Top 20 GO categories (BP and MF) enriched for *cbf5-D95A upf1Δ vs. upf1Δ*

	GO term	Adjusted *P* value	Number DE	Total number
***cbf5-D95A upf1Δ vs. upf1Δ*, up-regulated**				
GO:0055114	oxidation-reduction process (BP)	1.04E-10	43	460
GO:0005975	carbohydrate metabolic process (BP)	1.12E-06	29	292
GO:0044712	single-organism catabolic process (BP)	1.66E-06	29	324
GO:0015291	secondary active transmembrane transporter activity (MF)	2.89E-06	17	107
GO:0044723	single-organism carbohydrate metabolic process (BP)	3.04E-06	25	242
GO:0016491	oxidoreductase activity (MF)	3.99E-06	30	338
GO:0044710	single-organism metabolic process (BP)	4.70E-06	76	1474
GO:0044282	small molecule catabolic process (BP)	5.77E-06	18	122
GO:0016052	carbohydrate catabolic process (BP)	3.43E-05	15	94

	GO term	Adjusted *P* value	Number DE	Total number
GO:0005984	disaccharide metabolic process (BP)	9.30E-05	9	32
GO:0031505	fungal-type cell wall organization (BP)	2.60E-04	21	204
GO:0009311	oligosaccharide metabolic process (BP)	2.85E-04	9	36
GO:0016614	oxidoreductase activity, acting on CH-OH group of donors (MF)	1.71E-03	12	83
GO:0022804	active transmembrane transporter activity (MF)	2.93E-03	17	170
GO:0016616	oxidoreductase activity, acting on the CH-OH group of donors, NAD or NADP as acceptor (MF)	5.38E-03	11	77
GO:0022857	transmembrane transporter activity (MF)	6.47E-03	25	350
GO:0015297	antiporter activity (MF)	6.75E-03	9	50
GO:1901476	carbohydrate transporter activity (MF)	1.08E-02	6	34
GO:0015144	carbohydrate transmembrane transporter activity (MF)	1.08E-02	6	34
GO:0000297	spermine transmembrane transporter activity (MF)	2.03E-02	3	4
***cbf5-D95A upf1Δ vs. upf1Δ*, down-regulated**				
GO:0007049	cell cycle (BP)	6.59E-11	39	783
GO:0022402	cell cycle process (BP)	5.01E-10	34	627
GO:0000278	mitotic cell cycle (BP)	1.99E-08	24	372

	GO term	Adjusted *P* value	Number DE	Total number
GO:1903047	mitotic cell cycle process (BP)	4.49E-08	23	352
GO:0071840	cellular component organization or biogenesis (BP)	1.98E-06	61	2438
GO:0044085	cellular component biogenesis (BP)	1.70E-04	33	1288
GO:0000280	nuclear division (BP)	2.24E-04	17	288
GO:0048285	organelle fission (BP)	3.83E-04	17	299
GO:0044770	cell cycle phase transition (BP)	2.08E-03	11	170
GO:0044772	mitotic cell cycle phase transition (BP)	2.08E-03	11	170
GO:0005200	structural constituent of cytoskeleton (MF)	4.13E-03	5	29
GO:1990939	ATP-dependent microtubule motor activity (MF)	2.03E-02	3	5

Cutoff for DE genes: fold change ≥ 2, adjusted *P* value cutoff of <0.05, by DEseq2. Number of DE genes and total number of genes in each of the top 20 GO terms are shown.

Table 17. Top 20 GO categories (BP and MF) enriched for *cbf5-D95A upf1Δ vs.* WT

	GO term	Adjusted *P* value	Number DE	Total number
***cbf5-D95A upf1Δ vs.* WT, up-regulated**				
GO:0055085	transmembrane transport (BP)	7.75E-15	117	462
GO:0006811	ion transport (BP)	2.02E-11	100	406
GO:0015688	iron chelate transport (BP)	1.94E-09	10	11
GO:0015891	siderophore transport (BP)	1.94E-09	10	11
GO:0031505	fungal-type cell wall organization (BP)	2.04E-09	53	204
GO:1901678	iron coordination entity transport (BP)	8.19E-09	10	16

	GO term	Adjusted *P* value	Number DE	Total number
GO:0045229	external encapsulating structure organization (BP)	8.79E-09	59	250
GO:0071555	cell wall organization (BP)	8.79E-09	59	250
GO:0071852	fungal-type cell wall organization or biogenesis (BP)	1.40E-08	57	236
GO:0005975	carbohydrate metabolic process (BP)	9.12E-08	73	292
GO:0022857	transmembrane transporter activity (MF)	1.42E-19	104	350
GO:0022804	active transmembrane transporter activity (MF)	2.13E-16	64	170
GO:0015291	secondary active transmembrane transporter activity (MF)	4.43E-15	47	107
GO:0005215	transporter activity (MF)	2.78E-14	109	436
GO:0022891	substrate-specific transmembrane transporter activity (MF)	4.26E-11	81	310
GO:0015075	ion transmembrane transporter activity (MF)	4.02E-10	71	264
GO:0015293	symporter activity (MF)	5.58E-10	25	46
GO:0008324	cation transmembrane transporter activity (MF)	6.82E-09	56	194
GO:0022892	substrate-specific transporter activity (MF)	1.03E-08	91	373
GO:0015294	solute:cation symporter activity (MF)	5.44E-08	21	39

	GO term	Adjusted *P* value	Number DE	Total number
***cbf5-D95A upf1Δ vs.* WT, down-regulated**				
GO:0002181	cytoplasmic translation (BP)	4.11E-26	90	202
GO:0032543	mitochondrial translation (BP)	6.97E-21	79	168
GO:0043933	macromolecular complex subunit organization (BP)	1.46E-18	196	718
GO:0065003	macromolecular complex assembly (BP)	1.68E-17	172	609
GO:0044085	cellular component biogenesis (BP)	2.44E-17	307	1288
GO:0034622	cellular macromolecular complex assembly (BP)	2.90E-17	161	557
GO:0071840	cellular component organization or biogenesis (BP)	7.43E-15	490	2438
GO:0010467	gene expression (BP)	8.79E-14	435	2120
GO:0006996	organelle organization (BP)	6.45E-13	314	1474
GO:0022607	cellular component assembly (BP)	9.25E-13	204	845
GO:0003735	structural constituent of ribosome (MF)	5.10E-75	158	233
GO:0005198	structural molecule activity (MF)	2.33E-51	188	396
GO:0005515	protein binding (MF)	1.03E-07	175	808
GO:0046983	protein dimerization activity (MF)	1.70E-06	31	75
GO:0046982	protein heterodimerization activity (MF)	5.44E-04	17	35
GO:0000988	transcription factor activity, protein binding (MF)	1.21E-03	43	137
GO:0044877	macromolecular complex binding (MF)	3.23E-03	40	128

	GO term	Adjusted *P* value	Number DE	Total number
GO:0000989	transcription factor activity, transcription factor binding (MF)	1.04E-02	39	129
GO:0004596	peptide alpha-N-acetyltransferase activity (MF)	1.38E-02	3	7
GO:0019843	rRNA binding (MF)	2.92E-02	41	145

Cutoff for DE genes: fold change ≥ 2, adjusted P value cutoff of <0.05, by DEseq2. Number of DE genes and total number of genes in each of the top 20 GO terms are shown.

Bibliography

1. Fox, G. E. Origin and evolution of the ribosome. *Cold Spring Harb. Perspect. Biol.* **2,** a003483 (2010).

2. Petrov, A. S. *et al.* History of the ribosome and the origin of translation. *Proc. Natl. Acad. Sci.* **112,** 15396–15401 (2015).

3. Woolford, J. L. & Baserga, S. J. Ribosome biogenesis in the yeast Saccharomyces cerevisiae. *Genetics* **195,** 643–81 (2013).

4. Schmeing, T. M. & Ramakrishnan, V. What recent ribosome structures have revealed about the mechanism of translation. *Nature* **461,** 1234–1242 (2009).

5. Blanchard, S. C., Kim, H. D., Gonzalez, R. L., Puglisi, J. D. & Chu, S. tRNA dynamics on the ribosome during translation. *Proc. Natl. Acad. Sci.* **101,** 12893–12898 (2004).

6. Ban, N. *et al.* The Complete Atomic Structure of the Large Ribosomal Subunit at 2.4 A Resolution. *Science (80-.).* **289,** 905–920 (2000).
7. Marygold, S. J. *et al.* The ribosomal protein genes and Minute loci of Drosophila melanogaster. *Genome Biol.* **8,** R216 (2007).

8. Kongsuwan, K. *et al.* A Drosophila Minute gene encodes a ribosomal protein. *Nature* **317,** 555–8 (1985).

9. Hart, K., Klein, T. & Wilcox, M. A Minute encoding a ribosomal protein enhances wing morphogenesis mutants. *Mech. Dev.* **43,** 101–10 (1993).

10. Andersson, S., Saebøe-Larssen, S., Lambertsson, A., Merriam, J. & Jacobs-Lorena, M. A Drosophila third chromosome Minute locus encodes a ribosomal protein. *Genetics* **137,** 513–20 (1994).

11. Saebøe-Larssen, S. & Lambertsson, A. A novel Drosophila Minute locus encodes ribosomal protein S13. *Genetics* **143,** 877–85 (1996).

12. Schmidt, A., Hollmann, M. & Schäfer, U. A newly identified Minute locus, M(2)32D, encodes the ribosomal protein L9 in Drosophila melanogaster. *Mol. Gen. Genet.* **251,** 381–7 (1996).

13. Saebøe-Larssen, S., Urbanczyk Mohebi, B. & Lambertsson, A. The Drosophila ribosomal protein L14-encoding gene, identified by a novel Minute mutation in a dense cluster of previously undescribed genes in cytogenetic region 66D. *Mol. Gen. Genet.* **255,** 141–51 (1997).

14. van Beest, M., Mortin, M. & Clevers, H. Drosophila RpS3a, a novel Minute gene situated between the segment polarity genescubitus interruptus and dTCF. *Nucleic Acids Res.* **26,** 4471–5 (1998).

15. Török, I. *et al.* Down-regulation of RpS21, a putative translation initiation factor interacting with P40, produces viable minute imagos and larval lethality with overgrown hematopoietic organs and imaginal discs. *Mol. Cell. Biol.* **19,** 2308–21 (1999).

16. Marygold, S. J., Coelho, C. M. A. & Leevers, S. J. Genetic Analysis of RpL38 and RpL5, Two Minute Genes Located in the Centric Heterochromatin of Chromosome 2 of Drosophila melanogaster. *Genetics* **169,** 683–695 (2005).

17. Alexander, S. J., Woodling, N. S. & Yedvobnick, B. Insertional inactivation of the L13a ribosomal protein gene of Drosophila melanogaster identifies a new Minute locus. *Gene* **368,** 46–52 (2006).

18. De Keersmaecker, K., Sulima, S. O. & Dinman, J. D. Ribosomopathies and the paradox of cellular hypo- to hyperproliferation. *Blood* **125,** 1377–82 (2015).

19. Nakhoul, H. *et al.* Ribosomopathies: mechanisms of disease. *Clin. Med. insights. Blood Disord.* **7,** 7–16 (2014).

20. Narla, A. & Ebert, B. L. Ribosomopathies: human disorders of ribosome dysfunction. *Blood* **115,** 3196–205 (2010).

21. Dameshek, W. Riddle: What do Aplastic Anemia, Paroxysmal Nocturnal Hemoglobinuria (PNH and 'Hypoplastic' Leukemia Have in Common? *Blood* **30,** 251–254 (1967).

22. Sulima, S. O., Hofman, I. J. F., De Keersmaecker, K. & Dinman, J. D. How Ribosomes Translate Cancer. *Cancer Discov.* **7,** 1069–1087 (2017).

23. Sulima, S. O. *et al.* Bypass of the pre-60S ribosomal quality control as a pathway to oncogenesis. *Proc. Natl. Acad. Sci. U. S. A.* **111,** 5640–5 (2014).

24. Diamond, L. K. & Blackfan, K. D. Hypoplastic anemia. *Am. J. Dis. Child.* **56,** 464–467 (1938).

25. Ball, S. E., McGuckin, C. P., Jenkins, G. & Gordon-Smith, E. C. Diamond-Blackfan anaemia in the U.K.: analysis of 80 cases from a 20-year birth

cohort. *Br. J. Haematol.* **94,** 645–653 (1996).

26. Willig, T.-N. *et al.* Identification of New Prognosis Factors from the Clinical and Epidemiologic Analysis of a Registry of 229 Diamond-Blackfan Anemia Patients. *Pediatr. Res.* **46,** 553–553 (1999).

27. Doherty, L. *et al.* Ribosomal Protein Genes RPS10 and RPS26 Are Commonly Mutated in Diamond-Blackfan Anemia. *Am. J. Hum. Genet.* **86,** 222–228 (2010).

28. Landowski, M. *et al.* Novel deletion of RPL15 identified by array-comparative genomic hybridization in Diamond–Blackfan anemia. *Hum. Genet.* **132,** 1265–1274 (2013).

29. Armistead, J. & Triggs-Raine, B. Diverse diseases from a ubiquitous process: the ribosomopathy paradox. *FEBS Lett.* **588,** 1491–500 (2014).

30. Gazda, H. T. *et al.* Ribosomal protein L5 and L11 mutations are associated with cleft palate and abnormal thumbs in Diamond-Blackfan anemia patients. *Am. J. Hum. Genet.* **83,** 769–80 (2008).

31. McKusick, V. A. & Hamosh, A. # 105650 DIAMOND-BLACKFAN ANEMIA 1; DBA1. *Online Mendelian Inheritance in Man* (2018). at <https://www.omim.org/entry/105650?search=%23 105650&highlight=105650>

32. Vlachos, A. *et al.* Diagnosing and treating Diamond Blackfan anaemia: results of an international clinical consensus conference. *Br. J. Haematol.* **142,** 859–876 (2008).

33. Burgert, E. O., Kennedy, R. L. J. & Pease, G. L. Congenital Hypoplastic Anemia. *Pediatrics* **13,** (1954).

34. Cmejla, R., Cmejlova, J., Handrkova, H., Petrak, J. & Pospisilova, D. Ribosomal protein S17 gene (RPS17) is mutated in Diamond-Blackfan anemia. *Hum. Mutat.* **28,** 1178–1182 (2007).

35. Draptchinskaia, N. *et al.* The gene encoding ribosomal protein S19 is mutated in Diamond-Blackfananaemia. *Nat. Genet.* **21,** 169–175 (1999).

36. van Dooijeweert, B. *et al.* Pediatric Diamond-Blackfan anemia in the Netherlands: An overview of clinical characteristics and underlying molecular defects. *Eur. J. Haematol.* **100,** 163–170 (2018).

37. Gazda, H. T. *et al.* Frameshift mutation in p53 regulator RPL26 is associated with multiple physical abnormalities and a specific pre-

ribosomal RNA processing defect in diamond-blackfan anemia. *Hum. Mutat.* **33,** 1037–1044 (2012).

38. Gazda, H. T. *et al.* Ribosomal protein S24 gene is mutated in Diamond-Blackfan anemia. *Am. J. Hum. Genet.* **79,** 1110–8 (2006).

39. Farrar, J. E. *et al.* Abnormalities of the large ribosomal subunit protein, Rpl35a, in Diamond-Blackfan anemia. *Blood* **112,** 1582–92 (2008).

40. Willig, T.-N. *et al.* Mutations in Ribosomal Protein S19 Gene and Diamond Blackfan Anemia: Wide Variations in Phenotypic Expression. *Blood* **94,** (1999).

41. Boria, I. *et al.* The ribosomal basis of diamond-blackfan anemia: mutation and database update. *Hum. Mutat.* **31,** 1269–1279 (2010).

42. Gripp, K. W. *et al.* Diamond-Blackfan anemia with mandibulofacial dystostosis is heterogeneous, including the novel DBA genes TSR2 and RPS28. *Am. J. Med. Genet. A* **164A,** 2240–9 (2014).

43. Sankaran, V. G. *et al.* Exome sequencing identifies GATA1 mutations resulting in Diamond-Blackfan anemia. *J. Clin. Invest.* **122,** 2439–43 (2012).

44. Lipton, J. M., Atsidaftos, E., Zyskind, I. & Vlachos, A. Improving clinical care and elucidating the pathophysiology of Diamond Blackfan anemia: An update from the Diamond Blackfan Anemia Registry. *Pediatr. Blood Cancer* **46,** 558–564 (2006).

45. McKusick, V. A. & O'Neill, M. J. F. # 271400 ASPLENIA, ISOLATED CONGENITAL; ICAS. *Online Mendelian Inheritance in Man* (2014). at <https://www.omim.org/entry/271400?search=%23 271400&highlight=271400>

46. Bolze, A. *et al.* Ribosomal protein SA haploinsufficiency in humans with isolated congenital asplenia. *Science* **340,** 976–8 (2013).

47. Gilbert, B. *et al.* Familial isolated congenital asplenia: a rare, frequently hereditary dominant condition, often detected too late as a cause of overwhelming pneumococcal sepsis. Report of a new case and review of 31 others. *Eur. J. Pediatr.* **161,** 368–372 (2002).

48. Mahlaoui, N. *et al.* Isolated congenital asplenia: a French nationwide retrospective survey of 20 cases. *J. Pediatr.* **158,** 142–8, 148.e1 (2011).

49. Ban, N. *et al.* A new system for naming ribosomal proteins. *Curr. Opin. Struct. Biol.* **24,** 165–169 (2014).

50. McKusick, V. A. & Converse, P. J. # 153550 CHROMOSOME 5q DELETION SYNDROME. *Online Mendelian Inheritance in Man* (2016). at <https://www.omim.org/entry/153550?search=%23153550&highlight=153550>

51. Van Den Berghe, H. *et al.* Distinct haematological disorder with deletion of long arm of No. 5 chromosome. *Nature* **251,** 437–438 (1974).

52. Giagounidis, A. A. N., Germing, U. & Aul, C. Biological and prognostic significance of chromosome 5q deletions in myeloid malignancies. *Clin. Cancer Res.* **12,** 5–10 (2006).

53. Ebert, B. L. *et al.* Identification of RPS14 as a 5q- syndrome gene by RNA interference screen. *Nature* **451,** 335–339 (2008).

54. 5q minus syndrome. *Genetics Home Reference, National Library of Medicine* (2015). at <https://ghr.nlm.nih.gov/condition/5q-minus-syndrome>

55. Heaney, M. L. & Golde, D. W. Myelodysplasia. *N. Engl. J. Med.* **340,** 1649–1660 (1999).

56. Boultwood, J., Lewis, S. & Wainscoat, J. The 5q-syndrome. *Blood* **84,** (1994).

57. Sokal, G. *et al.* A new hematologic syndrome with a distinct karyotype: the 5 q-- chromosome. *Blood* **46,** (1975).

58. Heiss, N. S. *et al.* X-linked dyskeratosis congenita is caused by mutations in a highly conserved gene with putative nucleolar functions. *Nat. Genet.* **19,** 32–8 (1998).

59. Knight, S. W. *et al.* X-linked dyskeratosis congenita is predominantly caused by missense mutations in the DKC1 gene. *Am. J. Hum. Genet.* **65,** 50–8 (1999).

60. McKusick, V. A. & Kniffin, C. L. # 305000 DYSKERATOSIS CONGENITA, X-LINKED; DKCX. *Online Mendelian Inheritance in Man* (2018). at <http://omim.org/entry/305000?search=305000&highlight=305000>

61. Jády, B. E., Ketele, A. & Kiss, T. Human intron-encoded Alu RNAs are processed and packaged into Wdr79-associated nucleoplasmic box H/ACA RNPs. *Genes Dev.* **26,** 1897–910 (2012).

62. Ge, J. & Yu, Y.-T. RNA pseudouridylation: new insights into an old modification. *Trends Biochem. Sci.* **38,** 210–8 (2013).

63. Ni, J., Tien, A. L. & Fournier, M. J. Small Nucleolar RNAs Direct Site-Specific Synthesis of Pseudouridine in Ribosomal RNA. *Cell* **89,** 565–573 (1997).

64. Charette, M. & Gray, M. W. Pseudouridine in RNA: what, where, how, and why. *IUBMB Life* **49,** 341–51 (2000).

65. Jiang, W., Middleton, K., Yoon, H. J., Fouquet, C. & Carbon, J. An essential yeast protein, CBF5p, binds in vitro to centromeres and microtubules. *Mol. Cell. Biol.* **13,** 4884–93 (1993).

66. Zebarjadian, Y., King, T., Fournier, M. J., Clarke, L. & Carbon, J. Point Mutations in Yeast CBF5 Can Abolish In Vivo Pseudouridylation of rRNA. *Mol. Cell. Biol.* **19,** 7461–7472 (1999).

67. Carlile, T. M. *et al.* Pseudouridine profiling reveals regulated mRNA pseudouridylation in yeast and human cells. *Nature* **515,** 143–146 (2014).

68. Paolini, N. A. *et al.* A Ribosomopathy Reveals Decoding Defective Ribosomes Driving Human Dysmorphism. *Am. J. Hum. Genet.* **100,** 506–522 (2017).

69. Wolfe, K. H. & Shields, D. C. Molecular evidence for an ancient duplication of the entire yeast genome. *Nature* **387,** 708–713 (1997).

70. Léger-Silvestre, I. *et al.* Specific Role for Yeast Homologs of the Diamond Blackfan Anemia-associated Rps19 Protein in Ribosome Synthesis. *J. Biol. Chem.* **280,** 38177–85 (2005).

71. Choesmel, V. *et al.* Impaired ribosome biogenesis in Diamond-Blackfan anemia. *Blood* **109,** 1275–83 (2007).

72. Flygare, J. *et al.* Human RPS19, the gene mutated in Diamond-Blackfan anemia, encodes a ribosomal protein required for the maturation of 40S ribosomal subunits. *Blood* **109,** 980–6 (2007).

73. Wang, R. *et al.* Loss of function mutations in *RPL27* and *RPS27* identified by whole-exome sequencing in Diamond-Blackfan anaemia. *Br. J. Haematol.* **168,** 854–864 (2015).

74. Komatsu, N. *et al.* Establishment and characterization of an erythropoietin-dependent subline, UT-7/Epo, derived from human

leukemia cell line, UT-7. *Blood* **82,** 456–64 (1993).

75. O'Donohue, M.-F., Choesmel, V., Faubladier, M., Fichant, G. & Gleizes, P.-E. Functional dichotomy of ribosomal proteins during the synthesis of mammalian 40S ribosomal subunits. *J. Cell Biol.* **190,** 853–66 (2010).

76. Mohler, K. & Ibba, M. Translational fidelity and mistranslation in the cellular response to stress. *Nat. Microbiol.* **2,** 17117 (2017).

77. Delarue, M. Aminoacyl-tRNA synthetases. *Curr. Opin. Struct. Biol.* **5,** 48–55 (1995).

78. Perona, J. J. & Gruic-Sovulj, I. in 1–41 (Springer, Dordrecht, 2013). doi:10.1007/128_2013_456

79. Jakubowski, H. & Goldman, E. Editing of errors in selection of amino acids for protein synthesis. *Microbiol. Rev.* **56,** 412–429 (1992).

80. Guo, M. *et al.* Paradox of mistranslation of serine for alanine caused by AlaRS recognition dilemma. *Nature* **462,** 808–812 (2009).

81. Beebe, K., De Pouplana, L. R. & Schimmel, P. Elucidation of tRNA-dependent editing by a class II tRNA synthetase and significance for cell viability. *EMBO J.* **22,** 668–675 (2003).

82. Perret, V. *et al.* Relaxation of a transfer RNA specificity by removal of modified nucleotides. *Nature* **344,** 787–789 (1990).

83. Söll, D. The accuracy of aminoacylation — ensuring the fidelity of the genetic code. *Experientia* **46,** 1089–1096 (1990).

84. Hopfield, J. J., Yamane, T., Yue, V. & Coutts, S. M. Direct experimental evidence for kinetic proofreading in amino acylation of tRNAIle. *Proc. Natl. Acad. Sci. U. S. A.* **73,** 1164–8 (1976).

85. Lin, S. X., Baltzinger, M. & Remy, P. Fast kinetic study of yeast phenylalanyl-tRNA synthetase: role of tRNAPhe in the discrimination between tyrosine and phenylalanine. *Biochemistry* **23,** 4109–4116 (1984).

86. Yamane, T. & Hopfield, J. J. Experimental evidence for kinetic proofreading in the aminoacylation of tRNA by synthetase. *Proc. Natl. Acad. Sci. U. S. A.* **74,** 2246–50 (1977).

87. Ellis, N. & Gallant, J. An estimate of the global error frequency in translation. *MGG Mol. Gen. Genet.* **188,** 169–172 (1982).

88. Plant, E. P., Wang, P., Jacobs, J. L. & Dinman, J. D. A programmed -1 ribosomal frameshift signal can function as a cis-acting mRNA destabilizing element. *Nucleic Acids Res.* **32,** 784–90 (2004).

89. Dinman, J. D., Icho, T. & Wickner, R. B. A -1 ribosomal frameshift in a double-stranded RNA virus of yeast forms a gag-pol fusion protein. *Proc. Natl. Acad. Sci. U. S. A.* **88,** 174–8 (1991).

90. Wohlgemuth, I., Pohl, C. & Rodnina, M. V. Optimization of speed and accuracy of decoding in translation. *EMBO J.* **29,** 3701–9 (2010).

91. Kurland, C. G. Translational Accuracy And The Fitness Of Bacteria. *Annu. Rev. Genet.* **26,** 29–50 (1992).

92. Edelmann, P. & Gallant, J. Mistranslation in E. coli. *Cell* **10,** 131–137 (1977).

93. Loftfield, R. B. The frequency of errors in protein biosynthesis. *Biochem. J.* **89,** 82–92 (1963).

94. Loftfield, R. B. & Vanderjagt, D. The frequency of errors in protein biosynthesis. *Biochem. J.* **128,** 1353 (1972).

95. Parker, J. Errors and alternatives in reading the universal genetic code. *Microbiol. Rev.* **53,** 273–98 (1989).

96. Jacks, T. & Varmus, H. E. Expression of the Rous sarcoma virus pol gene by ribosomal frameshifting. *Science* **230,** 1237–42 (1985).

97. Jacks, T., Madhani, H. D., Masiarz, F. R. & Varmus, H. E. Signals for ribosomal frameshifting in the Rous sarcoma virus gag-pol region. *Cell* **55,** 447–58 (1988).

98. Jacks, T. *et al.* Characterization of ribosomal frameshifting in HIV-1 gag-pol expression. *Nature* **331,** 280–283 (1988).

99. Dinman, J. D. Mechanisms and implications of programmed translational frameshifting. *Wiley Interdiscip. Rev. RNA* **3,** 661–73 (2012).

100. Advani, V. M. Establishing link between translational recoding and human disease. (University of Maryland, 2015). doi:10.13016/M2FP6V

101. Belew, A. T., Hepler, N. L., Jacobs, J. L. & Dinman, J. D. PRFdb: a database of computationally predicted eukaryotic programmed -1 ribosomal frameshift signals. *BMC Genomics* **9,** 339 (2008).

102. Belew, A. T. & Dinman, J. D. Cell cycle control (and more) by programmed -1 ribosomal frameshifting: implications for disease and therapeutics. *Cell Cycle* **14,** 172–8 (2015).

103. Belew, A. T., Advani, V. M. & Dinman, J. D. Endogenous ribosomal frameshift signals operate as mRNA destabilizing elements through at least two molecular pathways in yeast. *Nucleic Acids Res.* **39,** 2799–808 (2011).

104. Advani, V. M., Belew, A. T. & Dinman, J. D. Yeast telomere maintenance is globally controlled by programmed ribosomal frameshifting and the nonsense-mediated mRNA decay pathway. *Transl. (Austin, Tex.)* **1,** e24418 (2013).

105. Belew, A. T. *et al.* Ribosomal frameshifting in the CCR5 mRNA is regulated by miRNAs and the NMD pathway. *Nature* **512,** 265–9 (2014).

106. Advani, V. M. & Dinman, J. D. Reprogramming the genetic code: The emerging role of ribosomal frameshifting in regulating cellular gene expression. *Bioessays* **38,** 21–6 (2015).

107. Liao, P.-Y., Choi, Y. S., Dinman, J. D. & Lee, K. H. The many paths to frameshifting: kinetic modelling and analysis of the effects of different elongation steps on programmed -1 ribosomal frameshifting. *Nucleic Acids Res.* **39,** 300–12 (2011).

108. Plant, E. P. & Dinman, J. D. Torsional restraint: a new twist on frameshifting pseudoknots. *Nucleic Acids Res.* **33,** 1825–33 (2005).

109. Matsufuji, S. *et al.* Autoregulatory frameshifting in decoding mammalian ornithine decarboxylase antizyme. *Cell* **80,** 51–60 (1995).

110. Belcourt, M. F. & Farabaugh, P. J. Ribosomal frameshifting in the yeast retrotransposon Ty: tRNAs induce slippage on a 7 nucleotide minimal site. *Cell* **62,** 339–352 (1990).

111. Wang, X., Wong, S.-M. & Liu, D. X. Identification of Hepta- and Octo-Uridine stretches as sole signals for programmed +1 and -1 ribosomal frameshifting during translation of SARS-CoV ORF 3a variants. *Nucleic Acids Res.* **34,** 1250–1260 (2006).

112. Ivanov, I. P., Matsufuji, S., Murakami, Y., Gesteland, R. F. & Atkins, J. F. Conservation of polyamine regulation by translational frameshifting from yeast to mammals. *EMBO J.* **19,** 1907–17 (2000).

113. Ivanov, I. P., Anderson, C. B., Gesteland, R. F. & Atkins, J. F. Identification of a new antizyme mRNA+ 1 frameshifting stimulatory pseudoknot in a subset of diverse invertebrates and its apparent absence in intermediate species. *J. Mol. Biol.* **339,** 495–504 (2004).

114. Wills, N. M., Gesteland, R. F. & Atkins, J. F. Evidence that a downstream pseudoknot is required for translational read-through of the Moloney murine leukemia virus gag stop codon. *Proc. Natl. Acad. Sci. U. S. A.* **88,** 6991–5 (1991).

115. Yoshinaka, Y., Katoh, I., Copeland, T. D. & Oroszlan, S. Murine leukemia virus protease is encoded by the gag-pol gene and is synthesized through suppression of an amber termination codon. *Proc. Natl. Acad. Sci. U. S. A.* **82,** 1618–22 (1985).

116. Leibundgut, M., Frick, C., Thanbichler, M., Böck, A. & Ban, N. Selenocysteine tRNA-specific elongation factor SelB is a structural chimaera of elongation and initiation factors. *EMBO J.* **24,** 11–22 (2005).

117. Schomburg, L., Schweizer, U. & Köhrle, J. Selenium and selenoproteins in mammals: Extraordinary, essential, enigmatic. *Cell. Mol. Life Sci.* **61,** 1988–1995 (2004).

118. Hao, B. *et al.* A new UAG-encoded residue in the structure of a methanogen methyltransferase. *Science (80-.).* **296,** 1462–1466 (2002).

119. Harger, J. W. & Dinman, J. D. An in vivo dual-luciferase assay system for studying translational recoding in the yeast Saccharomyces cerevisiae. *RNA* **9,** 1019–1024 (2003).

120. Rakauskaite, R., Liao, P.-Y., Rhodin, M. H. J., Lee, K. & Dinman, J. D. A rapid, inexpensive yeast-based dual-fluorescence assay of programmed--1 ribosomal frameshifting for high-throughput screening. *Nucleic Acids Res.* **39,** e97 (2011).

121. Loughran, G., Howard, M. T., Firth, A. E. & Atkins, J. F. Avoidance of reporter assay distortions from fused dual reporters. *RNA* **23,** 1285–1289 (2017).

122. Jacobs, J. L. & Dinman, J. D. Systematic analysis of bicistronic reporter assay data. *Nucleic Acids Res.* **32,** e160 (2004).

123. Gietz, R. D. & Schiestl, R. H. High-efficiency yeast transformation using the LiAc/SS carrier DNA/PEG method. *Nat. Protoc.* **2,** 31–34 (2007).

124. Ito, H., Fukuda, Y., Murata, K. & Kimura, A. Transformation of intact yeast

cells treated with alkali cations. *J. Bacteriol.* **153,** 163–8 (1983).

125. Hegemann, J. H., Güldener, U. & Köhler, G. J. Gene disruption in the budding yeast Saccharomyces cerevisiae. *Methods Mol. Biol.* **313,** 129–44 (2006).

126. Gueldener, U., Heinisch, J., Koehler, G. J., Voss, D. & Hegemann, J. H. A second set of loxP marker cassettes for Cre-mediated multiple gene knockouts in budding yeast. *Nucleic Acids Res.* **30,** e23 (2002).

127. Bolger, A. M., Lohse, M. & Usadel, B. Trimmomatic: a flexible trimmer for Illumina sequence data. *Bioinformatics* **30,** 2114–2120 (2014).

128. Langmead, B. & Salzberg, S. L. Fast gapped-read alignment with Bowtie 2. *Nat. Methods* **9,** 357–359 (2012).

129. Li, H. *et al.* The Sequence Alignment/Map format and SAMtools. *Bioinformatics* **25,** 2078–9 (2009).

130. Anders, S., Pyl, P. T. & Huber, W. HTSeq--a Python framework to work with high-throughput sequencing data. *Bioinformatics* **31,** 166–169 (2015).

131. Leek, J. T. & Storey, J. D. Capturing Heterogeneity in Gene Expression Studies by Surrogate Variable Analysis. *PLoS Genet.* **3,** e161 (2007).

132. Gagnon-Bartsch, J. A. & Speed, T. P. Using control genes to correct for unwanted variation in microarray data. *Biostatistics* **13,** 539–552 (2012).

133. Ritchie, M. E. *et al.* limma powers differential expression analyses for RNA-sequencing and microarray studies. *Nucleic Acids Res.* **43,** e47–e47 (2015).

134. Love, M. I., Huber, W. & Anders, S. Moderated estimation of fold change and dispersion for RNA-seq data with DESeq2. *Genome Biol.* **15,** 550 (2014).

135. Robinson, M. D., McCarthy, D. J. & Smyth, G. K. edgeR: a Bioconductor package for differential expression analysis of digital gene expression data. *Bioinformatics* **26,** 139–140 (2010).

136. Reimand, J. *et al.* g:Profiler-a web server for functional interpretation of gene lists (2016 update). *Nucleic Acids Res.* **44,** W83-9 (2016).

137. Song, H., Baxter-Roshek, J. L., Dinman, J. D. & Vakharia, V. N. Efficient expression of the 15-kDa form of infectious pancreatic necrosis virus VP5

by suppression of a UGA codon. *Virus Res.* **122,** 61–68 (2006).

138. Plant, E. P. *et al.* Differentiating between near- and non-cognate codons in Saccharomyces cerevisiae. *PLoS One* **2,** e517 (2007).

139. Rakwalska, M. & Rospert, S. The Ribosome-Bound Chaperones RAC and Ssb1/2p Are Required for Accurate Translation in Saccharomyces cerevisiae. *Mol. Cell. Biol.* **24,** 9186–9197 (2004).

140. Wilson, W. *et al.* HIV expression strategies: Ribosomal frameshifting is directed by a short sequence in both mammalian and yeast systems. *Cell* **55,** 1159–1169 (1988).

141. Shigemoto, K. *et al.* Identification and characterisation of a developmentally regulated mammalian gene that utilises -1 programmed ribosomal frameshifting. *Nucleic Acids Res.* **29,** 4079–88 (2001).

142. Manktelow, E., Shigemoto, K. & Brierley, I. Characterization of the frameshift signal of Edr, a mammalian example of programmed -1 ribosomal frameshifting. *Nucleic Acids Res.* **33,** 1553–63 (2005).

143. Shedlovskiy, D., Zinskie, J. A., Gardner, E., Pestov, D. G. & Shcherbik, N. Endonucleolytic cleavage in the expansion segment 7 of 25S rRNA is an early marker of low-level oxidative stress in yeast. *J. Biol. Chem.* **292,** 18469–18485 (2017).

144. Karthikeyan, G., Lewis, L. K. & Resnick, M. A. The mitochondrial protein frataxin prevents nuclear damage. *Hum. Mol. Genet.* **11,** 1351–1362 (2002).

145. Payne, T. *et al.* Transcript-specific translational regulation in the unfolded protein response of Saccharomyces cerevisiae. *FEBS Lett.* **582,** 503–509 (2008).

146. Xue, S. & Barna, M. Specialized ribosomes: a new frontier in gene regulation and organismal biology. *Nat. Rev. Mol. Cell Biol.* **13,** 355–69 (2012).

147. Gilbert, W. V. Functional specialization of ribosomes? *Trends Biochem. Sci.* **36,** 127–32 (2011).

148. Kondrashov, N. *et al.* Ribosome-mediated specificity in Hox mRNA translation and vertebrate tissue patterning. *Cell* **145,** 383–397 (2011).

149. Mills, E. W. & Green, R. Ribosomopathies: There's strength in numbers. *Science* **358,** eaan2755 (2017).

150. Lackner, D. H. *et al.* A network of multiple regulatory layers shapes gene expression in fission yeast. *Mol. Cell* **26,** 145–55 (2007).

151. Marguerat, S. *et al.* Quantitative analysis of fission yeast transcriptomes and proteomes in proliferating and quiescent cells. *Cell* **151,** 671–83 (2012).

152. Marshall, E., Stansfield, I. & Romano, M. C. Ribosome recycling induces optimal translation rate at low ribosomal availability. *J. R. Soc. Interface* **11,** 20140589 (2014).

153. Ludwig, L. S. *et al.* Altered translation of GATA1 in Diamond-Blackfan anemia. *Nat. Med.* **20,** 748–753 (2014).

154. Jack, K. *et al.* rRNA pseudouridylation defects affect ribosomal ligand binding and translational fidelity from yeast to human cells. *Mol. Cell* **44,** 660–6 (2011).

155. Kirwan, M. & Dokal, I. Dyskeratosis congenita: a genetic disorder of many faces. *Clin. Genet.* **73,** 103–112 (2007).

156. Mitchell, J. R., Wood, E. & Collins, K. A telomerase component is defective in the human disease dyskeratosis congenita. *Nature* **402,** 551–555 (1999).

157. Parenteau, J. *et al.* Preservation of Gene Duplication Increases the Regulatory Spectrum of Ribosomal Protein Genes and Enhances Growth under Stress. *Cell Rep.* **13,** 2516–2526 (2015).

158. Lawler, J. F., Merkulov, G. V, Boeke, J. D. & Boeke, J. D. Frameshift signal transplantation and the unambiguous analysis of mutations in the yeast retrotransposon Ty1 Gag-Pol overlap region. *J. Virol.* **75,** 6769–75 (2001).

159. Kervestin, S. & Jacobson, A. NMD: a multifaceted response to premature translational termination. *Nat. Rev. Mol. Cell Biol.* **13,** 700–12 (2012).

160. Held, K. D., Sylvester, F. C., Hopcia, K. L. & Biaglow, J. E. Role of Fenton Chemistry in Thiol-Induced Toxicity and Apoptosis. *Radiat. Res.* **145,** 542 (1996).

161. Zhou, M., Diwu, Z., Panchuk-Voloshina, N. & Haugland, R. P. A stable nonfluorescent derivative of resorufin for the fluorometric determination of trace hydrogen peroxide: Applications in detecting the activity of phagocyte NADPH oxidase and other oxidases. *Anal. Biochem.* **253,**

162–168 (1997).

162. Votyakova, T. V & Reynolds, I. J. DeltaPsi(m)-Dependent and -independent production of reactive oxygen species by rat brain mitochondria. *J. Neurochem.* **79,** 266–77 (2001).

163. Mohanty, J. G., Jaffe, J. S., Schulman, E. S. & Raible, D. G. A highly sensitive fluorescent micro-assay of H2O2 release from activated human leukocytes using a dihydroxyphenoxazine derivative. *J. Immunol. Methods* **202,** 133–141 (1997).

164. Song, C., Al-Mehdi, A. B. & Fisher, A. B. An immediate endothelial cell signaling response to lung ischemia. *Am. J. Physiol. Lung Cell. Mol. Physiol.* **281,** L993–L1000 (2001).

165. Elbein, A. D. The tunicamycins — useful tools for studies on glycoproteins. *Trends Biochem. Sci.* **6,** 219–221 (1981).

166. Kozutsumi, Y., Segal, M., Normington, K., Gething, M.-J. & Sambrook, J. The presence of malfolded proteins in the endoplasmic reticulum signals the induction of glucose-regulated proteins. *Nature* **332,** 462–464 (1988).

167. Cox, J. S., Shamu, C. E. & Walter, P. Transcriptional Induction of Genes Encoding Endoplasmic-Reticulum Resident Proteins Requires a Transmembrane Protein-Kinase. *Cell* **73,** 1197–1206 (1993).

168. Mori, K., Ma, W., Gething M, J. & Sambrook, J. A transmembrane protein with a cdc2-positive-cdc28-related kinase activity is required for signaling from the er to the nucleus. *Cell* **74,** 743–756 (1993).

169. Welihinda, A. A. & Kaufman, R. J. The unfolded protein response pathway in Saccharomyces cerevisiae. Oligomerization and trans-phosphorylation of Ire1p (Ern1p) are required for kinase activation. *J. Biol. Chem.* **271,** 18181–7 (1996).

170. Shamu, C. E. & Walter, P. Oligomerization and phosphorylation of the Ire1p kinase during intracellular signaling from the endoplasmic reticulum to the nucleus. *EMBO J.* **15,** 3028–39 (1996).

171. Cox, J. S. & Walter, P. A novel mechanism for regulating activity of a transcription factor that controls the unfolded protein response. *Cell* **87,** 391–404 (1996).

172. Yoshida, H., Matsui, T., Yamamoto, A., Okada, T. & Mori, K. XBP1 mRNA is induced by ATF6 and spliced by IRE1 in response to ER stress to produce a highly active transcription factor. *Cell* **107,** 881–91 (2001).

173. Calfon, M. *et al.* IRE1 couples endoplasmic reticulum load to secretory capacity by processing the XBP-1 mRNA. *Nature* **415,** 92–96 (2002).

174. Warner, J. R. The economics of ribosome biosynthesis in yeast. *Trends Biochem. Sci.* **24,** 437–440 (1999).

175. François, J. & Parrou, J. L. Reserve carbohydrates metabolism in the yeast Saccharomyces cerevisiae. *FEMS Microbiol. Rev.* **25,** 125–45 (2001).

176. Kniffin, C. L. # 617412 BRACHYCEPHALY, TRICHOMEGALY, AND DEVELOPMENTAL DELAY; BTDD. *Online Mendelian Inheritance in Man* (2017). at <https://www.omim.org/entry/617412>

177. Stark, H. *et al.* Ribosome interactions of aminoacyl-tRNA and elongation factor Tu in the codon-recognition complex. *Nat. Struct. Biol.* **9,** 849 (2002).

178. Yates, J. L. Role of ribosomal protein S12 in discrimination of aminoacyl-tRNA. *J. Biol. Chem.* **254,** 11550–11554 (1979).

179. Lodmell, J. S. & Dahlberg, A. E. A conformational switch in Escherichia coli 16S ribosomal RNA during decoding of messenger RNA. *Science* **277,** 1262–7 (1997).

180. Ogle, J. M. *et al.* Recognition of cognate transfer RNA by the 30S ribosomal subunit. *Science* **292,** 897–902 (2001).

181. Sharma, D., Cukras, A. R., Rogers, E. J., Southworth, D. R. & Green, R. Mutational Analysis of S12 Protein and Implications for the Accuracy of Decoding by the Ribosome. *J. Mol. Biol.* **374,** 1065–1076 (2007).

182. Anthony, R. A. & Liebman, S. W. Alterations in ribosomal protein RPS28 can diversely affect translational accuracy in Saccharomyces cerevisiae. *Genetics* **140,** (1995).

183. Synetos, D., Frantziou, C. P. & Alksne, L. E. Mutations in yeast ribosomal proteins S28 and S4 affect the accuracy of translation and alter the sensitivity of the ribosomes to paromomycin. *Biochim. Biophys. Acta (BBA)-Gene Struct. Expr.* **1309,** 156–166 (1996).

184. Singleton, R. S. *et al.* OGFOD1 catalyzes prolyl hydroxylation of RPS23 and is involved in translation control and stress granule formation. *Proc. Natl. Acad. Sci. U. S. A.* **111,** 4031–6 (2014).

185. Loenarz, C. *et al.* Hydroxylation of the eukaryotic ribosomal decoding center affects translational accuracy. *Proc. Natl. Acad. Sci. U. S. A.* **111,** 4019–24 (2014).

186. Cukras, A. R., Southworth, D. R., Brunelle, J. L., Culver, G. M. & Green, R. Ribosomal proteins S12 and S13 function as control elements for translocation of the mRNA:tRNA complex. *Mol. Cell* **12,** 321–8 (2003).

187. Arimoto, K., Fukuda, H., Imajoh-Ohmi, S., Saito, H. & Takekawa, M. Formation of stress granules inhibits apoptosis by suppressing stress-responsive MAPK pathways. *Nat. Cell Biol.* **10,** 1324–1332 (2008).

188. Tourrière, H. *et al.* The RasGAP-associated endoribonuclease G3BP assembles stress granules. *J. Cell Biol.* **160,** 823–31 (2003).

189. Zhang, X. *et al.* Mutations in QARS, Encoding Glutaminyl-tRNA Synthetase, Cause Progressive Microcephaly, Cerebral-Cerebellar Atrophy, and Intractable Seizures. *Am. J. Hum. Genet.* **94,** 547–558 (2014).

190. Kedersha, N. *et al.* Evidence That Ternary Complex (eIF2-GTP-tRNA $_{i}^{Met}$)–Deficient Preinitiation Complexes Are Core Constituents of Mammalian Stress Granules. *Mol. Biol. Cell* **13,** 195–210 (2002).

191. Netzer, N. *et al.* Innate immune and chemically triggered oxidative stress modifies translational fidelity. *Nature* **462,** 522–526 (2009).

192. Warner, J. R. & McIntosh, K. B. How common are extraribosomal functions of ribosomal proteins? *Mol. Cell* **34,** 3–11 (2009).

193. Weisberg, R. A. Transcription by moonlight: structural basis of an extraribosomal activity of ribosomal protein S10. *Mol. Cell* **32,** 747–8 (2008).

194. Wool, I. G. Extraribosomal functions of ribosomal proteins. *Trends Biochem. Sci.* **21,** 164–165 (1996).

195. Gupta, V. & Warner, J. R. Ribosome-omics of the human ribosome. *RNA* **20,** 1004–13 (2014).

196. Herruer, M. H. *et al.* Transcriptional control of yeast ribosomal protein synthesis during carbon-source upshift. *Nucleic Acids Res.* **15,** 10133–44 (1987).

197. Lucioli, A. *et al.* Gene dosage alteration of L2 ribosomal protein genes in Saccharomyces cerevisiae: effects on ribosome synthesis. *Mol. Cell.*

Biol. **8,** 4792–8 (1988).

198. Rotenberg, M. O., Moritz, M. & Woolford, J. L. Depletion of Saccharomyces cerevisiae ribosomal protein L16 causes a decrease in 60S ribosomal subunits and formation of half-mer polyribosomes. *Genes Dev.* **2,** 160 (1988).

199. Simoff, I., Moradi, H. & Nygård, O. Functional characterization of ribosomal protein L15 from Saccharomyces cerevisiae. *Curr. Genet.* **55,** 111–125 (2009).

200. Fan, Y. *et al.* Protein mistranslation protects bacteria against oxidative stress. *Nucleic Acids Res.* **43,** 1740–1748 (2015).

201. Singer, M. A. & Lindquist, S. Thermotolerance in Saccharomyces cerevisiae: the Yin and Yang of trehalose. *Trends Biotechnol.* **16,** 460–468 (1998).

202. Thevelein, J. M. Regulation of trehalase mobilization in fungi. *Microbiol. Rev.* **48,** 42–59 (1984).

203. Seo, Y., Kingsley, S., Walker, G., Mondoux, M. A. & Tissenbaum, H. A. Metabolic shift from glycogen to trehalose promotes lifespan and healthspan inCaenorhabditis elegans. *Proc. Natl. Acad. Sci. U. S. A.* **115,** E2791–E2800 (2018).

204. Chen, Q., Ma, E., Behar, K. L., Xu, T. & Haddad, G. G. Role of trehalose phosphate synthase in anoxia tolerance and development in Drosophila melanogaster. *J. Biol. Chem.* **277,** 3274–9 (2002).

205. Jia, Q. *et al.* Transcriptome Analysis of the Zebrafish Model of Diamond-Blackfan Anemia from RPS19 Deficiency via p53-Dependent and -Independent Pathways. *PLoS One* **8,** e71782 (2013).

206. Payne, E. M. *et al.* L-leucine improves the anemia and developmental defects associated with Diamond-Blackfan anemia and del(5q)MDSby activating themTORpathway. *Blood* **120,** 2214–2224 (2012).

207. Pereboom, T. C. *et al.* Translation of branched-chain aminotransferase-1 transcripts is impaired in cells haploinsufficient for ribosomal protein genes. *Exp. Hematol.* **42,** 394–403.e4 (2014).

208. Avondo, F. *et al.* Fibroblasts from patients with Diamond-Blackfan anaemia show abnormal expression of genes involved in protein synthesis, amino acid metabolism and cancer. *BMC Genomics* **10,** 442 (2009).